Optimal use of High Strength Steel grades within bridge

(OPTIBRI)

FINAL REPORT

Research and Innovation

EUR 29546 EN

Optimal use of High Strength Steel grades within bridge (OPTIBRI)

European Commission
Directorate-General for Research and Innovation
Directorate D - Industrial Technologies
Unit D.4 — Coal and Steel
Contact Hervé Martin
E-mail RTD-PUBLICATIONS@ec.europa.eu

European Commission
B-1049 Brussels

Manuscript completed in 2019.

Luxembourg: Publications Office of the European Union, 2019

PDF ISBN 978-92-79-98357-3 ISSN 1831-9424 doi: 10.2777/93807 KI-NA-29-546-EN-N

European Commission

Research Fund for Coal and Steel

Optimal use of High Strength Steel grades within bridge

(OPTIBRI)

A. M. Habraken
L. Duchêne, C. Bouffioux

University of Liège, MSM, B52/3, Quartier Polytech 1, Allée de la découverte 9, B-4000 Liège, Belgium

U. Kuhlmann, A. Zizza, S. Breunig, V. Pourostad

University of Stuttgart, Institute of Structural Design, Pfaffenwaldring 7, 70569 Stuttgart, Germany

L. da Silva, C. Rebelo, H. Gervasio, C. Rigueiro

Universidade de Coimbra, Dep. of Civil Engineering, Rua Luís Reis Santos - Polo 2 da Universidade, 3030-788 Coimbra, Portugal

F. Maas, T. Baaten, B. Droesbeke

Belgian welding institute, Technologiepark, 935, 9052 Zwijnaarde, Belgium

A. Reis, J. Pedro, C. Baptista, F. Virtuoso, C. Vieira

GRID SA, Av. João Crisostomo, 25 3rd Floor, 1050-125 Lisbon, Portugal

J. J. Dufrane, A. C. Vanderbecq, P. Toussaint

Industeel Belgium, 266, rue de Chatelet, 6030 Marchienne-au-pont, Belgium

Grant Agreement RFSR-CT-2014-00026
01.07.2014 – 30.06.2017

Final report

Directorate-General for Research and Innovation

2019 EUR 29546 EN

Table of contents:

1. Final summary

The project aims to generate guide lines for welded bridges using High Strength Steel.

The welded joints are the main reason why HSS grades have a very limited use in applications where fatigue is a critical issue, such as road bridges of medium span for instance. HSS material provides better fatigue properties than standard steels thanks to a longer initiation phase of cracks. However, in welded structures, the range of the crack initiation life is decreased to a shorter phase by the presence of small cracks like weld defects. If the use of improved welded joints could solve this problem, HSS steel grades could enhance lighter welded bridges and save material consumption. A cost comparison for a realised bridge example in S355 showed that the application of S690 and post weld treatment would have brought a cost advantage of 25% [1].

Using HSS grade within the design of a bridge deck allows slender components and thinner plates, but it is likely to be more susceptible to local buckling phenomena. Brittle fracture is slightly less dimensioning using HSS since thinner plates can be adopted, however girders are likely to be much more prone to fatigue, which proved to be the main issue of the design together with the local buckling phenomena.

As expressed before, initiation phase of a fatigue crack in HSS plates and in their improved welded joints becomes important. The OPTIBRI project prefers to use a multiaxial fatigue damage model (able to predict initiation and later growth phase of crack) to Probabilistic Fracture Mechanics only focused on crack propagation. As underlined within the BriFaG project, these multiaxial damage models have potentials, they do not follow the principle of SN curves requiring the definition of 'equivalent' or 'representative' uniaxial stress load history when the true behaviour depends on a tensor stress history. They also do not apply the additive linear damage rule of Miner, which is far from the true material behaviour. It is true that these models rely on a heavy identification phase; however, once validated, they have the advantage of being able to predict SN curves (required for comparison with standard normalized approaches) or to assess the fatigue life for any welded detail submitted to any stress history (constant or variable range of stress amplitude).

The OPTIBRI choice to select a single HSS grade and only two types of weld improvements allows performing an extensive static and fatigue test campaign covering characterization of Base Metal (BM), Heat Affected Zone (HAZ) and Weld Metal (WM) associated to both selected welded joints post treatment methods. The model identification on material samples (scale of the order of maximum 100 mm) is further improved to take into account a first scale effect and the set of parameters is enhanced thanks to the comparison of simulation results and experiments on small scale tests (more than 100 fatigue tests on plates with transverse welded stiffeners covering different thicknesses and the two types of welded joint post treatments: PIT and TIG remelting). These small case tests (scale of the order of 1 meter) have transversal welded stiffeners (with post treated welded joints) as according bridge designers, this feature is known as a strong limitation to pass the verification of fatigue limit state.

Within OPTIBRI, seven fatigue beam tests with the optimal post treated welded joint allow the identification of the SN curve of real bridge pieces taking into account a second scale effect. The adapted set of material parameters of the model able to reproduce the results of the fatigue beam tests will be used to perform the evaluation of existing design rules (FAT class) for a set of welded details present in welded bridges.

[1] Kuhlmann, U.; Dürr, A.; Günther, H.-P.: Improvement of fatigue strength of welded HSS by application of post-welded treatment methods. In: Proceedings of the IABSE Symposium in Budapest, September 13-15, 2006, S. 440-441

Steel bridges often consist of slender plates (even more slender with HSS use) which are stiffened in longitudinal as well as in transverse directions. Since the cross-section is affected by several internal forces, the plates are submitted to multiaxial stresses. However, the design of plated structures done by the current state of EN 1993-1-5 does not provide a reliable check for multiaxial loaded plates. For instance the "effective width method" does not provide any possibility of checking plates subjected to biaxial loading and the "reduced stress method" does not allow taking into account tensile stresses and their positive effect on the buckling behaviour. The positive effect of tensile stresses is well known, but cannot be quantified since no investigation has been conducted in this field, neither for the case tension/compression nor tension/shear. The OPTIBRI project experimentally studies the buckling of multiaxial stressed plates in S690QL: six large tests of multiaxially loaded panels are performed. The plate dimensions are in realistic scale according to the plate thicknesses usually used in bridge design as checked by GRID partner. Validated FE simulations on previous experiments will allow performing a reliable parametric study, yielding the evaluation of the true buckling behaviour and the development of enhanced Eurocode rules. The new knowledge generated by OPTIBRI goes until proposal of an enhancement of the code rules given in EN 1993-1-5.

The OPTIBRI project addresses for HSS bridges:

-the fatigue verification of structural piece with post treated welded joints (by PIT and TIG remelting),

-the prediction of FAT class through a validated FE model and a fatigue model and the comparison with FAT class present in Eurocode

-the buckling behaviour of plates submitted to multiaxial stresses and their verification according Eurocode rules as well as a comparison between experiment and available rules of the Eurocode

-the quantification of the interest (cost, environment and social impact) of using HSS within bridges

The quantification of the advantage of using HSS within bridges is performed on a 21.5 m wide highway bridge, with a typical 80 m long inner span and a composite steel-concrete twin plate girder deck. It presents clear fatigue and stability issues.

Three designs of this bridge are compared: the first bridge design (A) uses only standard S355 steel grade whereas the second design (B) uses also HSS S690 QL steel but relies on current state of Eurocodes. Finally, the third design (C) is performed based on the real measured behaviour of HSS S690 QL steel and post treated welded joints. Through different variants of the design (C), the project results demonstrate the need of updating of Eurocode to take into account the enhanced material properties of HSS and the buckling of multiaxial stressed plates.

Five partners, each one with complementary skills are gathered within OPTIBRI project:

University of Liège – Belgium; ULiège

Materials and Solid Mechanics (MSM) team consists in a group of 10 to 20 scientists (professor, research director, research engineer, post doc and PhD students). It belongs to Structures, Fluids and Solid Mechanics MS²F division in ArGEnCO department. It is focused on MATERIAL BEHAVIOUR (steel, Ti, Al, Ni... metals + coating). It means the development and identification of constitutive thermo-mechanical-metallurgical laws such as macroscopic phenomenological laws, multi-scale approaches and crystal plasticity models, fatigue models. These rheological models are applied within Finite Element codes to predict damage and rupture during forming processes, specific static or fatigue loading cases. Since 1984 MSM team has developed its own non linear finite element code Lagamine. Experiments are conducted within the Laboratory of Materials and Structures Mechanics (M&S) where a lot of material testing devices were acquired under the impulsion of AM Habraken. As leader of MSM group, she coordinated and participated to multiple projects

(Industrial projects, Walloon Region projects, BELSPO projects with foreign partners, PAI Intemate, ALECASPIF Pat project), she also participated in VIF Virtual Intelligent Forging (2004-2008), Coordinate Action EU and former BRITE EURAM projects on forging. Within OPTIBRI, she will be helped by Laurent Duchêne (Prof. in charge of Multi scale analysis of materials and structures in Civil Engineering field) and Chantal Bouffioux, research engineer skilled in finite element analysis and material identification.

University of Stuttgart – Germany; UStutt

The Institute of Structural Design (University of Stuttgart) headed by Prof. Ulrike Kuhlmann is part of the faculty of Civil and Environmental Engineering and has a strong focus on steel structures.

The Institute was coordinator of the RFCS projects "Robustness", "INFASO" and "COMBRI+" and is a coordinator of "SBRI", "ROBUSTIMPACT" and a partner in "HSS-SERF", "DISCCO" and "SAFEBRICTILE". Prof. KUHLMANN is chair-person of CEN/TC250 SC3 Steel Structures and Technical Working Group 8.3 (Plate buckling) as well as a member of TC6, TC8 and TC11 of ECCS. This will guarantee the possibility throughout the project to prepare and present results in Eurocode format. A number of research projects dealing with the implementation of design rules into code formulations have already been realized on national and international level. In what concerns OPTIBRI, USTUTT acts as the task leader of WP3 (investigations on plate buckling) and mainly interacts with WP1 inserting the experience in design of steel structures.

University Coimbra – Portugal; UC

The University of Coimbra is a research and education organization located in central Portugal, which was established in 1290. In the Faculty of Science and Technology (FCTUC), Dept. of Civil Engineering, the research Group on Steel and Composite Construction is represented by Prof. Luis da SILVA, who is Chairman of TMB of ECCS and also member of ECCS TC8, TC10, TC14 and the evolution group of EN 1993-1-1, President of Portuguese Steelwork Association (cmm), an experienced person in European Steel R&D activity, heavily involved in RFCS projects. He chairs the research group on Steel and Mixed Building Technology of the research unit ISISE (Institute for Sustainability and Innovation in Structural Engineering) that comprises 50 people, including 30 PhD students, with a shared laboratory and modern equipment for mechanical testing and instrumentation. Within OPTIBRI, UC leads the task of quantifying the impact of using HSS within bridges and relying on close material behavior and not current state of the standard rules.

Belgian Welding Institute - Belgium; BWI

BWI is a collective research centre. BWI has extensive recognised expertise in testing of materials and a worldwide reputation in testing of weld attachments. It is an independent non-profit organisation, combining the functions of research and development, education, training and transferring knowledge and all service relevant information to the industry. BWI has more than 30 years of experience in research for welding and related technologies, weldability of various materials and the behaviour of welded components and structures in service. It has carried out research with many technologies and has assisted companies with the implementation. In OPTIBRI, BWI is in charge of generating welded specimens with optimal welded joints or post weld treatment. BWI develops also a qualification procedure for the HFMI treatment of welds joints.

GRID Consultas, Estudos e Projectos de Engenharia - Portugal; GRID

Started in 1980, GRID is specialized in structural engineering and its main sectors are bridges, special structures and buildings. Its activity consists in consulting engineering, structural and foundation design and also technical assistance to construction works. GRID has a staff of 44 people and also has a permanent group of external consultants. The company has been involved in more than 500 studies and designs in Europe, Africa, South America. GRID has a large net of computer facilities with specific software for the static and dynamic analyses of structures and for time dependent analyses of concrete bridges.

GRID's Technical Director is António José Luis dos Reis who has a civil engineering degree by Technical University of Lisbon and a Ph.D by the University of Waterloo-Canada. He is Professor of Bridges and Structural Engineering at the Technical University of Lisbon, since 1985, and Invited Professor at the École Polytechnique Fédérale de Lausanne – EPFL, in Switzerland, in 2013. In the scope of his activity, António Reis has been involved since 1972 in a variety of projects such as long span bridges and special structures.

GRID tasks in OPTIBRI concern the studied bridge case designs, the definition of experiments to be representative of bridge details, the data for LCA, LCC, LCP assessment and the redaction of Guidelines about the optimal use of HSS within bridges.

INDUSTEEL BELGIUM; Industeel

Industeel is a company of the Arcelormittal group of companies. It is a sister company of INDUSTEEL France (Le Creusot and Chateauneuf). INDUSTEEL BELGIUM is based in Charleroi (B) where it employs 1200 workers approx.

INDUSTEEL BELGIUM produces special plates with improved mechanical or technological characteristics in numerous different grades: carbon, special and alloy, stainless steels.

The production of plates is in the range of 200 kt (kilotons) to 250 kt per year depending on the economic situation. The plate size ranges from 5 to 150 mm thick, 4 meter wide and up to 16 tons unit Weight. In its panel of produced grades of steel, Extra High Strength steels are of major importance. Produced grades range from 690 MPa up to 1100 MPa yield strength. This production is at a level of 25 kt per year i.e. 10 to 15 % of the total production.

The world potential market is estimated to 700 kt. INDUSTEEL BELGIUM ambition is to increase its market share in this field of activity. Typical applications for these grades are: lifting and handling operations, yellow goods, offshore, transport vehicles, mining. The structural applications in buildings and bridges are today not taking the best profit of these steels with a wide potential.

Mr JJ Dufrane, Manager Arcelormittal who is in charge of Industeel Business Transformation has followed OPTIBRI project at its start. He got experience within numerous internal research projects such as "Structural offshore steels with YS :355 to 460 Mpa for fixed and mobile offshore structures", "Development of 9 % Ni steels for LNG storage", "Duplex and superduplex stainless steels for critical subsea application development of 960 MPa steels for mobile cranes application", "Development of modified 9 % Cr steel for steam production". During the project Mr JJ Dufrane left Industeel and was replace by Anne-Claude Vanderbecq and Patrick Toussaint.

Within OPTIBRI, INDUSTEEL provides the material, its transportation and a part of its cutting.

The project flowchart (Fig. 1) and deliverables are presented hereafter:

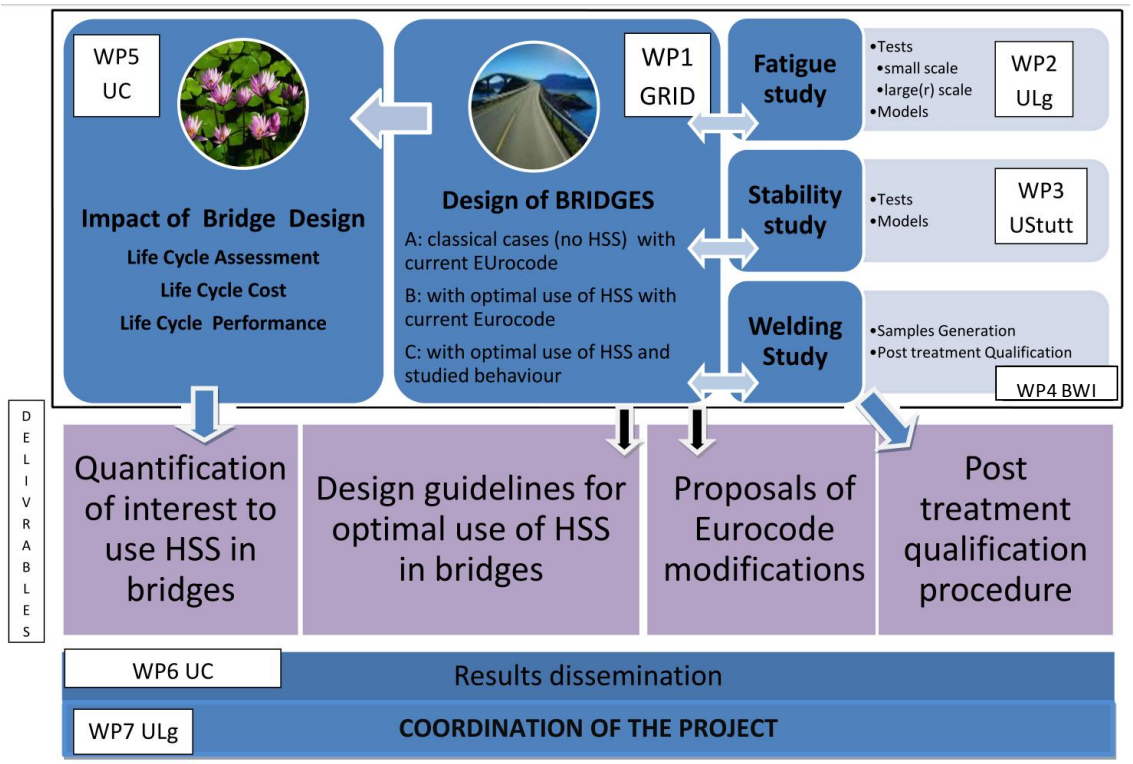

Figure 1: Optibri flowchart

In summary, the main OPTIBRI results are :

- ✓ guidelines for optimal use of HSS in bridges (see WP1 and Deliverable 1.5)
- ✓ a methodology to get reliable identification method of multiaxial damage fatigue model of Lemaitre type as well as a validated set of parameters (see WP2)
- ✓ - experimental and numerical results about SN curves of beams, bridge critical details and small case tests. It has been demonstrated that a slope m = 5 as well as an increased FATclass can be associated to the studied S690 QL with welded joints post treated by PIT. However some care must be taken before direct generalisation to all HSS bridges and critical details as low statistical data are available and care about R ratio must be paid due to higher mean stress in HSS components because thinner plates and higher yield stress (see WP2).
- ✓ proposition of Eurocode modifications about buckling of multiaxial stressed plates (see WP3)
- ✓ the selection of PIT treatment as optimal to enhance fatigue properties based on the measurements of induced residual stresses, the fatigue test results, a sensitivity analysis of the effect of PIT parameters (see WP2 and WP4)
- ✓ a quantification by LCA, LCC and LCP of the interest of using HSS in bridges (see WP5)

More details about project results can be found in Table 1 of Project overview section, or in Deliverables (section 4 provides their identification) or in WP summary hereafter. The major deviation between the initial project and the performed work concerns the drop of the activity about the TT weld joint that was replaced by TIG remelting post treatment. Finally section 5 provides a more extensive description of the work and results of each WP.

WP 1: Design of Bridges

The use of High Strength Steel (HSS) S690 QL or QL1 in highway bridges decks is not yet widespread. A research program to look for the optimal use of HSS S690QL within bridges was conducted.

A comparative design was preformed for a 21.5 m wide highway bridge, with a typical 80 m long inner span and a composite steel-concrete twin plate girder deck. Three designs were compared, using the Eurocodes: Design (A) adopted standard S355 NL steel grade whereas Design (B) used HSS S690 QL or QL1 on the main girders, and Design (C) used the same HSS S690, but profiting from the improvement of fatigue behaviour by using welded joint treatments and exploring different designs and possible enhancement of the presents Eurocode rules.

The highway bridge is composed by a continuous plate girder steel concrete composite deck with 2x2 lanes and a total width of 21.5 m. The total length of the bridge is 360 m, with 3 internal spans of 80 m and lateral spans of 60 m.

The bridge deck was designed for standard steel S355, and also for high-strength steel S690. Deck steel design and detailing was performed using European standards EN 1990, EN 1991, EN 1993 and EN 1994. Structural behaviour at ultimate limit states (ULS) was evaluated by finite frame element models, with due account for rheological effects from concrete. Construction stages were taken into account by superposition of results from:

- ✓ steel structure frame model, for the application of its own weight and the slab concrete weight;
- ✓ composite structure frame models with modular ratios for concrete, assessed for short-term actions, permanent actions and shrinkage effects (following EN 1994-2).

Longitudinal safety verifications included namely:

- ✓ ULS – bending and shear girders resistance;
- ✓ SLS – stress limitations on structural steel, reinforcement and concrete slab;
- ✓ ULS – fatigue of girders structural steel and stud connectors;
- ✓ Flange induced buckling of the webs and transverse stiffeners according with EN 1993-1-5.

Comparison between the three designs shows that using S690 enables reductions of 25% to 32% on the steel weight and about 50% on full penetration welding volume, compared to design with standard steel S355 NL.

The deck can be slender using HSS and have thinner plates, but it is likely to be more susceptible to local buckling phenomena. Brittle fracture is slightly less dimensioning using HSS since thinner plates can be adopted, but girders are likely to be much more prone to fatigue, which proved to be the main issue of the design together with the local buckling phenomena.

Plate buckling of the webs near supports proved to be a key issue when using HSS; close intermediate transverse stiffeners were introduced in Design B to increase web shear buckling resistance, whereas Design C explored the benefits of using one strong trapezoidal longitudinal stiffener at the outside of each plate girder web, which proved to be a suitable design option.

The critical fatigue welded joints were analysed according to EN 1993-1-9. For plate girders with transverse stiffeners, fatigue presents a major design constraint, namely on span sections, due to allowable plate stresses range near the welded joints.

Standard fatigue load model FLM3 with the damage equivalent factor concept was used for fatigue design of several plate girder details. Fatigue resistance of the welded joint between the transverse stiffeners and the bottom tension flange proved to be the most relevant aspect of the design of the composite steel-concrete twin plate girder deck designed for HSS S690.

Comparison between the three designs have shown that the use of HSS enables a reduction of 25-30% of the steel weight compared to the standard plate girder deck in S355 NL. Furthermore, the comparative designs reveal that using HSS S690:

- The deck to be slender;
- Thinner plates can be adopted but more susceptible to local buckling phenomena;

- Trapezoidal longitudinal stiffeners are very efficient to reduce local buckling of the webs;
- Brittle fracture is less dimensioning;
- A substantial cut on the volume of full penetration welding is obtained by using thinner plates;
- Girders are much more prone to fatigue, that proves to be the main issue of the design together with the buckling phenomena;
- The critical fatigue detail is the FAT80 occurring at the welded joints between the bottom flange and the transverse stiffeners;
- The use of welded treatments of these critical welded joints increases this FAT category and allows for an additional reduction of steel at the span's bottom flanges.

WP 2: Fatigue study

In order to study the fatigue behaviour of HSS welded connections and more specifically critical bridge details, numerical studies are performed, requiring, in particular, a detailed description of the static and fatigue behaviours of the three materials present in these connections: the base material S690QL (BM), the heat affected zone (HAZ) and the weld metal (WM).

From the static tests, the parameters of the laws of Hooke, Hill, Voce and Armstrong-Frederick are defined for the elasticity and for the plasticity with a combined isotropic-kinematic hardening.

Then, an important testing campaign is conducted to study the fatigue behaviour of four different kinds of HSS steel specimens: the small samples (extracted from plate thickness), the plates, the welded plates with/without post-treatment and the beams. For each geometry, the fatigue endurance is analysed, compared, numerically studied, aiming to get a deeper understanding of each effect affecting the lifetime of the pieces. Finally, an accurate description of the fatigue behaviour of large connections such as critical bridge details is provided.

Fig. 2 gathers S-N curves defined from the experiments and compares the different cases. The combined effect of the size, the surface roughness and the residual stresses is observed through the difference between Small samples and Plates curves. The welding effect is defined by Plates results versus Welded plates ones. In addition, the effect of post treatment choice: PIT or TIG remelting is also shown.

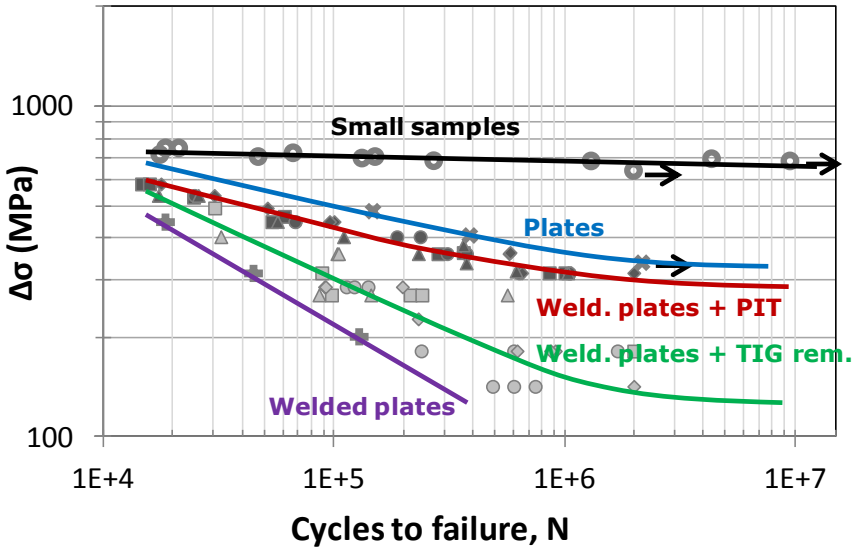

Figure 2: Fatigue tests performed on S690QL specimens

With the aim to identify a reduction factor for the size effect between plate tests and bridge case for the PIT-treated transverse attachment out of high strength steels, a beam testing program was developed and successfully executed.

Note that for the single as-welded case of the beam test campaign, a very high lifetime was achieved. This could be shown comparing this single result with the fatigue resistance of transverse stiffener according to EN 1993-1-9 and also in comparison to the small case series without post-treatment.

The fatigue resistance improvement of the weld toes of the transverse attachment due to the PIT-treatment led in most of the cases to failure mechanisms that are detached from that improved detail. In some cases base material failure of the tensioned bottom flange could be reached. In other cases external equipment led to deviant failure modes.

Nonetheless all of the test results can be used as minimum strengths for the investigated detail category. So two values for the nominal fatigue resistance $\Delta\sigma_c$ depending on the assumption of two different slopes for the linear regression have been determined. A PIT-improved reference value for the fatigue resistance at 2 million load cycles could be determined to be $\Delta\sigma_{c,\ imp}$ = 134 N/mm² under the assumption of a fix slope m = 5. Whereas the evaluation of the PIT-treated beam test series with a free slope of m = 3.2 results in a fatigue resistance of $\Delta\sigma_{c,\ imp}$ = 123 N/mm², see Fig.3, left.

The determination of a real scale factor for PIT-treated transverse stiffener by the comparison of small scale and beam test results was complicated by the shifted failure modes achieved at the beam tests. So that only a minimum, conservative reduction factor of around 71-73%can be defined by the relation of the beam test fatigue strength to small scale strength, see Fig.3, left .It shows the evaluation following the linear regression according to Background Document (Sedlacek et al, 2007) of EN 1993-1-9 with a fixed slope of m = 5. Following the linear regression analysis the fatigue strength of the PIT-treated beam test results could be determined around $\Delta\sigma_c$ = 134 N/mm² for 2 million cycles, see black lines. Dashed lines represent the 95% survival probability and continuous line the mean value graph of test results. The evaluation with the variable slope of 3.2 and thus a steeper slope leads to a fatigue strength $\Delta\sigma_c$ = 123 N/mm² for 2 million cycles, see Fig. 3, left (blue lines), also dashed for 95% probability and continuous for 50 % probability.

This factor takes into account, all the beam tests, so it includes the one where no post treatment at all was applied.

If this test is dropped, the reduction factor becomes 78% (see Fig.3, right) which can be seen as a less conservative value. Note also that Fig.3, right does not applied statistic approach of EN 1993-1-9 and is based on failure initiation. Table 3 provides, for two beams, the comparison between the number of cycles at the crack initiation and failure.

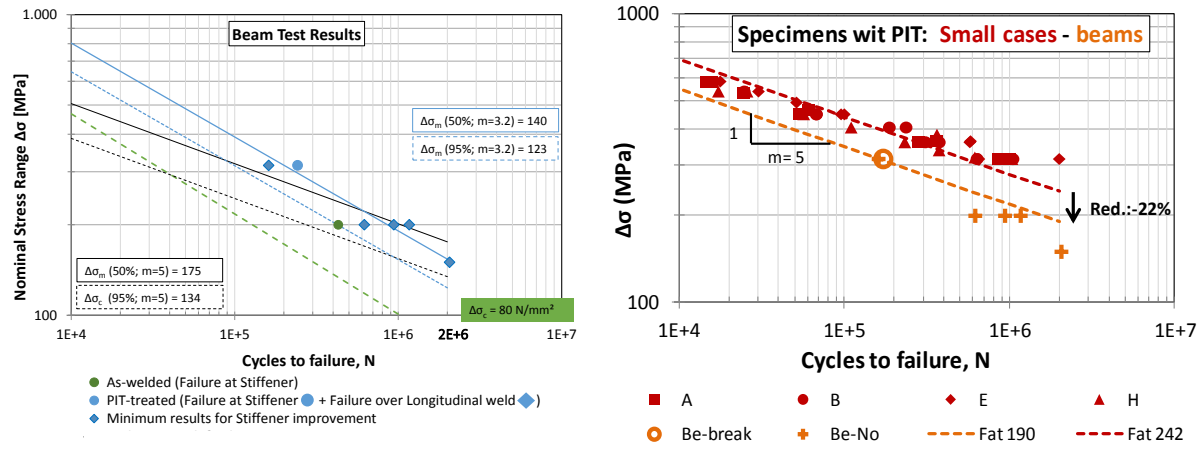

Figure 3: S-N diagram with fatigue resistance for PIT-treated beam tests for transverse stiffener with a slope of m = 5.0 and free slope of m = 3.2 (left) and fatigue tests results on S690QL PIT post-treated specimens: small cases ("A", "B", "E", "H") and beams "BE-break" for the beam with rupture at transverse stiffener welded joint and "Be-No" for the beams without rupture on the PIT treated welded joints + S-N curves with a slope m=5 : FAT242 for small cases and FAT190 for beams (right)

Table 1: Experimental fatigue beam tests: number of cycles at crack initiation Ni and at total failure Nf, on beam with PIT treatment and rupture on Stiffener Welded joint: "PIT-SW", on beam with As Welded joint and rupture on Stiffener Welded joint: "AW-SW"

Name	R	Δσ	Rupt.:0/1	Ni	Nf
		Mpa			
PIT-SW	0.1	315	1	172 175	242 468
AW-SW	0.1	200	1	168 825	429 250

It could be shown that this PIT-treated welded detail can be shifted to an uncritical stage and that the attention of fatigue has also to be shifted to details that are not known to be critical in terms of fatigue failure.

A high fatigue resistance has been shown for the automatic longitudinal fillet welded joint. Besides the planned investigations during the execution of the beam tests, the interest to improve the fatigue resistance of the longitudinal fillet welded joint systematically has been awakened.

For the prediction of the fatigue crack initiation, the Lemaître Chaboche multiaxial fatigue model improved by the stress gradient method is used. A first set of fatigue damage material parameters (SET 1) is identified from the testing program on small samples. A second set of parameters (SET 2) is determined for plates and a final set (SET 3) for the beams. Reduction factors link the data sets SET23, SET2 and SET 1.

Numerical models simulate in a first step the welded plates and in a second step the beams with the most efficient post-treatment (PIT). The residual stresses, measured by X-ray, are taken into account in the models. For each case, the fatigue data (SET2 or SET 3) are adapted to take into account of the size of the welded connection for a correct prediction of the crack initiation. The SET 3 allows simulating the bridge connections, with a model validated by the experiments.

A critical detail of a bridge design with S690QL steel has been studied in two stages: i) a global model of a main girder and a stiffener; ii) a submodel representing the welded connection with a very fine mesh and the residual stresses from the welding process and the PIT post-treatment. The number of cycles at the crack initiation, computed for several stress ranges, determines a new S-N curve. It contributes to define the general guidelines for bridge design with HSS steel.

WP 3. Buckling of multiaxially stressed plates

In order to investigate the buckling behaviour of slender plates subjected to multiaxial stress states, six large size tests were realized at the laboratory in University of Stuttgart. The test setup consisted of a portal frame equipped with a hydraulic jack for introducing compression to the plate. Additional hydraulic jacks were arranged laterally for introducing tension stresses to the plate and generating the desired multiaxial stress state. The tests subdivided into "A" and "B". "A"-tests are conducted on plates with a width of 900 mm having a square test panel of 900 mm x 900 mm. The tension/compression ratio β also varied between 0, -0.25 and -0.5. "B" tests were conducted on plates with a width of 500 mm having a test panel of 1500 mm x 500 mm. The tension/compression ratio β varied between 0, -1.5 and -1.0. In each group β=0 was used as a reference for the evaluation of the test results. The influence of the tension stresses on the buckling behaviour can be seen on the out-of-panel deformation and on the ultimate load. In both test series "A" and "B" a distinct increase of the ultimate load is observed, if tensile stresses act at the same time as compression.

The tests are simulated with Finite Element Method with measured imperfections and material parameters measured by tensile tests. The FE results showed a good agreement with the test results. The experiments were also simulated using imperfections according to Annex C, EN 1993-1-5. Good results have been found for square panels under compression and tension stress with one, two and three half-wave imperfection shapes.

The tension stresses may change the failure mode of a square panel from one half-wave into more half-waves. Furthermore, the results show that tensile stresses increase the buckling resistance of the investigated panels.

The buckling curves have been recalculated for different boundary conditions as well as for bending and shear forces for high strength steel.

The proposal of (Zizza:2016) [41] developed for mild steel is investigated for S690QL panels subjected to compression and tension. It is concluded, that the proposal of (Zizza:2016) [41] leads to good results also for this case. It is concluded that considering the positive effect of tension stresses on the reduction factors, enhances the accuracy of the "reduced stress method" and leads to a more economic design of the panels. At this point, it seems reasonable to take into account tensile stresses in the design of multiaxially loaded plates. Application of reduced stress method for panels subjected to shear and tension stresses shows a good agreement with numerical results.

In contrast to reduced stress method, the effective width method does not consider the positive effect of tension stresses and reduces the shear resistance in the same way as for compression stresses. In order to consider the beneficial effects of tension stresses the following proposal in case of panels subjected to normal, bending and shear forces is made:

If $|\sigma_t| > |\sigma_c|$ and the stress ratio $\psi \geq -0.5$ the slenderness $\overline{\lambda}_w$ may be taken the same $\overline{\lambda}_p$ acc. to eq. (10.2) from section 10 of (EN 1993-1-5:2006).

$\Rightarrow \overline{\lambda}_w = \overline{\lambda}_p = \sqrt{\frac{\alpha_{ult,k}}{\alpha_{cr}}}$ if $|\sigma_t| > |\sigma_c|$ and the stress ratio $\psi \geq -0.5$

where:

σ_t: Tension stress

σ_c: Compression stress

$\overline{\lambda}_w$: Slenderness for calculation of shear buckling resistance

$\overline{\lambda}_p$: Slenderness acc. to eq. (10.2) from section 10 of (EN 1993-1-5:2006)

The resistance of panels should be determined according to the following interaction acc. to 7.1(5) of (EN 1995-1-5:2006) :

$$\eta_1 + (2\bar{\eta}_3 - 1)^2 \leq 1.0$$

with:

$$\eta_1 = \frac{N_{Ed}}{\frac{f_y A_{eff}}{\gamma_{M1}}} + \frac{M_{Ed} + N_{Ed} e_N}{\frac{f_y W_{eff}}{\gamma_{M1}}}, \bar{\eta}_3 = \frac{V_{Ed}}{V_{bw,Rd}}$$

However, the basis of this investigation is limited on unstiffened panels neglecting the load-shedding with flanges. In future, the effect of tension stresses should be further numerically investigated for panels with stiffeners being part of a section with flanges.

WP 4: Samples generation and post-weld treatment qualification

Weld Procedure Qualification testing has been carried out to define the welding parameters for each set up for the small scale fatigue samples, in S690QL. Using these welding procedures, all small scale fatigue samples were generated (and parameters logged). Two different post-weld treatments have been carried out on these samples: Pneumatic Impact Treatment (PIT) as well as TIG (or GTAW) dressing. The first treatment results in a geometrical change, as well as introduction of compressive stresses (at the surface), the second one results in a geometrical change, but also a microstructural change.

Welding of HSS Supralsim S690QL, both in a laboratory environment, and in a company workshop, has been found to be quite straightforward, with very limited preheat (only necessary for the thicker material). The time needed to carry out the post-weld heat treatment (in the industrial case) was very limited compared to the actual welding, inspection and repair time.

For the different plate thicknesses, the temperature cycle during actual welding has been measured in different regions next to the welded joint. The differences in temperature cycle result in different microstructures, and therefore properties in this region. Of course, in a real welded joint this 'Heat Affected Zone' has changing microstructures and properties, over a small distance. In this project it has been shown that, by replicating the thermal cycle, as measured on the actual welded joint, it has been possible to recreate samples where material characteristics of a certain area of the heat

affected zone of the welded attachment can be obtained in a homogeneous zone of relative size (>10mm length). This method could be used for other applications (damage modelling, weld structure/properties modelling).

For the Pneumatic Impact Treatment, different parameter settings have been used to investigate differences in hardness profiles/fatigue life results. Based on the dataset available it has not been possible to show any differences. Therefore, the original proposal to develop a 'Post Welding Treatment Procedure' has been abandoned, referral to the IIW recommendations for post treatment is given.

Post mortem analyses of the fatigued – weld post treated specimens, has however shown that fatigue crack often starts in the treated area. This is something that needs to be analysed further, to see if improvements and/or adaptations of the treatments can avoid this.

WP 5: Impact of bridge design

Framework

The main aim of this WP is to provide an appropriate methodology for the lifetime assessment of HSS bridges, from bridge construction to the end-of-life stage, taking into account structural, environmental and cost criteria. Divided in 4 steps this WP will perform researches for all the missing data related to HSS bridges then will cover systematically the difference between Design A, B and C of the studied bridge cases.

WP 5.1 – Life cycle performance of HSS bridges

WP 5.2 – Life cycle environmental analysis of HSS bridges

WP 5.3 – Life cycle cost analysis of HSS bridges

WP 5.4 – Application to case studies

Principal Conclusions

The following observations and conclusions were made from the lifecycle assessment of the 3 bridges designed by GRID in WP1, from the construction, over the operation and maintenance stage, until the demolition at the end-of-life.

Environmental outputs include emissions to air, water and soil. In this work, most of input and output data were collected from the professional database and extension database provided by the Gabi software. Considering the same impacts for the conventional and High-Strength Steel, LCA showed that Designs B & C, which make use of a high-strength steel - S690, caused on average 22.5% and 29.2% less environmental impacts as compared to Design A that makes use of a conventional S355 steel grade. The use of longitudinal stiffeners, instead of vertical stiffeners, accompanied by post-weld treatments led to a significant reduction in the amount of steel required.

With no LCI data available for HSS, sensitivity analysis was performed and an estimated 33 - 47% increment in impact factors for HSS were to be required for the latter two design equivalent to the first design in terms of environmental impacts.

Despite being designed from HSS, design B registered costs practically the same as design A in the lifecycle cost analysis. Moreover, Design C was found to be 5.1% cheaper compared to design A. In terms of Social/user costs, 2.2% - 3.2% cheaper alternatives were made possible.

Clear advantages had already been seen in the early stages of the design as a significantly reduced amount of steel is required when using high-strength steel. Reduction of the steel volume is achieved by using HSS. And even more reduction is possible by using longitudinal stiffeners in place of vertical ones.

In summary, the following advantages were identified for high-strength steel:

- LCA – Better environmental performance due to the reduction volume of steel required and subsequent reduction in weld volumes.
- LCC – Cheaper as a result of the lighter structures achieved and the use of improved knowledge on the structural behaviour of HSS

- LCS – reduced user costs as a result of reduced maintenance operations comes as a direct result of reduced surface are of the steel that requires corrosion protection

Possible Actions

From the lifecycle environmental analysis point of view, it is therefore essential to explicitly consider the LCI impacts associated to welding in order to appropriately compare solutions using HSS.

From the lifecycle costs analysis point of view it is therefore important to identify the costs associated with specific maintenance actions related to HSS solutions.

From the lifecycle social analysis it is therefore essential to detail the duration of the erection and maintenance operations in terms of duration in a detailed way.

WP 6: Result dissemination

A webpage was implemented in the European Convention for Constructional Steelwork (ECCS) web site (https://www.steelconstruct.com/site/) for the public dissemination of the main results of the research programme.

A private part in this website was created for the organization of internal documents and project deliverables during the execution of the research programme. This private part can be accessed only by the partners of the project.

A dedicated workshop was organized which gathered 29 specialized participants from different countries.

The dissemination material (copy of the slides of the 10 presentations) was provided to the 170-200 participants of Stahlbaukalendertag 2017 organized by Institute of Structural Design Stuttgart.

During the department day of ArGEnCo, held on 2 May 2017, at ULiège, in Liège, Belgium, a poster summarising Optibri results has been presented.

Currently the results of the project have been currently presented three time in international conferences and one time in a national conference. A new presentation is already planned about environmental impact.

Publications in journals to large technical audience (Lastechniek – Metallurgie) will be submitted by BWI.

Other scientific journals are foreseen to be submitted to international structural, material and environmental journals by the partners now that final Deliverables forced everybody to write the information in a structured way.

The gathered knowledge will also be disseminated through PhD theses: A. Zizza (2016, Stuttgart) and S. Breunig, V. Pourostad, current PhD students of Prof. Kuhlman. The final application of C. Canales ULiège PhD could be based on OPTIBRI project, however this is not yet confirmed. What is sure is that further investigations of the fatigue behaviour of bridge details are on going through a Master thesis in ULiège.

2. Scientific and technical description of the results

Objectives of the project

1. to quantify by LCA, LCC and LCP the interest of using HSS in bridges
2. to provide guidelines for optimal use of HSS in bridges
3. to propose a HFMI post treatment qualification procedure of HSS welded joint
4. to propose Eurocode modifications about fatigue assessment for HSS welded bridges
5. to propose Eurocode modifications about buckling of multiaxially stressed plates

WP 1: Design of Bridges

WP 1.1: Design cases A B C

The highway bridge studied is composed by a continuous plate girder steel concrete composite deck with 2x2 lanes and a total width of 21.5 m. The total length of the bridge is 360 m, with 3 internal spans of 80 m and lateral spans of 60 m (Fig. 1.1).

The bridge deck is designed for standard steel S355 (Design A, Fig. 1.2 and 1.3), and also for high-strength steel S690 (Design B, Fig. 1.4 and 1.5, and Design C, Fig. 1.6 and 1.7). Design A using standard S355 (J2 or N/NL) steel grade and relying on present versions of the Eurocodes, while Design B uses HSS S690 (QL/QL1) and is based on present versions of the Eurocodes. Finally, Design C also uses HSS S690 (QL/QL1), but is supported by the fatigue tests performed by WP2, and on an enhanced verification approach for the buckling, proposed in WP3. Annex 1 includes three drawings with the detail definition of each solution.

Deck steel design and its description are performed using European standards EN 1990, EN 1991, EN 1993 and EN 1994. Structural behaviour at ultimate limit states (ULS) is evaluated by finite frame element models, with due account for rheological effect from concrete. Construction stages are taken into account by superposition of results from the steel structure frame model, for the application of its own weight and the slab concrete weight; and the composite structure frame models with modular ratios for concrete, assessed for short-term actions, permanent actions and shrinkage effects (following EN 1994-2 [1]).

Longitudinal safety verifications included namely:

a) ULS – bending and shear girders resistance;

b) SLS – stress limitations on structural steel, reinforcement and concrete slab; and

c) ULS – fatigue of girders structural steel and stud connectors.

Flange induced buckling and transverse stiffeners are also designed with EN 1993-1-5 [2]. Plate buckling of the webs near supports is a key issue when using HSS. Close intermediate transverse stiffeners are introduced in Design B to increase web shear buckling resistance, whereas Design C explored the benefits of using one strong trapezoidal longitudinal stiffener at the outside of each plate girder web, which proved to be a suitable design option.

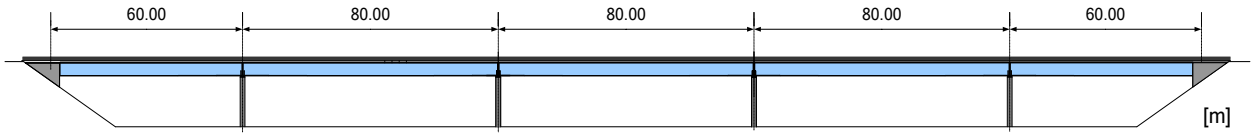

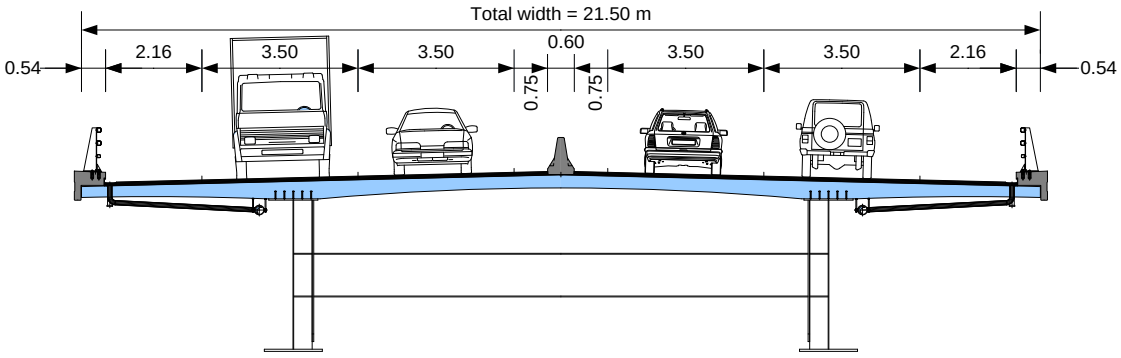

Figure 1.1: Longitudinal view and deck cross-section with the highway platform data

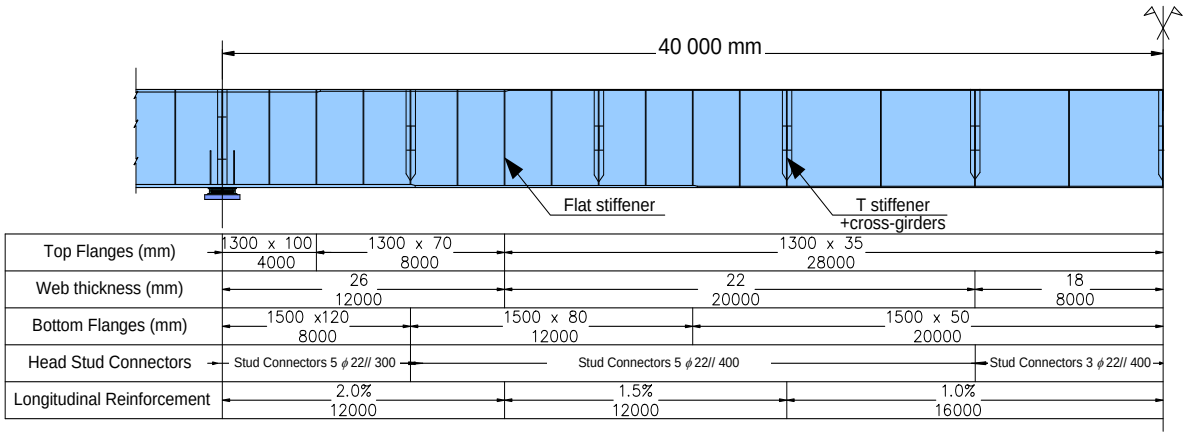

Figure 1.2: Structural steel distribution for the main girder typical span for Design A with S355 NL

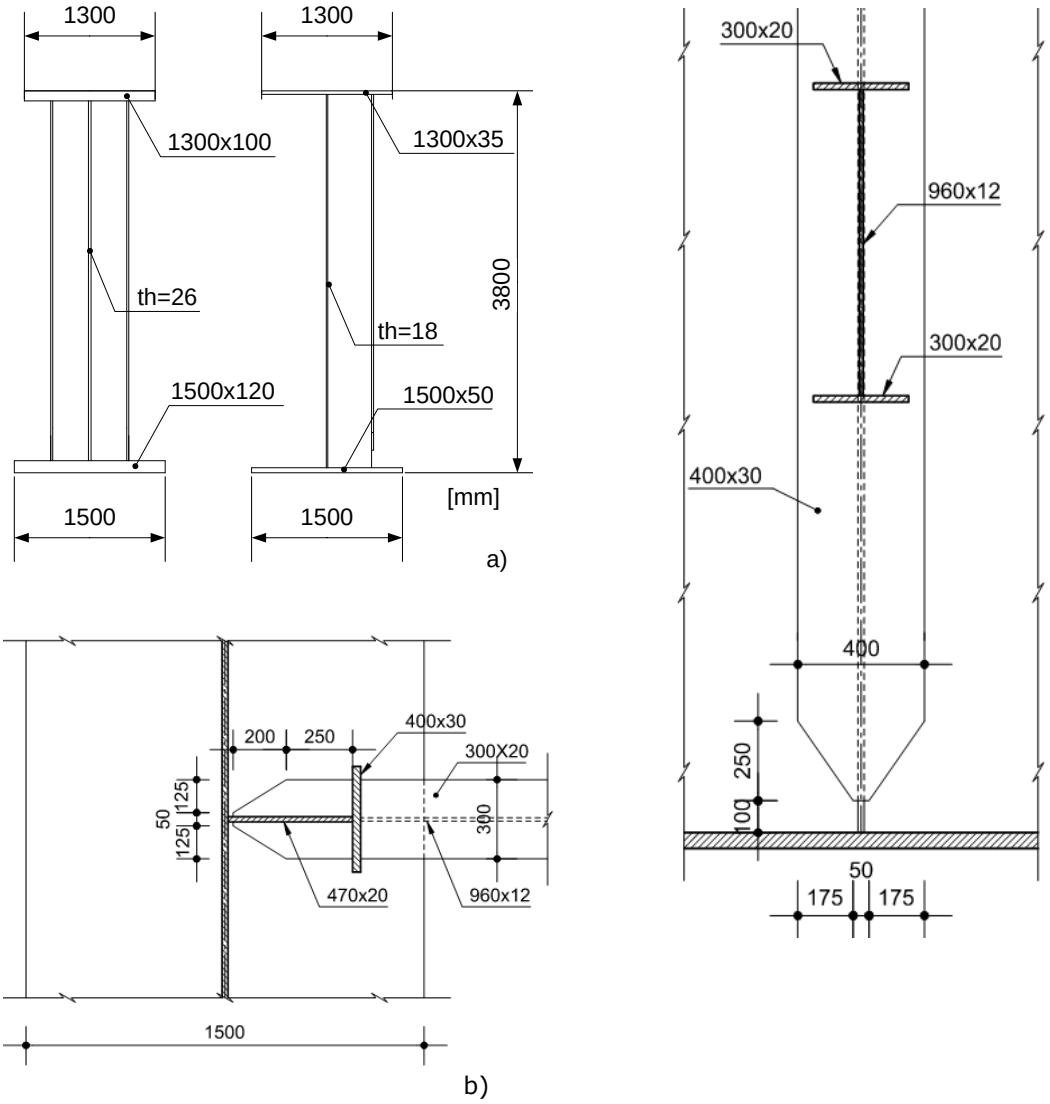

a) Plate girder cross-sections – support / mid-span

b) T stiffener and cross-girders detailing – plan section and elevation

Figure 1.3: Details of main girders and transverse stiffeners for Design A with S355 NL

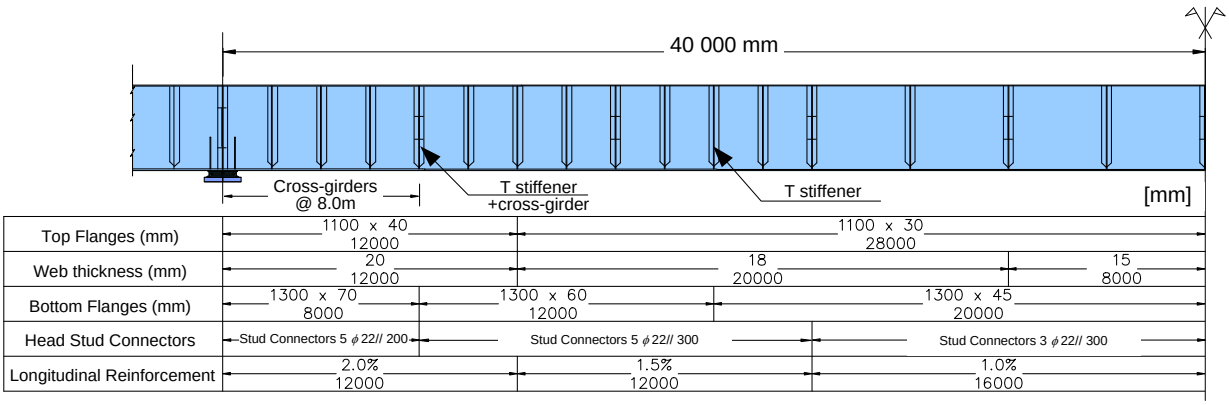

Figure 1.4: Structural steel distribution for the main girder typical span for Design B with S690 QL

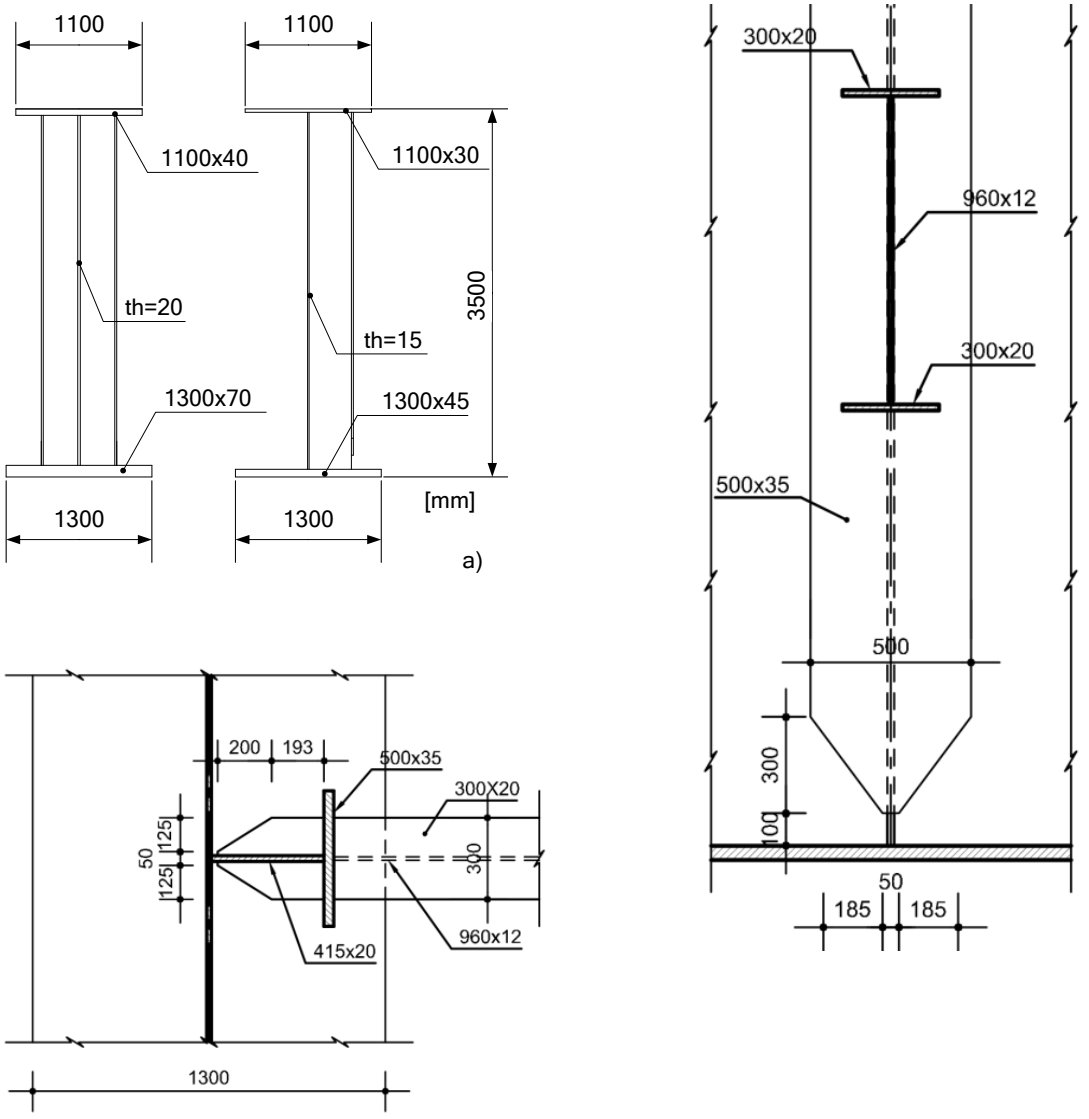

a) Plate girder cross-sections – support / mid-span

b) T stiffener and cross-girders detailing – plan section and elevation

Figure 1.5: Details of main girders and transverse stiffeners for Design B with S690 QL

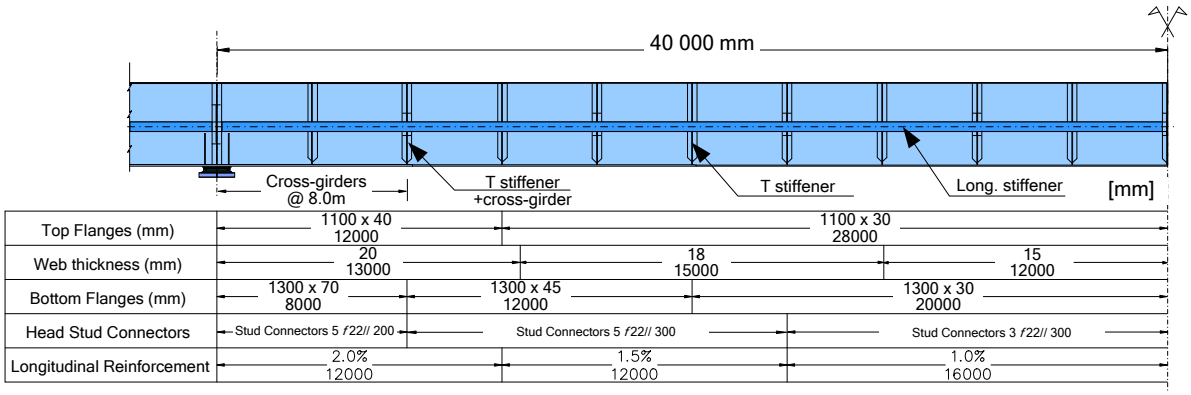

Figure 1.6: Structural steel distribution for the main girder typical span for Design C with S690 Q

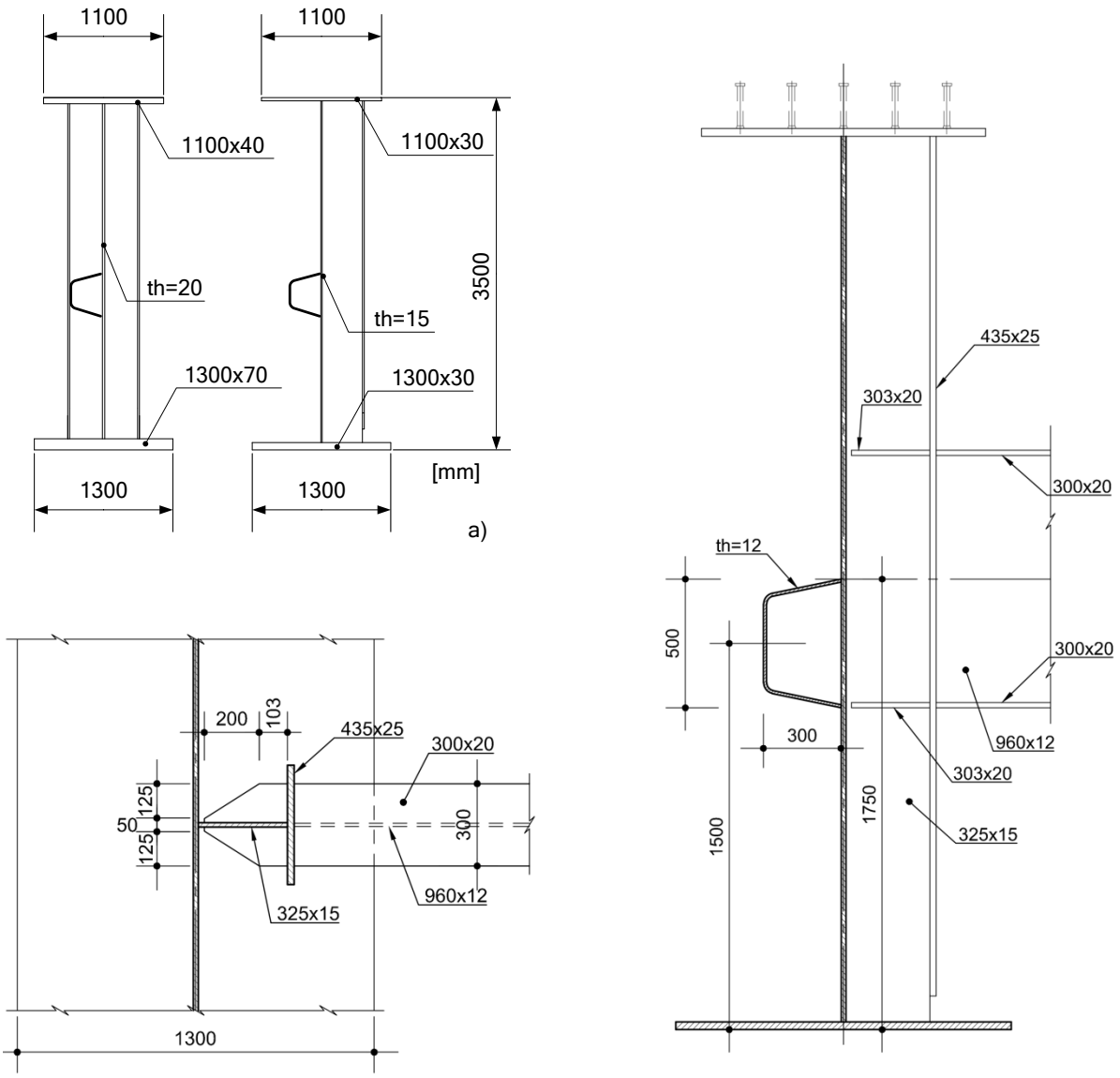

a) Plate girder cross-sections – support / mid-span

b) T stiffener and cross-girders detailing – plan section and elevation

Figure 1.7: Details of main girders and transverse stiffeners for Design C with S690 QL

Execution scheme – The following construction phases have been adopted:

1. installation of the steel structure of the deck ;
2. on-site pouring of the concrete slab segments by casting them in a selected order:

It is assumed in the design that the structural steel of the deck will be executed by incremental launching from one abutment to the other. The structural analysis of these construction stages was performed and it does not govern the design.

The concrete slab may be casted on-site by segments in a selected order with a forming carriage running on the main girders. The slab is executed in 10.0 m length segments, eight segments by span, of which five at the mid-span will be concreted in the first passage of the forming carriage; the other segments located over the supports, will be casted at a later stage (Fig. 1.8). The self-weight of the mobile formwork is estimated to be equivalent to a uniform load of 2 kN/m².

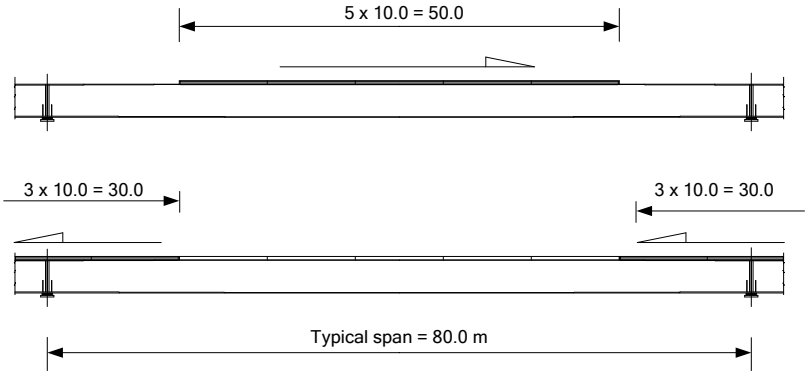

Figure 1.8: Distribution and order of concreting of the slab segments in a typical span

The time taken to pour and prestress each slab segment is assessed at 4 days. The first day is for concreting, the second day to its hardening, the third day to prestressing and the fourth day to moving the falsework. In result, one may assume that the 36 segments slab can be completed in 144 days. The non structural bridge equipment, such as waterproofing, asphalt, safe barriers and drainage system may be completed in about 45 days. This time schedule is adopted to estimate the age of concrete at time of loading, for creep effects calculations.

It should be point out that a minor variation in these times during the construction phases has little influence on the values of the modular ratio and even less on the values of internal forces and moments obtained from the global analysis. Therefore, it was considered that the slab construction stages are not relevant for the main aim of the study, which is the comparison between different structural steel grades and potential competitiveness of the High Strength Steel (HSS) application to bridges. Therefore, the structural analysis in this design is made assuming the slab as completely casted at one single stage over the main girders.

Materials – The following structural steels were considered for the three designs:

- ✓ Design A – Steel S355 NL (EN 10025-3 [3]),
- ✓ Designs B and C – Steel S690 QL (EN 10025-6 [4]).

Both solution adopted a concrete slab made of concrete C35/45 (EN 1992-1 [5]) and reinforcement B500B (EN 10080 [6]). Head stud connectors S235 with tensile strength of 450 MPa in accordance with EN 13918 [7] and EN 1994-2 [1] are adopted in three designs.

Actions – The following actions were considered for the design of the three deck solutions:

- ✓ Steel self weight – the main girders weight is considered by using unit weight of structural steel as 77 kN/m^3; Additional self-weight of stiffeners, connectors, cross-girders and other bracing elements is modelled by a uniform distributed load of 3.5 kN/m applied directly on each main girder.
- ✓ Slab self weight – for a total width of 21.5 m and an average thickness of 0.32 m, slab weigh representing an applied uniform load of 86.0 kN/m per main girder.
- ✓ Superimposed dead loads – including asphalt layer and waterproofing, safety barriers, and the drainage system, corresponds to a distributed load of 29.9 kN/m on each main girder.
- ✓ Total shrinkage – corresponds to an axial slab deformation of 173.1x10^{-6} at traffic opening and 324.1x10^{-6} at infinite time.
- ✓ Creep effect – is considered in the analysis by taking the appropriate modular ratio n_L for the concrete rendering the steel-concrete composite section into an equivalent steel section; values n_L = 6.2, 14.3 and 15.7 respectively for short term actions, shrinkage effect and superimposed dead loads action applied at an age of the concrete of 95 days.
- ✓ Traffic loads – Load Model 1 is used for the global ULS and SLS longitudinal analysis according with EN 1991-2 [8], by adopting a Tandem System (TS) of 600+400+200 kN, and an Uniform Distributed Load (UDL) of 70.5 kN/m, both positioned longitudinally and transversally on the deck so as to achieve the most unfavourable effect for the studied main girder; Fatigue assessment of the bridge deck is made using the Load Model 3 of

EN 1991-2, being composed by four axles with a total weight of 480 kN and a second vehicle of 144 kN, distant 40m apart.

- ✓ Thermal gradient – linear thermal gradients of $\Delta T_{M,heat}$ = 15°C and $\Delta T_{M,cool}$ = −18°C, between the top of the slab and the bottom of the girder, according with the approach 1 of EN 1991-1-5 [9].

WP 1.2: ULS analysis of HSS bridge (Design B)

1.2.1 Bending resistance

The flange widths and thickness of the main plate girders were first defined to achieve the required bending resistance. Then, span flanges were re-assessed based on fatigue requirements. The final main girders geometry is presented in Figs. 2 to 5, for standard steel S355 and HSS S690.

Differently to Class 3 sections usually adopted in design of support sections, when using HSS the bottom flange and web at support sections are Class 4, due to the compact thickness required and the very low value of $\varepsilon = \sqrt{235/f_y}$ = 0.584. Therefore, to take into account for local plate buckling effects by EN 1993-1-5 [2], effective width sections are used. Reduction factors ρ = 0.94 and 0.49 respectively for support section compressed bottom flange and web are adopted. The design of the bottom flange nearby internal supports, further considers the reduction factor χ_{LT} =0.72 due to lateral torsional buckling. Even so, an important reduction of steel can be achieved on both flanges by using HSS S690. All deck sections can still be designed elastically, as confirmed by the results from Table 1.1 confirm. In fact, ULS bending resistance is not a critical design issue when using HSS 690.

Table 1.1: Elastic bending resistance at support and mid-span deck cross-sections

Mid-span section	Design A S355	Design B S690	Design C S690
$\{\sigma_{Ed} / (f_{yf} / \gamma_{M0})\}$ Bottom flange < 1	0.93	0.65	0.87
Support section	**Design A S355**	**Design B S690**	**Design C S690**
$\{\sigma_{Ed} / (f_{yf} / \gamma_{M0})\}$ Effective bottom flange at support < 1	0.95	0.88	0.88
$\{\sigma_{Ed} / (\chi_{LT} f_{yf} / \gamma_{M1})\}$ Eff. bottom flange at *h*w/2 from support < 1	0.92	0.97	0.97

1.2.2 Shear resistance

The shear resistance is evaluated using the effective width method presented in sections 4 to 7 of EN 1993-1-5 [2]. The shear resistance at support panels is attained only by the web contribution, since the flanges are completely used for bending. The web resistance is evaluated considering shear buckling. To increase the shear critical stress τ_{cr}, on Designs A and B closed spaced transverse stiffeners are adopted, a=2 m apart at support panels and a=4 m apart at mid-span region. However, Design C increased the spacing between transverse stiffeners to a constant value of a=4 m, and adopted a closed longitudinal stiffener at the outside of the web. This solution proved to be a better option for increasing the shear resistance when using HSS, as Table 1.2 resumes the main results for the support panel.

Additionally, (M,V) interaction is checked according to §7.1 of EN 1993-1-5 [2], at the web section located at min$\{h_w/2; a/2\}$=1 m from the support. When using HSS S690, it is possible to reduce the thickness of the webs from 26 mm to 20 mm, but the interaction (M,V) makes the support panels work at the limit, if consistently a unique safety coefficient γ_{M1} =1.1 is adopted, for both bending and shear resistances.

1.2.3 Intermediate transverse stiffeners design

Transverse stiffeners increase shear resistance, provide lateral supports to the web and to longitudinal stiffeners when they exist, carry concentrated transverse forces and together with cross-girders reduce distortional deformations of the deck cross-section.

Table 1.2: Elastic shear resistance at support panels

Support section	Design A S355	Design B S690	Design C S690
h_w x t_w (mm^2)	3580x26	3390x20	3390x20
τ_{cr} (MPa)	211.6	127.9	146.4
$\bar{\lambda}_w = 0.76\sqrt{f_{yw}/\tau_{cr}}$	0.97	1.77	1.65
χ_w	0.86	0.56	0.58
$V_{Ed}/V_{bw,Rd} = V_{Ed}/(\chi_w h_w t_w f_{yw}/\sqrt{3}\gamma_{M1})$	0.86	0.91	0.87
(M/V) Interaction with $\gamma_{M1=1.1}$	No interaction	1.00	0.94

One first survey used the same two types of intermediate HSS stiffeners as adopted in Design A – flat and T stiffeners (Fig. 1.3), but it was concluded that EN 1993-1-5 requirements for flat transverse stiffeners are very difficult to fulfil with HSS. Therefore, only T shape stiffeners were adopted in the Design B and C (Figs. 1.5 and 1.7). When checking the buckling resistance, stiffener cross-section is taken as the gross area comprising the stiffener plus a width of web plate equal to 15 εt_w , which is smaller for the HSS due to the significant reduction of ε and t_w.

The intermediate transverse stiffeners are designed according to section 9 of EN 1993-1-5 [2], cheeking the following requirements:

– Minimum stiffness for shear verification of the webs – by imposing a second moment of the area of a stiffener I_{st} higher than:

$$If\ a/h_w < \sqrt{2}:\ I_{st} \geq 1.5\, h_w^3 t^3/\, a^2$$
$$If\ a/h_w \geq \sqrt{2}:\ I_{st} \geq 0.75\, h_w t^3 \qquad (1.1)$$

This requirement is easily verified and does not demand very strong stiffeners.

– Resistance requirement – verified with the axial force N_{st} imposed by the tension field action (and additionally the destabilising influence of web direct stress), and given by:

$$N_{st} = V_{Ed} - \frac{1}{\bar{\lambda}_w^2}\frac{f_{yw} h_w t}{\sqrt{3}\,\gamma_{M1}} = V_{Ed} - V_{cr,w} \qquad (1.2)$$

where V_{Ed} is taken at the distance 0.5 h_w from the edge of the panel with the largest shear force and $V_{cr,w}$ corresponds to the elastic shear buckling resistance of the web.

This requirement is considerable more demanding for the intermediate single-sided HSS stiffeners, since slender webs are working with very high V_{Ed} , producing high eccentric axial forces N_{st} , that should be taken into account in the beam-column verification of the stiffeners.

– Safety to torsional buckling – design rules for open stiffeners assume that torsional buckling is completely prevented when loaded axially; thus EN 1993-1-5 provides the following general requirement that should be fulfilled for open T or L stiffeners with warping stiffness:

$$\sigma_{cr} \geq \theta\, f_y \text{ with } \theta = 2 \text{ for flat stiffeners and } \theta = 6 \text{ for torsional rigid stiffeners} \qquad (1.3)$$

where σ_{cr} is the elastic critical stress of a stiffener at torsional buckling. Out of the three criteria, this is the one governing the design, so when using HSS this condition was adopted replacing f_y with the maximum actual stress $\sigma_{max,Ed}$ that occurs in the transverse stiffener under consideration [10].

Further Research – Presently, it is clear that axial forces considered in the intermediate stiffener verifications, resulting from the tension field model, are very conservative. In fact, the tension field model for the determination of web panels shear resistance was replaced by the rotated stress field in the current version of EN1993-1-5.

In the last two decades several research studies with experimental work and/or numerical simulations have concluded that transverse stiffeners are predominantly loaded by bending induced by their restraint to web lateral deflection and not by in-plane tension field forces (Lee[2003], Xie[2003], Kim Yoon Duk[2004], Presta[2008], Sinur[2012] [11–15]). Nevertheless, there is at present no established method to substitute the EN1993-1-5 method for transverse stiffeners design, based on numerical investigations and prototype experimental tests of high strength steel strength panels.

According to the available test results and numerical simulations, Eq. (1.2) overestimates the average axial force installed at the stiffeners N_{st} (by a factor of 2), and therefore overestimates also the design of the stiffeners cross-section. Therefore, important savings can be achieved in the cross-section of the transverse stiffeners. The conclusion from Sinur's work, which was focused in longitudinal and transverse stiffened panels, was taken to assess the potential reduction in stiffener weight of Design C. In their experimental tests, using steel grade S355 and transverse flat stiffeners, the force measured in the stiffeners from the prototype represented, at the limit, 56% of the force calculated according to EN1993-1-5 method. This percentage was applied to stiffeners design force N_{st} evaluated and a new design of the stiffeners was performed for Design C on Table 1.3.

Using this assumption, it was concluded that "T" stiffeners are only needed to link cross girders, 8.0 m apart and to assure resistance to lateral buckling of the compressed bottom flange. Therefore, flat stiffeners would be sufficient for the remaining intermediate transverse stiffeners. These results lead to a 33% reduction in intermediate stiffeners weight. However, it should be noted that new test results should be added to verify the shear buckling behaviour of high strength stiffened panels, before extrapolating the available test results to HSS design, without further research.

Table 1.3: Alternative geometrical definition of the transverse stiffeners of Design C adopting the proposition of Sinur 2012 [15]

Support section Design A S355		Design C	Design C + Sinur
T Stiffeners (mm)	web	335x15	330x15
	flange	435x25	350x20
Flat stiffeners (mm)		---	250x35
Intermediate transverse stiffeners weight (ton)		15.4	10.3
structural steel weight ratio (kg/m^2)		9.0	6.0

1.2.4 Flange induced buckling

When a girder is subjected to bending, the induced curvature (deformed shape of the girder) combined with the compression in the flange of area A_f and yielding stress f_{yf} leads to a vertical force applied to the web plane. These flange vertical deviation forces introduce vertical compressive stresses into the web that can induce its buckling. The web buckling phenomenon is modeled as a column buckling of a vertical web stripe, ignoring the vertical transverse stiffeners. Assuming several assumptions a simplified web slenderness limit is proposed in section 8 of EN 1993-1-5, to prevent flange induced buckling of the web of area $A_w = h_w t_w$:

$$\frac{h_w}{t_w} \leq k \frac{E}{f_{yf}} \sqrt{\frac{A_w}{A_f}} \qquad (1.4)$$

with $k = 0.55$ or 0.40 if elastic or plastic moment resistance is adopted. This criterion is not usually relevant for deck designs using S355 steel. However, when HSS S690 is adopted, the high deviation force given by $f_{yf} A_f$ together with high web slenderness, makes this conservative limit much more difficult to fulfil.

Therefore, the assumptions were reassessed:

- It is assumed in eq. (1.4) that two identical flanges (with area A_{f}) are entirely yielded when buckling occurs. However, for the case of a composite section with a concrete flange, the

substantial area and bending stiffness prevents a very localized buckling. The deviation force induced in the web is governed by the tensile force in the tension flange [16], with the actual installed stress σ_{Ed} at ULS, much lower than f_{yf} (as it was observed by ratios σ_{Ed}/f_{yf} on Table 1.1); the same occurs in the bottom compressed flange over the supports, where f_{yf} may also be substituted by σ_{Ed} at ULS;

- The I girder was originally considered symmetrical for calculating the radius of curvature in eq. (1.4); but composite decks have rarely symmetrical cross-sections, and the actual position of the neutral axis at ULS can be defined by h_i/h, being h_i the distance of the neutral axis to the flange where σ_{Ed} is considered, and h the height of the steel girder;
- Peak residual stresses of 0.5 f_{yf} in the flange due to web/flange welded joint are kept.

Eq. (1.4) can therefore be written using an additional coefficient β, by:

$$\frac{h_w}{t_w} \le k\frac{E}{\beta f_{yf}}\sqrt{\frac{A_w}{A_{fc}}} \qquad \text{with } \beta = \left[\frac{h\alpha}{3h_i}(\alpha+0.5)\right]^{0.5} \le 1 \qquad \text{and } \alpha = \sigma_{Ed}/f_{yf} \qquad (1.5)$$

Table 1.4 presents the assessment of flange induced buckling of the web at mid-span and support panels, when using S355 and HSS S690, using eq. (1.4) and (1.5) with k=0.55. For HSS, at span sections, this improvement confirms the web slenderness is still under the limit, even without considering the contributions of the transverse stiffeners, while at support sections it is verified by a small margin, but several stiffeners exist over the supports and nearby.

Table 1.4: Flange induced buckling of the webs at support and mid-span panels

	Design A - S355		Design B / C - S690	
Panel	Support	Mid-span	Support	Mid-span
$A_w = h_w \times t_w$ (mm^2)	3580x26	3715x18	3390x20	3425x15
$A_f = b_{f,eff} \times t_f$ (mm^2)	1500x120	1500x50	1230x70	1300x45 / 30
$\frac{h_w}{t_w} \le k\frac{E}{f_{yf}}\sqrt{\frac{A_w}{A_{fc}}}$	138<282 ✓	206<326 ✓	170 > 158 ×	228 > 157 ×
h_i/h	---	---	0.483	0.629
$\alpha = \sigma_{Ed}/f_{yf}$	---	---	0.88	0.65
$\beta = \left[\frac{h\alpha}{3h_i}(\alpha+0.5)\right]^{0.5}$	---	---	0.915	0.629
$\frac{h_w}{t_w} \le k\frac{E}{\beta f_{yf}}\sqrt{\frac{A_w}{A_{fc}}}$	---	---	170 < 173 ✓	228 < 250 ✓

WP 1.3: SLS analysis of HSS bridge (Design B)

1.3.1 Deflection

The maximum in service deflections for the frequent value of the highway live loads, and the limit $L/500$ imposed by SIA 260 [17] are resumed in Table 1.5. As usually occurs, this limitation is verified by far for highway bridges.

Table 1. 5: Deflection for frequent highway live loads and SIA 260 limit

Condition	Design A S355	Design B S690	Design C S690
$\delta(\psi_1 Q_{k1}) \le L/500 = 160$ mm	49 mm (= L/1632)	74 mm (= L/1081)	90 mm (= L/889)

1.3.2 In service stresses

Table 1.6 resumes the highest in service stress ratios obtained for the main girder. Due to the use of HSS, the ratios for Design B are lower that when using S355. In Design C, the additional reduction in the bottom flange thickness in the span sections implies higher stresses in service, which are close to Design A mid-span results.

Concrete C35/45 and reinforcement B500B stress ratios are also low, as often occurs in composite steel-concrete decks.

Table 1.6: Stress ratios in structural steel ($\sigma_{Ed,ser,max}/f_y$), concrete slab ($\sigma_{c,ser,max}/0.6\,f_{ck}$), and slab reinforcement ($\sigma_{rs,ser} \leq 0.8\,f_{sk}$)

	Design A S355		Design B S690		Design C S690	
Section	Support	Mid-span	Support	Mid-span	Support	Mid-span
Concrete slab / reinforcement	0.49	0.27	0.61	0.32	0.61	0.36
Top flange	0.71	0.35	0.59	0.26	0.59	0.27
Web	0.75	0.65	0.61	0.47	0.61	0.63
Bottom flange	0.73	0.68	0.53	0.48	0.53	0.64

1.3.3 Limitation of web breathing

Table 1.7 resumes the maximum webs slenderness obtained and the limit b/t to avoid fatigue problems due to web breathing. As usually occur, this limitation is verified in all designs.

Table 1.7: Limitation of web breathing in mid-span cross-sections

Condition	Design A S355	Design B S690	Design C S690
$b/t \leq 300$	206	228	229

WP 1.4: Fatigue in HSS bridge (Design B)

1.4.1 Fatigue assessment using FLM3

Fatigue assessment of steel girders is made according to the simplified approach proposed in the Eurocodes, adopting the Fatigue Load Model 3 (FLM3) and the damage equivalent factors. FLM3 defined in EN 1991-2 [8] is composed by four axles with a total weight of 480 kN. A second vehicle also with four axles and total weight of 144 kN, travels at a distance not less than 40 m. FLM3 is located at the centre of the lane corresponding to the real heavy traffic lane, and the internal forces envelopes in the main girders are directly evaluated by loading the correspondent influence lines.

For the definition of this model, the basic concept is to select a fatigue 'single vehicle' so that, assuming a conventional number of crossings of the bridge deck by this vehicle ($2\text{x}10^6$ per year for heavy vehicles at each slow lane for highways with 2 or more lanes per direction and high flow rates of lorries), and after a numerical adaptation with appropriate λ factors, it leads to the same damage as the real traffic during the intended lifetime of the bridge.

At each element under verification, the design value of the equivalent constant amplitude nominal stress ranges, resulting from the Load Model 3 crossing the bridge, is therefore compared to the corresponding detail category fatigue design value, as follows:

$$\gamma_{\mathrm{Ff}} \cdot \Delta\sigma_{\mathrm{E},2} \leq \frac{\Delta\sigma_c}{\gamma_{\mathrm{Mf}}} \rightarrow \gamma_{\mathrm{Mf}} \cdot \gamma_{\mathrm{Ff}} \cdot \Delta\sigma_{\mathrm{E},2} \leq \Delta\sigma_c = \mathrm{FAT} \tag{1.6}$$

being:

$\Delta\sigma_{E,2}$ equivalent constant amplitude stress range at 2x10^6 cycles;

$\Delta\sigma_c$ fatigue detail category (FAT), related to fatigue strength of the each detail at 2x10^6 cycles;

γ_{Mf} =1 partial factor for equivalent constant amplitude stress ranges;

γ_{Ff} partial factor for fatigue strength; for safe life γ_{Ff} = 1.35 - Table 3.1 of EN 1993-1-9 [18];

λ damage equivalent factor, depending on the traffic composition, bridge span and design life.

The equivalent constant stress ranges are obtained by Eq. (1.7) considering the most unfavourable design situation for each section. i.e. the main girder support section with the slab fully cracked, and span sections with the slab uncracked and composite short term properties:

$$\Delta\sigma_{E,2} = \lambda \left|\sigma_{FLM3,max} - \sigma_{FLM3,min}\right| \quad (1.7)$$

The damage equivalent factor is obtained from:

$$\lambda = \lambda_1 \times \lambda_2 \times \lambda_3 \times \lambda_4 \leq \lambda_{max} \quad (1.8)$$

Where λ_i factors are calculated according to EN 1993.2, 9.5.2 [19]:

- λ_1 is the factor for the damage effect of traffic and depends on the critical length of the influence line. In road bridges with continuous spans up to L=80 m, λ_1 may be taken as:
  - $\lambda_1 = 2.55 - 0.70\,\frac{L-10}{70} = 1.85$ for mid-span sections,
  - $\lambda_1 = 1.70 + 0.50\,\frac{L-30}{50} = 2.20$ for support sections.
- λ_2 depends on the traffic type and volume and is obtained by $\lambda_2 = \frac{Q_{m1}}{Q_0}\left(\frac{N_{obs}}{N_0}\right)^{1/5}$= 1.224 with
  - N_0 = 0.5x10^6 lorries per year and per slow lane;
  - Q_0 = 480 kN (for FLM3);
  - N_{obs} = 2.0x10^6 lorries per year and per slow lane;
  - $Q_{m1} = \left(\frac{\sum n_i Q_i^5}{\sum n_i}\right)^{1/5}$= 445 kN, i.e. the mean weight of the heavy traffic from FLM4 for long distance traffic [20].
- $\lambda_3 = \left(\frac{t_{Ld}}{100}\right)^{1/5}$= 1.0 for the design live of the bridge t_{Ld}=100 years.
- λ_4 accounts for the effect of heavy vehicles on the other lanes; for a double girder deck with a large distance between girders λ_4 = 1.0.

Therefore, the factor for the support and mid-span section are respectively $\lambda = 2.69 < \lambda_{max} = 2.70$ and $\lambda = 2.26 > \lambda_{max} = 2.00 \rightarrow \lambda = 2.00$.

1.4.2 Critical details and FAT categories

The fatigue strength corresponding to each relevant detail in the structural steel is presented in EN 1993-1-9 [18] for the most frequent situations as "detail categories". Fig. 1.9 presents the typical details for this bridge deck. The main critical details, the correspondent FAT categories and the stress ranges obtained are identified in Table 1.8. It was decided not to adopt cope holes in longitudinal butt welded joints between the web and the flanges. This detail would be a FAT 71, very difficult to verify when using HSS.

From the results presented in Table 1.8, the critical detail is the intermediate transverse stiffeners welded to the bottom flange. Therefore Design C adopted these welded joints treated, and according with the tests performed in WP2, the FAT increases considerable. Therefore, the following critical fatigue detail is at the bottom flange level is the FAT125, correspondent to the web to bottom flange longitudinal welded joint.

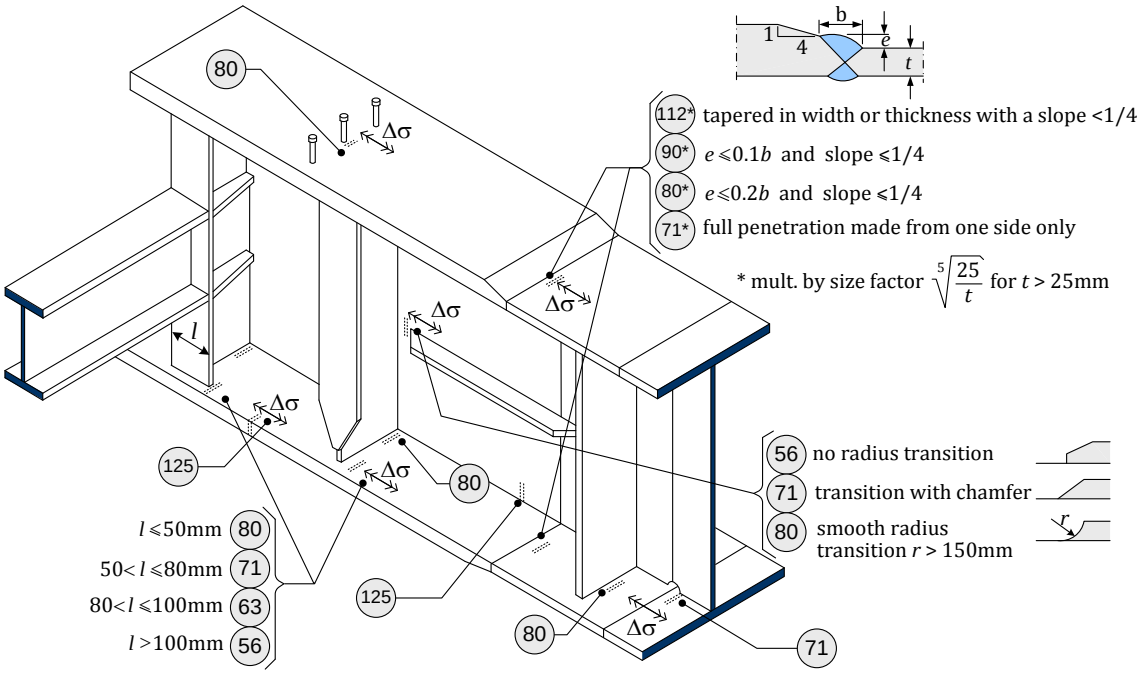

Figure 1.9: Typical FAT detail categories (Adapt. from [21])

Table 1.8: Fatigue assessment of the main girders welded joints using vehicle FLM3 and damage equivalent factors

Detail	FAT category	Design A	Design B	Design C
Top flange splices, with all welded joints ground flush to plate surface	FAT 112 x geometric size effect for plate thickness superior to 25 mm, given by $\sqrt[5]{\frac{25}{t_{ft}}}$	Support section $\gamma_{Mf}\,\Delta\sigma_{E,2}$ =22.6<85MPa Span section $\gamma_{Mf}\,\Delta\sigma_{E,2}$ =25.7<105MPa	Support section $\gamma_{Mf}\,\Delta\sigma_{E,2}$ =36.4<<102MPa Span section $\gamma_{Mf}\,\Delta\sigma_{E,2}$ = 28.9<<108MPa	Support section $\gamma_{Mf}\,\Delta\sigma_{E,2}$ =36.4<<102MPa Span section $\gamma_{Mf}\,\Delta\sigma_{E,2}$ =28.9<<108MPa
Bottom flange splices, with all welded joints ground flush to plate surface	FAT 112 x geometric size effect for plate thickness superior to 25 mm, given by $\sqrt[5]{\frac{25}{t_{ft}}}$	Support section $\gamma_{Mf}\,\Delta\sigma_{E,2}$ =25.5<82MPa Span section $\gamma_{Mf}\,\Delta\sigma_{E,2}$ =57.4<98MPa	Support section $\gamma_{Mf}\,\Delta\sigma_{E,2}$ = 49.8 < 91 MPa Span section $\gamma_{Mf}\,\Delta\sigma_{E,2}$ =77.8<100 MPa	Support section $\gamma_{Mf}\,\Delta\sigma_{E,2}$ = 49.8<91MPa Span section $\gamma_{Mf}\,\Delta\sigma_{E,2}$ =103<108MPa
Welded joint of transverse T stiffeners to the flange	FAT 56 for l > 100 mm	Support section $\gamma_{Mf}\,\Delta\sigma_{E,2}$ =22.6<56MPa	Support section $\gamma_{Mf}\,\Delta\sigma_{E,2}$ = 36.4 < 56 MPa	Support section $\gamma_{Mf}\,\Delta\sigma_{E,2}$ = 36.4<56MPa
Welded joint of support T stiffen to the bottom flange	**FAT 56** for l > 100 mm	Support section $\gamma_{Mf}\,\Delta\sigma_{E,2}$ =25.5<56MPa	Support section $\gamma_{Mf}\,\Delta\sigma_{E,2}$ = **49.8 < 56** MPa	Support section $\gamma_{Mf}\,\Delta\sigma_{E,2}$ = **49.8 < 56** MPa
Transverse stiffener welded joint to the bottom flange	**FAT 80** for l ≤ 50 mm	Span section $\gamma_{Mf}\,\Delta\sigma_{E,2}$ =**57.4<80**MPa	Span section $\gamma_{Mf}\,\Delta\sigma_{E,2}$ = **77.8 < 80** MPa	Span section $\gamma_{Mf}\,\Delta\sigma_{E,2}$ = **110.3<125**MPa with welded treatment
Shear studs welded on the top flange	FAT 80	Support section $_{Mf}\,\Delta\sigma_{E,2}$ =22.6<<80MPa	Support section $\gamma_{Mf}\,\Delta\sigma_{E,2}$ = 36.4 << 80 MPa	Support section $\gamma_{Mf}\,\Delta\sigma_{E,2}$ = 36.4 << 80 MPa
Cover plates on supports connecting the pot bearings to the girders bottom flanges	Welded detail **FAT40** for cover plate thickness smaller that the bottom flange with t>50mm; or FAT 90 for connection with preloaded high strength bolts	Support section $\gamma_{Mf}\,\Delta\sigma_{E,2}$ =25.5<40MPa or $\gamma_{Mf}\,\Delta\sigma_{E,2}$ =25.5<90MPa	Support section $\gamma_{Mf}\,\Delta\sigma_{E,2}$ = 49.8 > 40 MPa or $\gamma_{Mf}\,\Delta\sigma_{E,2}$ = 49.8 < 90 MPa	Support section $\gamma_{Mf}\,\Delta\sigma_{E,2}$ = 49.8 > 40 MPa or $\gamma_{Mf}\,\Delta\sigma_{E,2}$ = 49.8 < 90 MPa

As usually occurs in composite steel-concrete highway decks, the fatigue stress ranges are always verified at top flange level, since they are attached to the concrete slab. However fatigue assessment of bottom flange, which was not governing the Design A, is the major constraint for Designs B and C. In Design C, the weld treatment considered in the welded joint between the transverse stiffeners and the bottom flange of the main girders, has enabled higher stress ranges and thus a flange thickness reduction at span regions. Nevertheless, it is clear from Table 1.8 results that fatigue issues are a major constraint to the use plate girders design with HSS S690.

1.4.3 Brittle failure and welding

The allowable plate thickness that avoids direct calculation of brittle fracture was defined, depending on the steel grade, according to EN 1993-1-10 [22]. It was concluded that with the reference temperature T_{Ed} = −30°C, very restrictive maximum thickness are allowed, according to the simplified procedure proposed in EN 1993-1-10, namely when using the S355 steel grade.

In fact, S355 girders have plate thicknesses up to 120 mm, much higher that the limit of 92 mm obtained directly by Table 2.1 of EN 1993-1-10 [22] for steel grade NL and $\sigma_{Ed} = 0.63 f_y$. The use of HSS S690 somehow solves this issue. It allows reducing σ_{Ed} to $0.53 f_y$ and the plate thicknesses to 70 mm, almost in line with the 63 mm limit obtained by Table 2.1, if grade QL generally prescribed is replaced by QL1, for plate thickness higher than 50 mm. A more detailed verification, based on the fracture mechanics theory, shows that HSS S690 QL1 with 70 mm, at bottom flange-transverse stiffener welded joint, respects the brittle failure requirements for T_{Ed} = −30°C.

Full penetration welded joints requiring special welding procedures are identified in Fig. 1.10. The use of HSS thinner plates reduces the welding volumes of full penetration welding joints in about 50%, which is quite significant it terms of production benefits.

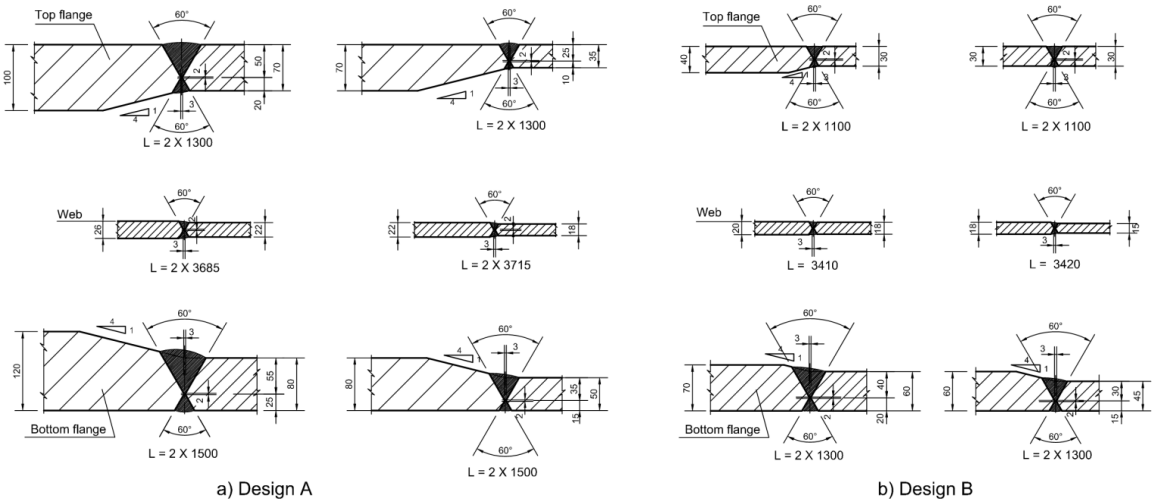

Figure 1.10: Typical plate girders full penetration welded joint details for: a) Design A – S355, and b) Design B – S690

WP 1.5: General guidelines covering main issues to be considered for HSS bridges

The comparative design was focused on a composite steel-concrete highway bridge composed by a continuous plate girder steel-concrete composite deck with 2x2 lanes and a total width of 21.5 m (total length of the bridge: 360 m, with 3 internal spans of 80 m and lateral spans of 60 m).

The design of two bridge decks with the Eurocodes, one using standard S355 NL and the other HSS S690 QL (or QL1 for plate thickness higher than 50 mm), confirmed benefits in using HSS.

Comparison between the three designs shows that the use of HSS enables a reduction of 25-30% of the steel weight compared to the standard plate girder deck in S355 NL. Table 1.9 presents the rations of steel weight for the three solutions.

Table 1.9: Comparative analysis – Structural steel average weight ratios (kg/m2)

Structural steel weight	Design A S355	Design B S690	Design C S690	Reduction A-B (%)	Reduction B-C (%)	Reduction A-C (%)
Total ratio of steel (kg/m^2)	219	165	149	-25%	-10%	-32%
Main girder sections (kg/m^2)	186	123	114	-34%	-8%	-39%
Cross-girders+stiffeners (kg/m^2)	33	42	35	+27%	-17%	+6%

For design A, the average weight of the structural steel is 219 kg/m^2, of which 186 kg/m^2 are from flanges and webs of the main girders, and 33 kg/m^2 are from cross-girders and stiffeners.

Design B, allows for and important reduction of structural steel to 165 kg/m^2, of which 123 kg/m^2 are from flanges and web of the main girders, and 42 kg/m^2 are from cross-girders and stiffeners, that have been increased with respect the Design A. By comparing these values with Design A (with S355), a 25% reduction can be obtained in structural steel in the deck and a 34% reduction is found on main girders weight only.

Design C, profits from the welded treatments of the welded joints at the bottom flange level, and a better design of the transverse and longitudinal stiffeners. In consequence, a further reduction of the average weight of the structural steel is attained to 149 kg/m^2, of which 114 kg/m^2 are from flanges and webs of the main girders, and 35 kg/m^2 are from cross-girders and stiffeners. By comparing the steel weight obtained with Design B and Design C, a further reduction of 10% is obtained, 8% in the main girders steel weight and 17% in the cross-girders and stiffeners.

Finally, the comparative design points out further important aspects:

- The deck can be slender using HSS S690;
- HSS allows the use of thinner plates but it is more susceptible to local buckling phenomena;
- The use of closed longitudinal stiffeners is efficient to reduce web local buckling;
- Brittle fracture is less dimensioning when using HSS;
- A substantial cut on the volume of full penetration welding is obtained by using thinner plates;
- Girders in HSS are much more prone to fatigue, that proves to be the main issue of the design together with the buckling phenomena;
- Fatigue detail assessment of the twin plate girder deck shown the critical steel detail is the FAT80 occurring at the welded joints between the bottom flange and the transverse stiffeners;
- The use of welded treatments of the critical welded joints increases this FAT category and allows for an additional reduction of steel at the bottom flanges of spans.

WP 2: Fatigue study

This fatigue study is based on an important experimental campaign testing small samples of 100 mm to beams of 4 m long. The welded joints and their post treatment is an important focus of this research. The fatigue analysis is performed with the numerical simulations of the cyclic loadings using the F.E. code "Lagamine" [23] and the determination of the number of cycles at the crack initiation by the use of a post-processor: "PostLag_Dam" [24]. Both codes have been developed at the University of Liège (Materials and Solid Mechanics MSM /Research Unit UEE/Engineering school). These softwares are under the responsibility of A.M. Habraken and L. Duchêne, leaders of MSM team (http://www.uee.uliege.be/cms/c_2383455/en/lagamine).

WP 2.1: Experimental study on material specimens

A testing campaign is performed to describe the mechanical and fatigue behaviours of the Base Material S690QL (BM), two representative Heat Affected Zones (HAZ1 and HAZ2) related to welded attachments (stiffeners-plates) and the Weld Metal (WM).

The samples of BM are extracted out of 6 or 15 mm thick plates depending on their shape.

The descriptions of the samples productions of HAZ1, HAZ2 and WM are detailed in WP 4.1.

The applied thermal history on samples HAZ1 and HAZ2 is representative of HAZ appearing during transversal stiffeners welding on 25 mm and 40 mm plates respectively. The micro hardness and the grain size have been examined to define representative cooling rates and to produce samples able to reproduce the behaviour of the zones affected by the welding process. One goal of these two HAZ sample types is to check whether the plate thickness has an impact on the HAZ behaviour.

The generation of the samples for the weld characterisation is explained in Fig. 2.1, where a groove is cut on a bulk sample of BM and is filled with WM. Then, samples are cut out the upper layer of the bulk sample with the WM localised in the central part. The final shape of these samples is adapted to analyse the behaviour of the WM.

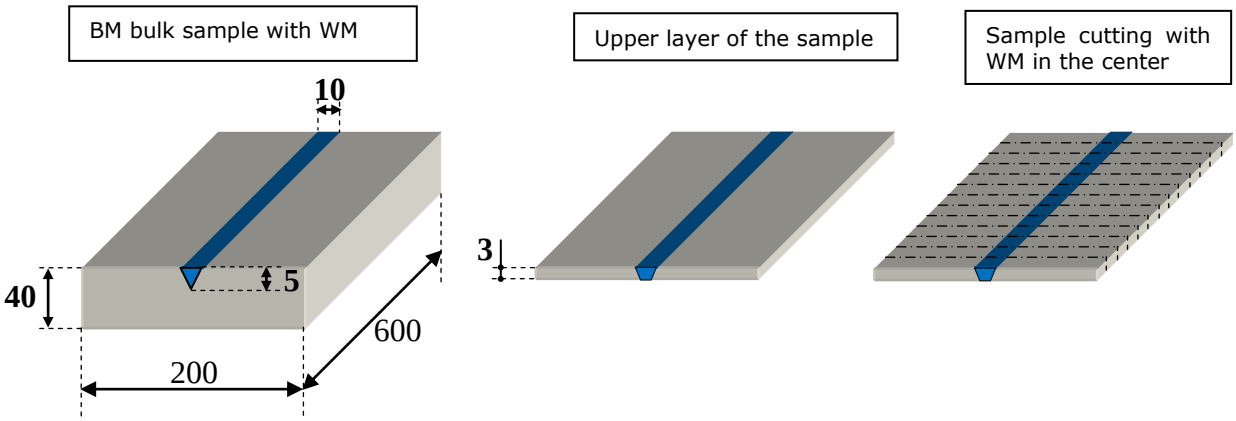

Figure 2.1: Method used to produce samples to test the behaviour of the weld metal

Static mechanical experimental procedure

Tensile tests in 1 or 3 directions, large tensile tests, shear and reverse shear (Bauschinger) tests (Fig. 2.2) are performed to study the mechanical behaviour of each material: the yield locus size and its hardening behaviour. Each test is repeated several times to verify its reproducibility and average curves are computed.

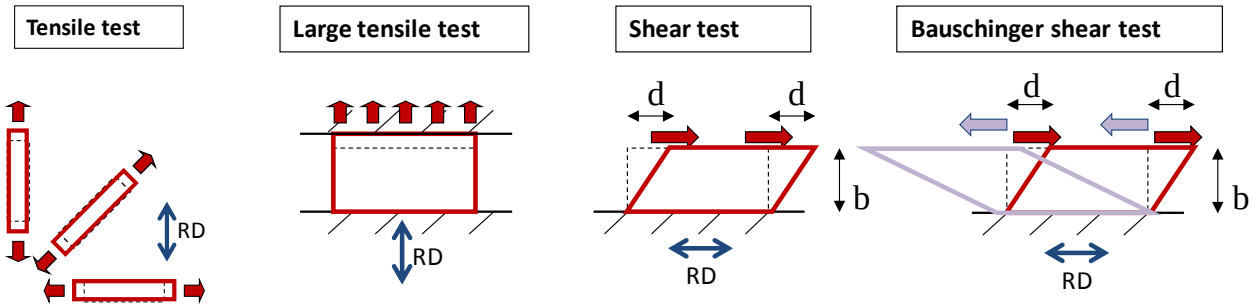

Figure 2.2: Description of the mechanical tests performed to describe the material behaviour of S690QL, HAZ1, HAZ2 or WM

The samples used for the tensile tests are classical (EN 10002-1). The ones used for the large tensile tests and the simple shear or reverse shear tests have a specific shape shown in Fig. 2.3. A speckle pattern is applied on the central surface of the samples and four 3D digital cameras combined to a numerical post processing are used to verify the homogeneity of the strain field in the central part of the pieces and to measure its value during the whole test. This method induces

a specific sample geometry. The experimental procedure, using the bi-axial machine developed by Flores, 2005 [25], presents the advantage of directly giving the stress-strain curves.

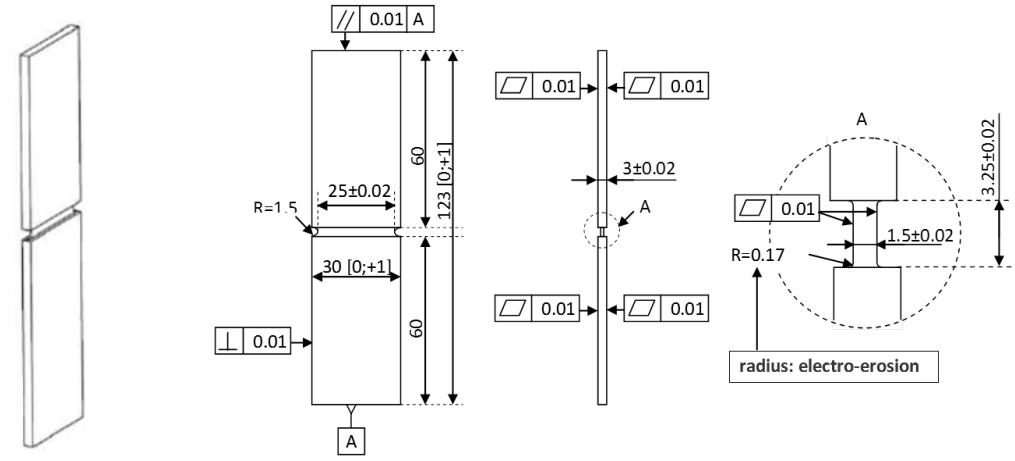

Figure 2.3: Description of the samples for the large tensile (WM), shear and reverse shear tests (S690QL, HAZ1, HAZ2 and WM)

Fatigue experimental procedure

A vibrophore is used for the fatigue tests on all the small size samples, with a frequency in the range [100-150] Hz depending on the load of the machine.

The frequency effect on fatigue tests was already studied by several authors, namely by Massonet [26] who observed an increase of 5% of the fatigue limit at zero mean stress on carbon steel at 170 Hz compared to tests at low frequency. Chang et al. (2009) [27] showed the link between the yield stress, the ultimate tensile strain, the elongation with the strain rate on SM570-TMC steel. Lamarche (2009) [28] defined a formula to link the static and dynamic yield stresses of steel. This link has been deeply studied and calibrated in the RFCS project Hitubes (2012) [29] on HSS, TS590 steel which has the same level of yield stress as our S690QL steel. Their formula has been adapted and used to adjust the fatigue tests at high frequency and to define the equivalent stress range at 1 Hz: $\Delta\sigma_{1Hz}$ (Eq. 2.1).

$$\Delta\sigma_{1Hz} = \frac{1+c\,(\dot{\varepsilon}_{1Hz})^n}{1+c\,(\dot{\varepsilon}_{xHz})^n}.\Delta\sigma_{xHz} \quad \text{with c= 0.085; n= 0.19} \qquad (2.1)$$

For all the experiments, the engineering stress formulation is used, $\sigma_{eng} = F/A_0$ (axial load, F divided by the original section area, A_0) with, for the notched specimens, the section area measured at the notch.

Each test is performed up to rupture at constant stress range $\Delta\sigma = \sigma_{max} - \sigma_{min}$ and stress ratio: $R = {}^{\sigma_{min}}/_{\sigma_{max}}$.

Examples of geometries of smooth and notched samples are shown in Fig. 2.4 to Fig. 2.5.

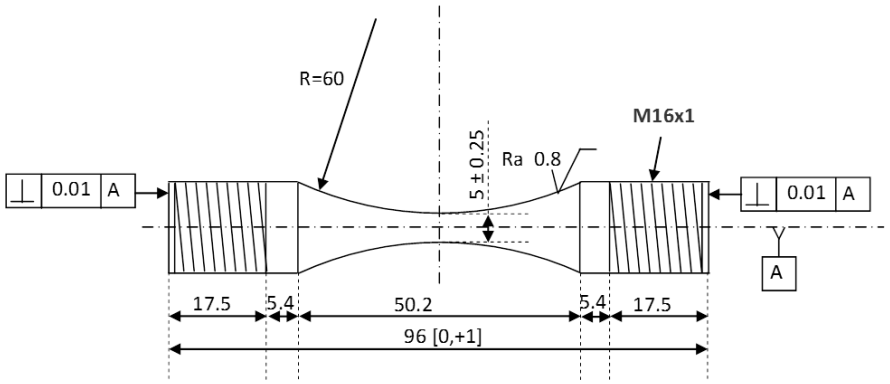

Figure 2.4: Smooth sample of BM (S690QL)

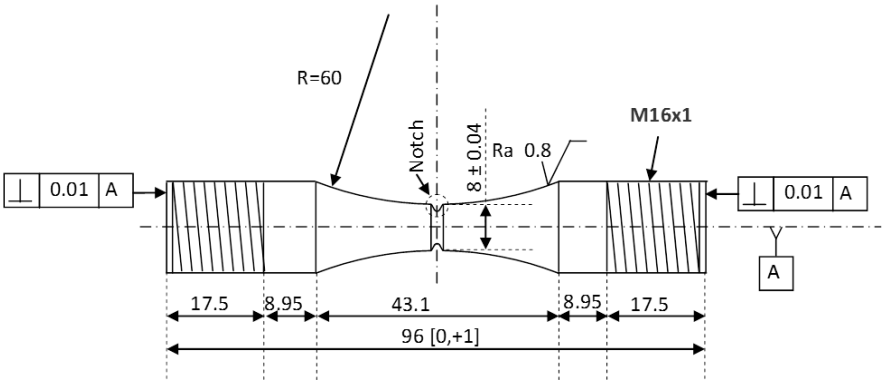

Figure 2.5: Sample of BM (S690QL) with notch

WP 2.2: Model identification (static mechanical and fatigue behaviour)

Static mechanical model

For the uniaxial and large tensile tests, the true stress/true strain formulation is required for any use in the F.E (Finite Element) code: "Lagamine" [23] software used in this study (Eqs. 2.2 and 2.3).

$$\sigma_{i,true} = F_i / A_i \tag{2.2}$$

$$\varepsilon_{i,true} = \ln(L_i / L_0) \tag{2.3}$$

The elastic range is described by Hooke's law.

The Hill 48 law (Eq. 2.4) is used for the plastic part where σ_{ij} are the stress tensor σ components and where σ_F is the yield stress.

$$F_{HILL}(\underline{\sigma}) = \frac{1}{2}\left[H(\sigma_{xx} - \sigma_{yy})^2 + G(\sigma_{xx} - \sigma_{zz})^2 + F(\sigma_{yy} - \sigma_{zz})^2 + 2N(\sigma_{xy}{}^2 + \sigma_{xz}{}^2 + \sigma_{yz}{}^2)\right] - \sigma_F^2 = 0 \tag{2.4}$$

The isotropic hardening is described by the Voce formulation: (Eq. 2.5)

$$\sigma_F = \sigma_0 + K(1 - exp(-n.\varepsilon^{pl})) \tag{2.5}$$

where σ_0 or ε_0, K and n are the material parameters and ε_{pl} is the equivalent plastic strain.

When a mixed isotropic-kinematic hardening is used, the stress tensor $\underline{\sigma}$ (in Eq. 2.4) is replaced by $(\underline{\sigma} - \underline{X})$, where $\underline{X}$ is the back-stress tensor. The evolution of the back-stress is described by the Armstrong-Frederick formulation (Eq. 2.6).

$$\dot{\underline{X}} = C_X\,(X_{sat}\,\underline{\dot{\varepsilon}^{pl}} - \dot{\bar{\varepsilon}}^{pl}.\underline{X}) \tag{2.6}$$

where C_X is the back stress saturation rate and X_{sat} is the initial back stress saturation value.

The inverse method "Optim" coupled with the F.E. code "Lagamine" [23] both developed at ULiège are used to identify the material data.

A set of tests, sensitive to the data to adjust and representative of the material stress state of the process studied, is selected. We have, on one side, the experimental tests and, on the other side, the F.E simulations of the tests and their numerical results which are compared to the experimental curves. Then, the Levenberg Marquart minimization algorithm is used to iteratively adjust the material data until the numerical simulations are able to predict the experimental results with a sufficient accuracy.

Static mechanical data

The following tables 2.1 and 2.2 summarize all the mechanical data for each material with Hooke's, Hill's, Voce's and Armstrong-Frederick's laws and with identical data for HAZ1 and HAZ2 since no difference was observed.

Fig. 2.6, left and right, shows the adequacy between the experiments and the numerical simulations of the tensile and shear tests and also the high tensile strength reached by HAZ. For

the WM, no experimental tensile curve is shown because it was replaced by large tensile tests for geometrical reasons.

In Table 2.2, the distinction is made between the ultimate engineering and true stresses.

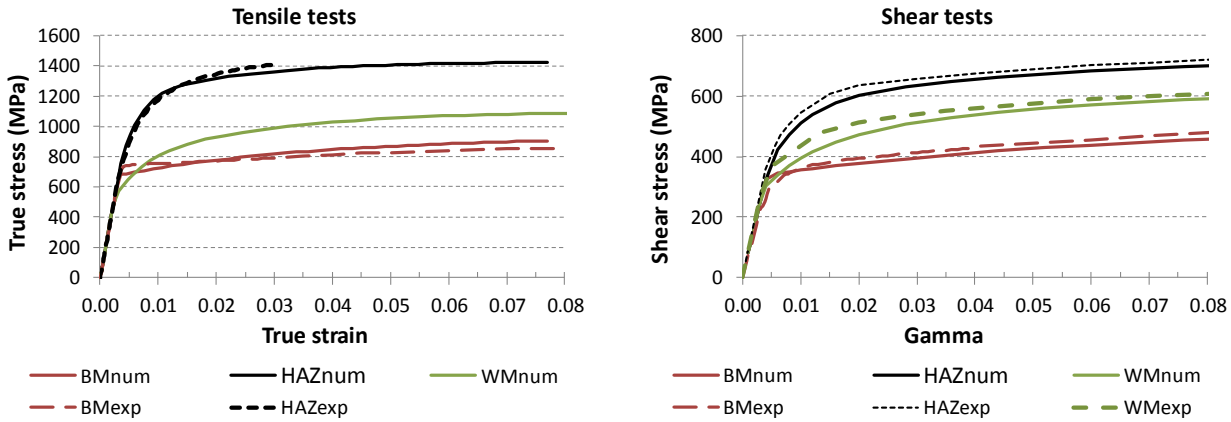

Figure 2.6: Comparison of numerical - experimental tensile & shear tests on BM, HAZ and WM

Table 2.1: Summary of material data chosen for the numerical simulations (unities: MPa, sec)

Data for Hooke, Hill, Voce and Armstrong-Frederick laws (units: MPa, s)											
	Elast. data Hooke		Yield locus Hill				Isotropic harden. Voce			Kinem. harden. Arm.-Fred.	
Material	E	v	F	G	H	N=L=M	K	σ_0	n	C_X	X_{sat}
BM	210 116	0.3	1	1	1	3.9	0	674	0	31.9	167
HAZ1, HAZ2	210 000	0.3	1	1	1	4.45	371	827	511	52.5	152
WM	210 000	0.3	1	1	1	3.2	241	531	285	42.6	218

Table 2.2: Summary of ultimate tensile strength (MPa)

	$\sigma_{u.eng}$	$\sigma_{u.true}$
BM	838	905
HAZ1, HAZ2	1338	1424
WM	1008	1101

Fatigue model

The multiaxial Lemaitre and Chaboche Fatigue Model (LCFM) [30] is used to describe the fatigue behaviour of the materials and to predict the number of cycle at rupture (N_f) for any stress ratio R, stress range Δσ, uniaxial stress state or tensorial stress state characterised by σ_{Hm} and σ_{eqmax} (Eq. 2.7 to Eq. 2.12). D is the damage scalar (0 for sound material, 1 for rupture) and N is the number of cycles.

The material parameters are: the ultimate tensile strength σ_u (see Deliverable D2.1), the fatigue limit at null mean stress σ_{l0}, b, β, a and M_0 with b= $1/\sigma_u$ and a in the range [0; 1].

$$\frac{\partial D}{\partial N} = \begin{cases} 0 & \text{if } f_D < 0 \\ \left[1-(1-D)^{\beta+1}\right]^a \left(\frac{A_{II}}{M_0\,(1-3.b.\sigma_{Hm}).(1-D)}\right)^{\beta} & \text{if } f_D \geq 0 \end{cases} \quad (2.7)$$

$$f_D = A_{II} - A_{II}^* \quad (2.8)$$

$$A_{II} = \frac{1}{2}\sqrt{\frac{3}{2}\left(\hat{\sigma}_{ijmax} - \hat{\sigma}_{ijmin}\right)\left(\hat{\sigma}_{ijmax} - \hat{\sigma}_{ijmin}\right)} \text{ with } \hat{\sigma}_{ij} = \sigma_{ij} - \sum_k \frac{1}{3}\sigma_{kk} \quad (2.9)$$

$$A_{II}^{*} = \sigma_{l0}\,(1 - 3.b.\sigma_{Hm}) \text{ (Sines' criterion)} \quad (2.10)$$

$$a = 1 - a\left\langle \frac{A_{II} - A_{II}^{*}}{\sigma_u - \sigma_{eqmax}} \right\rangle \quad (2.11)$$

$$\sigma_{Hm} = \frac{1}{3}\left[\frac{1}{T}\int_T \mathrm{Tr}\left(\underline{\underline{\sigma}}(t)\right)dt\right] \quad (2.12)$$

where f_D is the damage yield locus, A_{II} is the second invariant of the amplitude of the deviator $\underline{\underline{\hat{\sigma}}}$ of the stress tensor, A_{II}^{*} is the fatigue limit, $\hat{\sigma}_{ijmax}$ and $\hat{\sigma}_{ijmin}$ are the maximum and minimum components of the deviatoric stress, σ_{Hm} is the mean hydrostatic stress, σ_{eqmax} is the maximum Von Mises' stress per cycle and $\langle x \rangle = x$ if $x > 0$ else $= 0$.

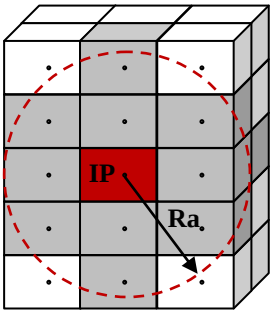

Figure 2.7: Volume averaged stress gradient method: elements with their integration point inside a sphere of radius Ra

LCFM is combined with the volume averaged stress gradient method and becomes **G**LCFM when required. In this case, for each element, the variables computed at its integration point $\chi_{ip,i}$ are replaced by an average value $\overline{\chi_{ip}}$ computed from the surrounding elements having their integration point inside a sphere of radius Ra and its centre at the integration point (Eq. 2.13 and Fig. 2.7).

$$\overline{\chi_{ip}} = \frac{\sum_{i=1}^{Nelem} \chi_{ip,i}.V_i}{\sum_{i=1}^{Nelem} V_i} \text{ with } \chi_{ip} = \{A_{II}, \sigma_{eqmax}, \sigma_{Hm}\} \quad (2.13)$$

Fatigue data

Table 2.3 summarises the optimised data of GLCFM for small samples. A single set of material data is defined for HAZ1 and HAZ2 since the fatigue endurance is similar for both.

Table 2. 3: Material data of GLCFM for small samples of BM (S690QL), HAZ, WM

Material	σ_U (Mpa)	σ_{l0} (Mpa)	b	β	a	M0	Ra (mm)	$a^*(M0^{-\beta})$
BM	905.0	580.0	1.10 E-03	0.17	1	5.385 E+30	0.06	5.966E-06
HAZ1, HAZ2	1424.0	428.4	7.02E-04	2.094	1	4.410E+05	0.06	1.516E-12
WM	1101.0	319.4	9.08E-04	0.161	1	7.245E+32	0.00	5.182E-06

WP 2.3: Fatigue experimental study on plates with welded transversal stiffeners

Fatigue experimental procedure

Here, the fatigue behaviour of medium-sized pieces, called "small case samples" (Fig. 2.8, left), intermediate cases between small samples used for the first fatigue characterisation and bridge connections, are studied. Simple plates and plates with welded stiffeners with or without post-treatment applied to the weld toes are tested in fatigue (Fig. 2.8, right).

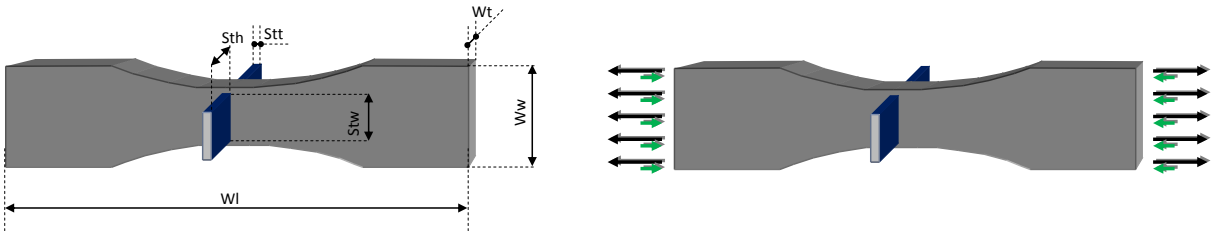

Figure 2.8: Geometries of the small case samples with Ww= 235 mm, Wl= 1070 mm, Sth= 40mm (left) and loading (right)

Several effects affecting the fatigue life and present in complex pieces are studied. In the first step, the comparison between small samples and simple plates shows the cumulative effects of the size, the surface roughness and the residual stresses due to the plate production. Here, the porosity hasn't any effect since no significant difference was measured on the samples. In the second step, the testing on the welded plates shows the effects of the stress concentration at the weld toes, the welding process modifying both the residual stress distribution and the material resistance at weld toes (heat affected zone). Finally, the effects of the post-treatment, PIT or TIG remelting, applied at the weld toes of some specimens is analysed. Here, no significant effect of the geometry was observed. Table 2.4 summarises all the cases tested. The results are shown in Fig. 2 and listed in Deliverable D2.2. A 2500 KN Schenck press has been used for all the experiments.

Table 2.4: Parameters of the small case tests and effects studied - sizes in Annex 1, Table A.1.1.

Case	Post-treatment	Plate thick. (mm)	Stiffen. thick. (mm)	Stiffen. length (mm)	Dist. to edge	Stress ratio R	Effect
		Wt	**Stt**	**Stw**			
Plate	No weld	25	-	-	-	0.1	No weld, no post-treat. // A
A	PIT	25	15	60	✓	0.1,0.3,0.5	**Reference case, 3R**
B	PIT	15	15	60	✓	0.1	Thickness ↘ // A
E	PIT	25	15	60	no	0.1	No edges dist. // A
H	PIT	40	15	60	no	0.1	Plate thickness ↗ // E
C	TIG rem.	15	15	60	✓	0.1	TIG rem. effect // B
D	TIG rem.	25	15	60	✓	0.1	TIG rem. effect // A
F	TIG rem.	25	15	40	✓	0.1	Stiffeners length ↘ // D
G	TIG rem.	15	6	60	✓	0.1	Stiffeners thickness ↘ // C
I	Nothing	15	15	60	✓	0.1	No post-treatment // B

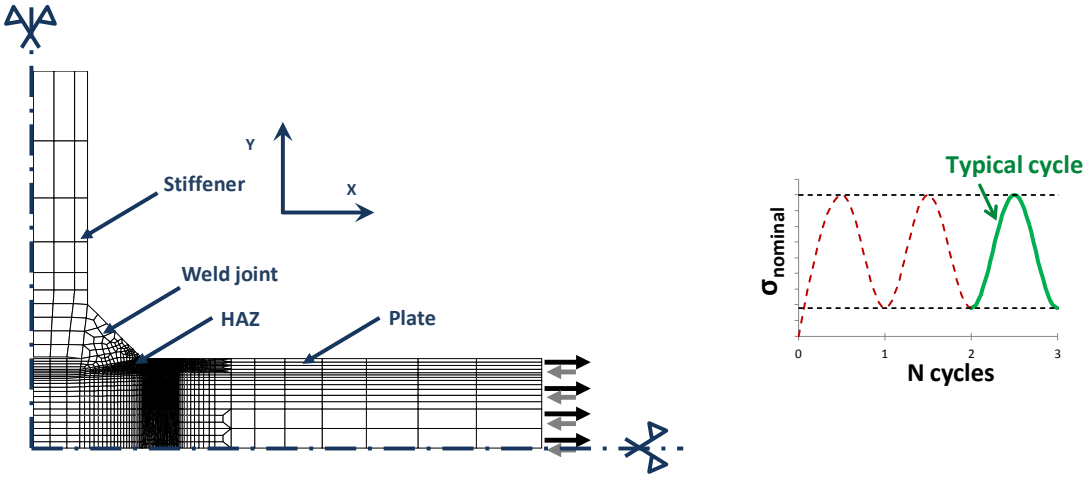

Figure 2.9: Optimised mesh used for F.E. simulations with very small mesh size at the weld toe (0.1 mm), position of the load and typical cycle (the third one).

The mesh of the model used for the numerical simulations of typical cycles (Fig. 2.9) and used to compute the numbers of cycles at the crack initiation for several stress ranges, has been optimised. The elements size is very small at the weld toe (0.1 mm) to avoid mesh dependent results and to take into account material changes (BM,HAZ,WM) and residual stresses. The load is applied on the web, in X direction and the stress ratio, R= $\sigma_{min}/\sigma_{max}$, is constant for all the simulations: 0.1.

The residual stress fields were measured for two reasons: i) a better understanding of the efficiency of the post-treatment methods, ii) their implementation in the numerical models. They were measured by X-ray and also by neutron diffraction on welded plates, with and without post-treatment for three different geometries, two positions (at mid-weld MW, at weld-edge WE), in longitudinal and transversal directions (respectively RD and TD), from the weld toe, up to a depth of 3 mm and up to a distance of 13 mm (Fig. 2.10 and Fig. 2.11). In D2.2, a complete description of cases A to I (Table 2.4) and measured stress fields can be found. The stress profiles at the weld toe for the different cases (see Fig. 2.12, left) show the high beneficial effect of the PIT post-treatment (cases A, B, E) by comparison with the other cases: without post-treatment (I) and with the Tig remelting post-treatment (C, D).

The residual stress profile from the case E is applied on the developed FE model at the initial state since they have the same geometry.

A post-processor is used to compute the number of fatigue cycles when the beginning of rupture appears for several stress ranges with Lemaitre and Chaboche fatigue model LCFM [30] combined with the volume averaged stress gradient method GLCFM (see model in WP2.2).

An adjustment is applied on the fatigue data of the small samples to determine the fatigue data of the plates (Table 2.5), taking into account of the size effect and able to correctly predict the crack initiation of all the experiments (Fig. 2.12, right).

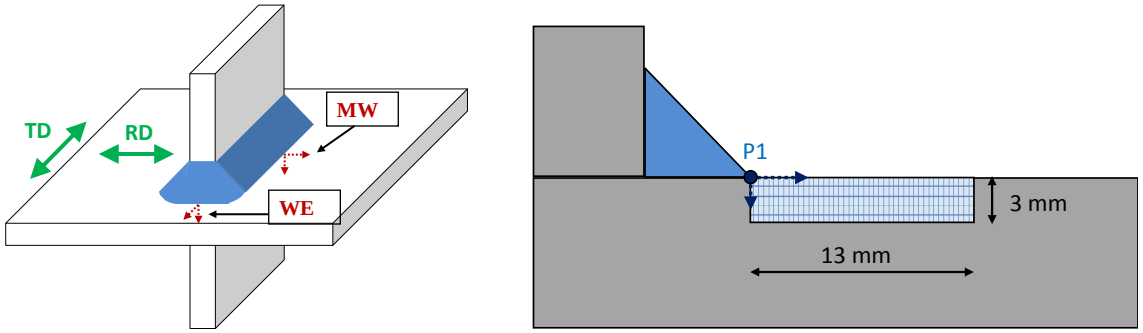

Figure 2.10: Specimen used to measure the residual stress profile, directions and location of the measurement section (left), measurement section: up to a depth of 3 mm and to a distance of 13 mm to the weld toe (right)

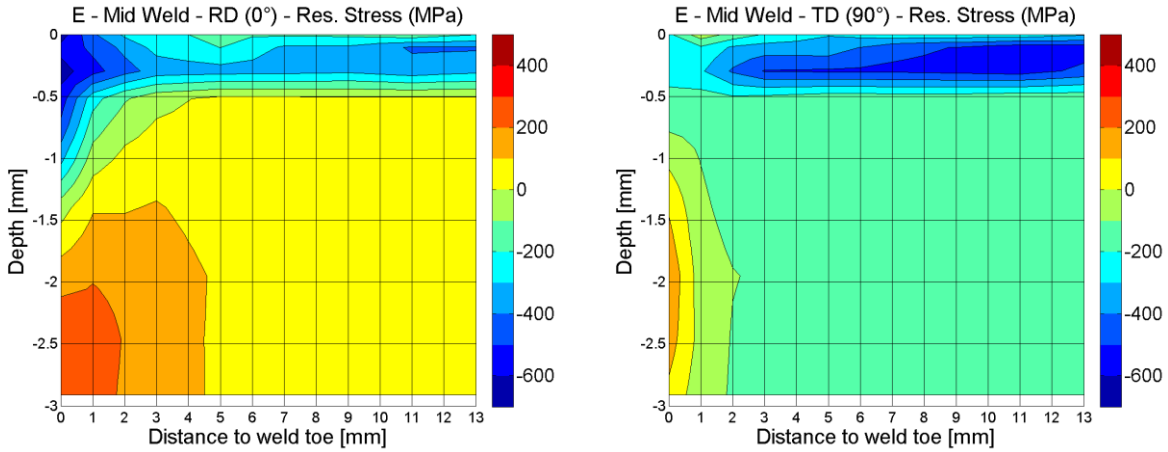

Figure 2.11: Residual stress by X-ray method, on the welded, PIT post-treated specimen, at mid-welded joint: in RD (left), in TD (right)

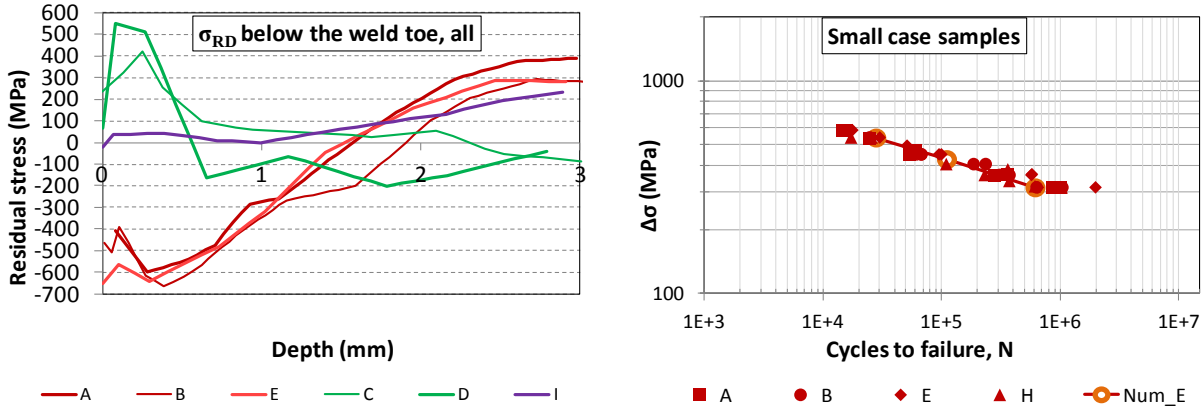

Figure 2.12: Comparison of residual stress distribution by X-ray method, in rolling direction and at weld toe and mid welded joint: with PIT post-treatment (A, B, E), with TIG remelting post-treatment (C, D) and without post-treatment (I) (left) and fatigue crack initiation from the experiments on PIT treated samples (A, B, E, H) and numerical prediction (Num_E) (right)

Table 2.5: Material data of GLCFM for fatigue analysis of welded specimens (small case samples)

Material	σ_U (Mpa)	σ_{l0} (Mpa)	b	β	a	M0	Ra (mm)	$a*(M0^{-\beta})$
BM-plate	905.0	203.0	1.10 E-03	0.17	1	5.385 E+30	0.06	5.966E-06
HAZ-plate	1424.0	149.9	7.02E-04	2.094	1	4.410E+05	0.06	1.516E-12

WP 2.4.a: Experimental tests on beams with transverse stiffeners

The performance of small scale tests (around 1 m long, see WP2.2 and WP2.3) is easier in operation, faster and therefore much more economical than fatigue beam tests. So time-consuming fatigue test series have been tested via "small" scale series. Nonetheless the small case test campaign cannot totally reflect the effect of the so-called size effect that reduces the fatigue resistance of the real bridge structures (multiple spans of 80 m long for instance). This size effect results of mainly three different aspects and is also known as plate thickness or component effect.

The size effect for notched and smoothened fatigue details has already been investigated extensively regarding different aspects e.g. for differing plate thicknesses for welded attachments by Gurney,1991 [31] and regarding welded girders by Helms et al., 1989 [32] for the untreated, as-welded state.

Dürr, 2006 [33] and Kuhlmann et al., 2006 [34] have already investigated the size effect between small scale tests and beam tests using HFMI (High Frequency Mechanical Impact) treatment on high strength steel S690 with welded transverse attachments. The weld toes of the transverse stiffener were improved by the HFMI-method UIT (Ultrasonic Impact Treatment). The conducted stress ratios were R = 0.5 and R = -1.0, whereas the girders with R = -1.0 led to no further assumptions due to a lower amount of results, for R = 0.5 the relation between girder and small scale tests could be quantified to be around 85 %, see Eq. 2.14. Table 2.6 compares the results of the conducted beam tests and the small case tests with R = 0.5 and N= number of tests.

Table 2.6: Comparison of former beam test results from Dürr, 2006 [33]

Literature	Steel grade	R	N	Type	m	Δσc, 50 % (MPa)	Δσc (MPa)
(Dürr, 2006)	S690	0.5	7	(Beam) Girder	5	151	121
(Dürr, 2006)	S690	0.5	14	Small scale	5	178	136

$$\frac{\Delta\sigma_{c,50\%}\,(Girder, UIT, R=0.5)}{\Delta\sigma_{c,50\%}\,(QS1, UIT, R=0.5)} = \frac{151\ N/mm^2}{178\ N/mm^2} = 0.85 \qquad (2.14)$$

Thus, according to Dürr, 2006 [33] the reduction considering the size effects using HFMI by applying UIT on the fillet welds connecting the transverse stiffener to the flange is around 15%. Since the beam tests of Dürr have been conducted under a stress ratio R = 0.5 and R = -1.0, the behaviour of the improved fatigue resistance with a variation of the mean stress ratio to R = 0.1 is still not known for the welded transverse attachment out of high strength steels.

Consequently, one aim of the OptiBri-project was to identify the reduction of PIT-improved fillet welded joints of transverse stiffeners on large scale structures of high strength steels for R = 0.1. Therefore a huge test program consisting of material tests, small scale tests with differing plate thicknesses and conditions and beam tests has been generated, see previous chapters. Within seven cyclic 4-point bending beam tests this reduction due to size effects should be identified comparing the fatigue resistances of the small specimen series tested in WP2.3 to those beam tests.

The test program consists of seven welded girder tests in sum with a welded transverse attachment in the mid span of the girder. In order to have a reference value for the unimproved as-welded state, there was one girder test planned without post-weld treatment. Six of the seven beam tests were treated with HFMI to show the improvement factor under the influence of the size effect, see Table 2.7. The fabrication and the welding procedure of the beam specimens were accompanied by the project partner BWI at the end of 2015 and are documented in Deliverable D4.3.

Table 2.7: Test program of beam tests

State	Number [-]	Stress ratio R [-]	Material
As-welded (AW)	1	0.1	S690
PIT-treated (PIT)	6	0.1	S690

Post-weld treatment

The tests have been PIT-treated by the PITec Company in Stuttgart. Therefore the same treatment parameters as for the small scale series SC_A have been used (see D 2.2). The treatment was conducted on both, the tensioned and compressed weld toes of the transverse stiffener so that knowledge of the improvement of the compressed flange weld toes could also be gained. Fig. 2.13 shows which weld toes had been treated in case of the tensioned flange.

During the testing process cracks appeared also on the longitudinal welded joint as a critical detail when the transverse attachment has been improved. So that in consequence the PIT treatment was also applied on the weld toes of the longitudinal welded joint at the tensioned flange for beam test T3. Within further tests, also cracks on the upper compressed longitudinal welded joint appeared, so that for the further test beams, the PIT-treatment was done on both weld toes of longitudinal welds, namely for the beam tests T4, T6 and T7.

Figure 2.13: Position of treated weld toes

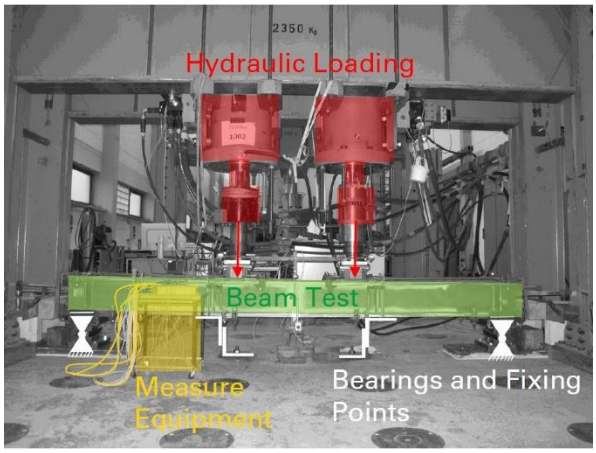

Figure 2.14: Test setup of beam tests

The 4-point-bending test setup mainly consisted of a test portal with two test cylinders, which were controlled servo-hydraulically with a maximum cyclic load capacity of 800 kN. The two supports were executed as pivot bearing in order to avoid constraints in the longitudinal direction of the beam. Due to the high applied loadings special bronze reinforced PTFE material was used inside the supports to reach a high durability in combination with a low friction. In the longitudinal direction there have been applied fixing points to avoid a slipping in the longitudinal direction of the beam in forms of angle sections with some bearing gap. Fig. 2.14 shows the test setup with its equipment.

Test results of beam tests

The expected failure mode of the beam test was supposed to be the weld toe failure at the PIT-treated weld at the transverse stiffener on the bottom flange. However during the testing procedure other cracks appeared. Therefore the failure modes had to be identified by visual inspection of the failed tests. General information on crack surface inspection and detailed information and description of each crack surface of the girder can be found in D2.3.

Table 2.8: Results of tested beams

Name	State	Location of PIT-treatment	Δσ [N/mm²] flange upper side	Δσ [N/mm²] flange bottom side	N [-]	Crack location
T1	PIT	Stiffener	315	381	161.357	Bottom Flange BM
T2	PIT	Stiffener	200	242	620.740	Bottom Flange FP
T3	PIT	Stiffener, longitudinal bottom	150	182	2.063.240	Upper Flange BM
T4	PIT	Stiffener, longitudinal both	200	242	940.020	Bottom Flange FP
T5	aw		200		429.250	Stiffener WT
T6	PIT	Stiffener, longitudinal both	315		242.468	Stiffener WT
T7	PIT	Stiffener, longitudinal both	200	242	1.169.436	Bottom Flange BM
T1	PIT	Stiffener	315	381	161.357	Bottom Flange BM

BM = base material; FP = fixing point; WT = Weld toe, N= number of cycles at failure (crack of a length minimum over half flange width).

An overview of the test results can be taken from Table 2.8. In addition to the overview in Table 2.8 which gives the crack position by name, Fig. A2.1 in Annex 2 shows an overview of the crack position for each beam test in the longitudinal view. Figs. A2.2 to A2.7 in Annex 2 show the corresponding crack surfaces of all beam tests. According to this analysis, the three main failure modes were defined.

Failure Mode 1: Weld toe failure at the weld connecting the transverse stiffener to the bottom flange

Failure Mode 2: Crossing crack over the longitudinal fillet weld (bottom or upper)

Failure Mode 3: Crossing crack over the longitudinal fillet weld induced from bottom flange side by fixing point.

Each of these failure modes is represented by photos in the following Table 2.9.

Table 2.9: Failure modes and corresponding signs in Figs. 2.15 , 2.16, 2.17.

Sign	Failure mode description	Corresponding failure mode sketch	Corresponding failure mode picture
○	Failure mode 1: crack from weld toe of transverse stiffener	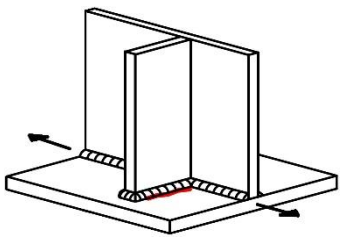	

□	Failure mode 2 or 3: crack from base material (see Fig. 2.16)	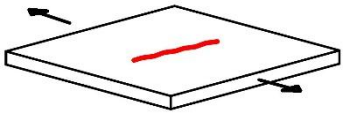	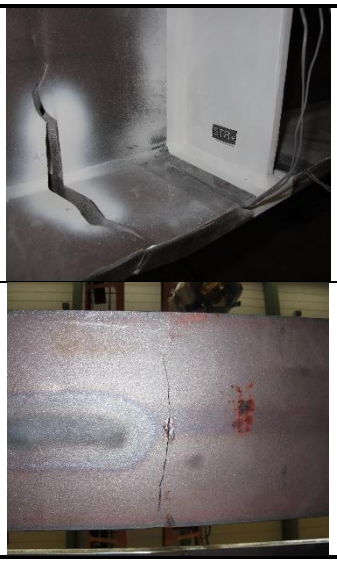
◇	Used as minimum result for evaluation (see. Figure 2.17)	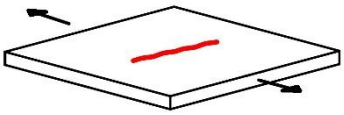	

A comparison to test results on S355 girder tests and failure modes of steel profiles with transverse attachments can be seen in Breunig [34].

Evaluation and interpretation of test results

The results are differentiated by their different failure modes in the S-N-diagrams, see Fig. 2.15, Fig. 2.16, Fig. 2.17. The corresponding failure modes have the same sign, to be able to interpret them. A dot means failure mode 1, squares stand for failure mode 2, diamonds are used as a minimum result, see Table 2.9.

As-welded beam test result

From Fig. 2.15 it can be seen that the achieved beam test result of the single as-welded beam is high compared to the fatigue resistance of the construction detail "transverse stiffener" according to EN 1993-1-9. Especially considering the scale effect of the beam test. This leads to the assumption that this high value for fatigue resistance might result from the combination of the use of S690 and the good quality of the weld and well-chosen welding parameters. It can be noticed, that the single as-welded beam test (green dot) reaches a fatigue resistance, which is even above the fatigue strength of the non-treated longitudinal welded joint 112 N/mm² and close to the fatigue detail of 125 N/mm².

Also in comparison to the small scale test series I (Table 2.4) without post-treatment the high beam test resistance is striking. The small scale tests meet the fatigue resistance according to EN 1993-1-9 rather well. In order to show the crack initiation N_i the point is given with a green dot and a red surrounding. Further information on this can be found in Deliverable D2.3 and Breunig [34].

PIT-treated beam test results

Due to the high improvement for the construction detail of the transverse stiffener the base material with a fatigue resistance of 160 N/mm² turned out to be the decisive detail category in 5 of 6 girder tests. Cracks appeared crossing the longitudinal welded joint starting from the base material bottom side of the bottom flange. The crack surfaces clearly showed that the crack initiation was on the bottom side, where there is a higher stress level than on the upper side for the failure at the transverse stiffener. The different stress ranges for the different failure modes are considered in the S-N-diagram, see Fig. 2.16.

Whereas the longitudinal welded attachment suffers from the same stress level, as the weld toe of the transverse stiffener, there was no failure of the longitudinal welded joint. Although the detail category for the longitudinal welded attachment can be estimated with $\Delta\sigma_c$ around 112 N/mm² (EN 1993-1-9) [18], since it is an automatically welded longitudinal weld connecting the web to the flanges, but with start and end positions. For none of the beam tests the cracks started from the longitudinal welds, so the fatigue resistance seemed to have been higher than 112 N/mm². The cracks from the base material, induced at the bottom flanges show resistances close to 160 N/mm², see Fig. 2.16.

In addition to Δσc = 112 N/mm² a choice of SN-curves according to (EN 1993-1-9) [18] is given to be compared to the beam test results, see different dashed lines and corresponding boxes with Δσc.

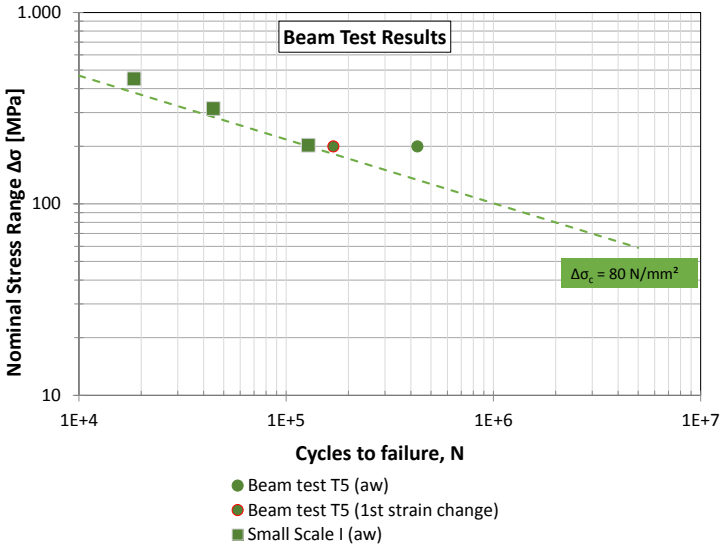

Figure 2.15: S-N curve for as-welded beam test (aw) in comparison to small case as welded tests (Small scale I (aw)) (left) and

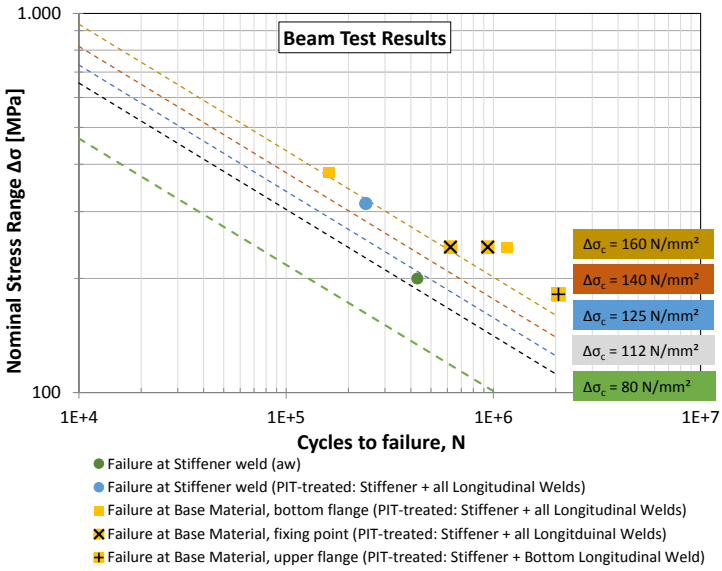

Figure 2.16: S-N curve for PIT-treated beam tests in comparison to EN 1993-1-9 fatigue resistance

Interpretation of test results regarding HFMI-treatment

In order to determine the fatigue resistance of the welded transverse stiffener after PIT treatment, the results of the failure in the base material can be used to define a minimum fatigue resistance. However it has to be emphasized that these are only minimum results and that there can be even more potential for the transverse stiffener detail.

The evaluation of the test results was conducted within the linear regression analysis according to the Background Document (Sedlacek et al., 2007) [36] to EN 1993-1-9 [18].

Generally the slope for the fatigue resistance of welded details is around 3, whereas the slope for HFMI-treated welded details is assumed to be around 5. In order to see the difference, the results have been evaluated with two different slopes.

Fig. 2.17 shows the evaluation following the linear regression according to Background Document (Sedlacek et al., 2007) [36] of EN 1993-1-9 with a fixed slope of m = 5. Following the linear regression analysis the fatigue strength of the PIT-treated beam test results could be determined around $\Delta\sigma c$ = 134 N/mm² for 2 million cycles see black lines. Dashed lines represent the 95% survival probability and continuous line the mean value graph of test results. The evaluation with the variable slope of 3.2 and thus a steeper slope leads to a fatigue strength $\Delta\sigma c$ = 123 N/mm² for 2 million cycles, see Fig. 2.17 blue lines, also dashed for 95% probability and continuous for 50 % probability.

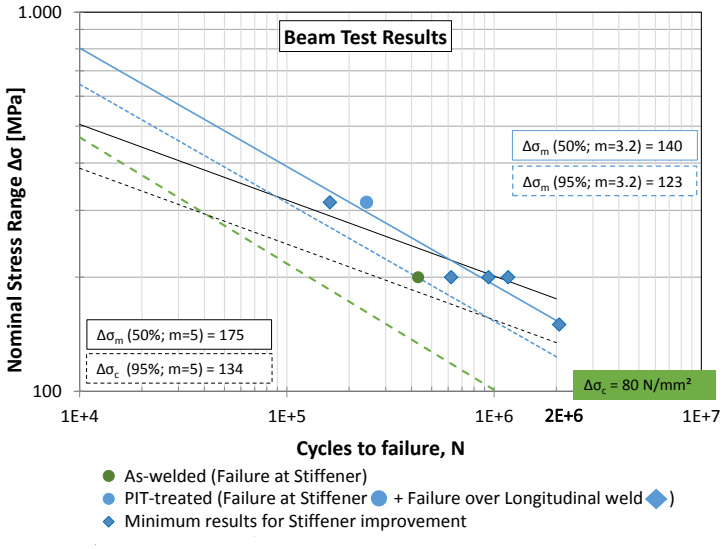

Figure 2.17: S-N diagram with fatigue resistance for PIT-treated beam tests for transverse stiffener with a slope of m = 5.0 and free slope of m = 3.2

Deliverable D2.3 gives further information on the fatigue resistance of the longitudinal welded joints.

WP 2.4b: Numerical study on beams with transverse stiffeners

Here, a new set of fatigue model parameters is defined to simulate the fatigue behaviour of large pieces, like beams (WP 2.4a). The geometry of the beam tests of WP 2.4a has a size which is similar to the bridge connections numerically studied in WP 2.5 and WP 2.6. The modified set of fatigue model parameters takes into account of a size factor and also the effect of the welding conditions (use of a robot for the small case samples and manual task for beam tests). This new data set present a reduction factor compared with the fatigue data of the small case samples (WP 2.3).

Note that the current fatigue numerical analysis of the beam tests and the bridge critical details (WP2.5) are done in parallel thanks to their similarities in size and in shape.

From the numerical study on bridges (WP2.5) with a load applied on the main girder, it has been observed that the stress distribution in the main girder bottom flange, at a short distance from the stiffener (i.e. 40 mm), is almost uniform and is not affected by the asymmetry of the section. The longitudinal stress computed by the F.E. code corresponds to the stress obtained by classical formula of elasticity theory. In conclusion, both models of beams and bridge details can be simplified and include only the girder bottom flange, the stiffener and the welded attachment.

The mesh of the model is very fine and similar to the mesh optimised in WP 2.3, for the fatigue analysis of the small case tests, with adjustment of the sizes of each parts.

The residual stresses due to the plates production, the welding process and the PIT post-treatment, measured by X-ray and presented in WP2.3, are applied in the model at its initial state.

The model is tested in fatigue bending with a constant amplitude and a stress ratio R= 0.1, like in the experimental procedure.

Table 2.10: Material parameter data set of GLCFM model for fatigue analysis of beams, called BM-large-plate & HAZ-large-plate

Material	σ_U (Mpa)	σ_{l0} (Mpa)	b	β	a	M0	Ra (mm)	$a^*(M0^{-\beta})$
BM-large plate	905.0	203.0	1.10 E-03	0.159	1	5.385 E+30	0.06	1.299E-05
HAZ-large plate	1424.0	150	7.02E-04	1.965	1	4.410E+05	0.06	8.104E-12

The number of cycles at rupture initiation is compute by a post-processor using the Lemaitre and Chaboche fatigue model [30] combined with the volume averaged stress gradient method (see model in WP2.2). Based on a sensitivity analysis, the new sets of fatigue data, adapted to large plates, are defined for BM and HAZ large plates (Table 2.10) to accurately predict the crack initiation in the beams (Fig 2.18). Here, only a single result of the experiments could be used for the fatigue characterisation since, on the other specimens, the crack didn't initiate on a PIT post-treated stiffener weld toe. However, these last results (called "Beam-Exp-No") could be used to show the zone where no crack did appear on the PIT treated welded joints and, finally, to validate the model showing an S-N curve with a slope m= 5 consistent with all the experiments on PIT post-treated welded joints.

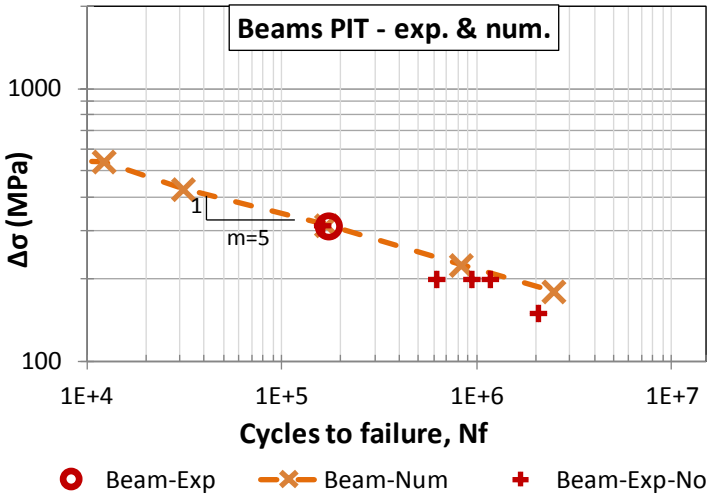

Figure 2.18: Fatigue crack initiation: comparison of the test on the beam: "Beam-Exp", numerical predictions from the model of beam: "Beam-Num" and results of the experiments where no crack did appear at the stiffener weld toe: "Beam-Exp-No"

WP 2.5: Application of the GLCFM model to bridge case design B and C

Two designs are numerically studied: the Design B where the standard S355 steel grade is replaced by HSS S690QL steel and is based on the present versions of the Eurocodes and the Design C with the use of the same steel but based on the true material behaviour.

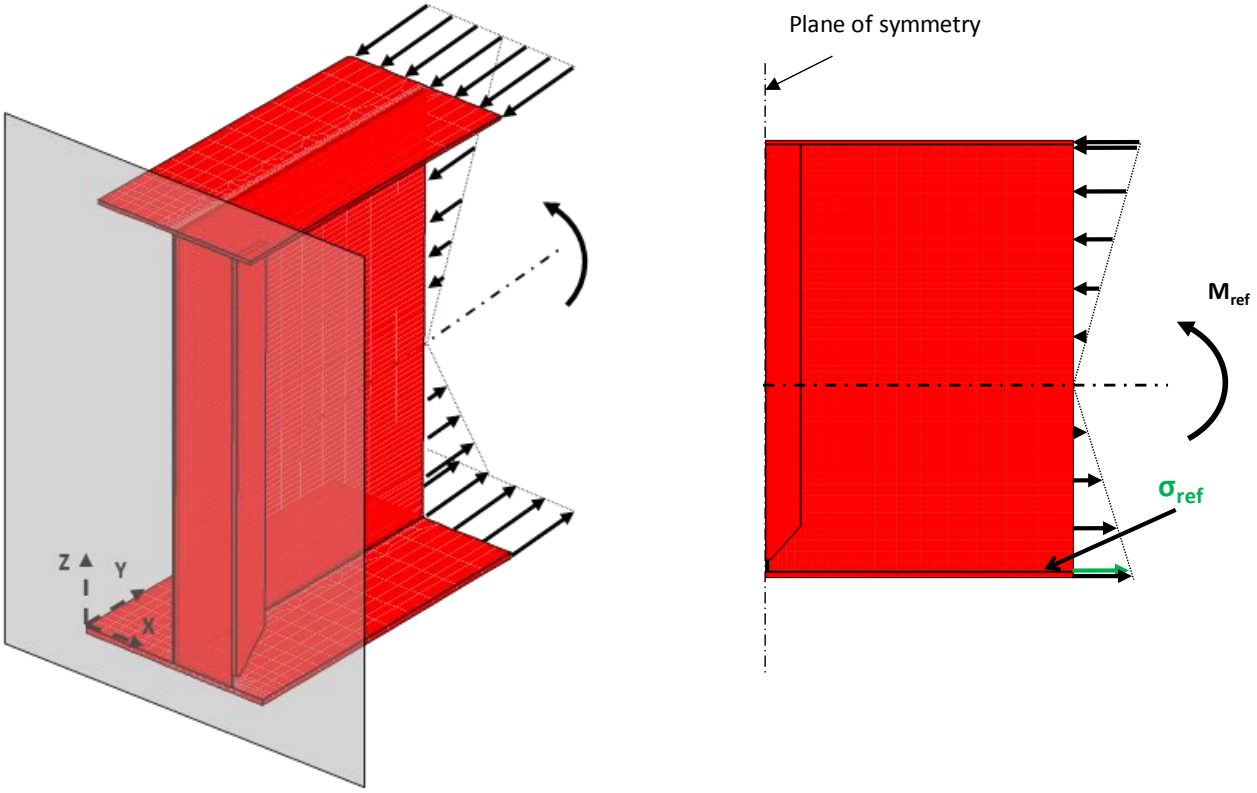

Figure 2.19: Forces applied at the free edge of the model and specific tensile stress (σref) on the upper surface of the bottom flange

A first model representing the Design B is defined with the main girder and a T-stiffener (Fig. 2.19). The effect of the transverse stiffener is neglected. Two materials are used in the model: the base material (BM) and the weld metal. The local effect of the transformation of BM to Heat Affected Zone is neglected for its low effect regarding the global stress distribution and its very low thickness (2mm) by comparison to the model size. On the contrary, the welded joints are all modelled for their impact on the model stiffness.

The girder length is the half of the distance between two T-stiffeners. The dimensions of each parts, the description of materials behaviours and the boundary conditions are detailed in D2.6.

A bending moment is applied on the girder (Fig. 2.19).

Following observations in the beam testing campaign, the critical section is the weld toe of the stiffener. The numerical simulation of the loading shows that the stress distribution in the main girder bottom flange, at short distance to the stiffener (i.e. 40 mm), is almost uniform and is not affected by the asymmetry of the section and the presence of the stiffener. On this section, the longitudinal stress level computed by the F.E. code corresponds to the stress obtained by classical formula of elasticity theory (verified for different levels of stress).

Conclusions of W.P. 2.5

- The model of bridge critical detail to use for the prediction of the number of cycles at the crack initiation can be replaced by a sub-model comprising the girder bottom flange, the stiffener and the welded attachment only.
- Since, the geometries of Designs B and C are similar except small variations in dimensions, the same conclusion can be extended to the Design C.
- A sub-model, with a very fine mesh, representing the Design C will be used to predict the crack initiation in both Designs B and C and also to participate to the determination of SN curve of bridge critical detail in WP 2.6.

WP 2.6: Application of the GLCFM model on typical welded connection detail

The critical section of Design C (D1.4) is the welded joint between the T-stiffener and the girder bottom flange. The geometry of the numerical model can be simplified in agreement with the observations in WP 2.5, with a sub-model representing the zone close to the studied section, with the girder bottom flange, the stiffener and the welded attachment (Fig. 2.20).

The geometry of the model and the boundary conditions are specified in D2.6.

The static material data are specified in Table 2.1 and the fatigue data of the BM and HAZ large plates are summarised in Table 2.10.

The model has a similar very fine mesh as the optimised one used for the "small case" specimens (see Deliverable D2.2) with very fine elements at the weld toe of the stiffener (0.1 mm) and with the transformation of the base material (BM) to heat affected zone (HAZ) near the welded joint.

The residual stress field measured by X-ray on a PIT post-treated sample, near the weld toe of the stiffener, is applied on the model at the initial state and with verification that the stress state is stable before the application of the load.

A cyclic bending moment with a constant amplitude is applied on the model. Three cycles are numerically simulated by F.E. method. From the stress history of the third cycle, the number of cycles at the crack initiation is computed by a post-processor. This procedure is repeated for several stress ranges $\Delta\sigma_{ref} = \sigma_{ref,max} - \sigma_{ref,min}$, with the reference stress measured at the upper surface of the bottom flange and with a stress ratio R of 0.1. The fatigue S-N curve, shown in Fig. 2.21, has a slope m= 5 and a stress range $\Delta\sigma i$ of 190 MPa at 2 million of cycles.

At lower stress ranges (for example, $\Delta\sigma$= 80 MPa), the numerical model doesn't predict any damage at 2.E8 cycles.

For all the stress ranges tested with the model (between 80 and 400 MPa), the crack appears in the HAZ and not in the BM. This is consistent with the observations on the beam test.

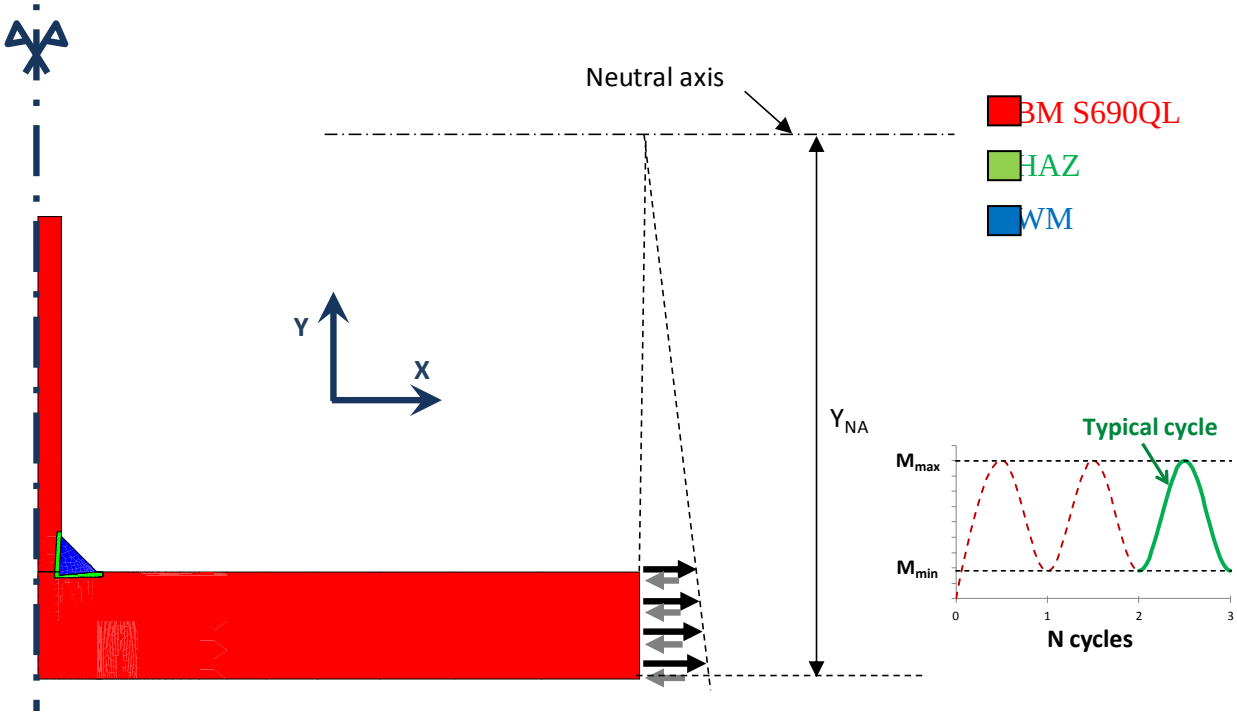

Figure 2.20: Load applied at the model with a level defined from the distance to the neutral axis of the girder (left), cyclic loading and typical cycle (right)

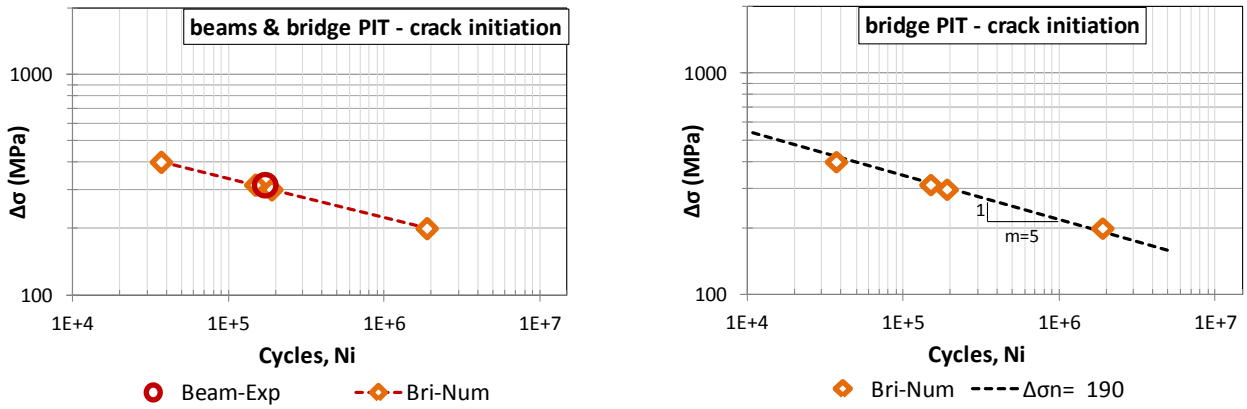

Figure 2.21: Fatigue crack initiation: comparison of the test on the beam (Beam-Exp) and numerical predictions from the model of critical bridge detail (Bri-num) (left) and determination of the FAT curve defined by the numerical analysis and a slope m= 5) - see experimental results in Annexe 2, Tables A.2.1

Conclusions of WP2

From the important static and fatigue testing campaign on small specimens, the behaviours of BM, HAZ and WM have been first deeply studied aiming to the definition of the complex static material laws and their data and also the fatigue laws and data adapted to small size specimens.

Then, from the whole fatigue testing procedure on plates and on welded plates, with several geometries, with and without post-treatment (PIT or TIG remelting), from the residual stress fields measured on welded post-treated specimens and from numerical analysis, a method has been developed to define new sets of fatigue material data for BM and HAZ plates. With this accurate description of the fatigue behaviours adapted to plates, the numerical model of a PIT post-treated welded connection subjected to axial loading as in the experiments, is able to predict the fatigue lifetime for any stress range and stress ratio, providing S-N curves for PIT post-treated welded detail with a size similar to the specimens tested here. Both the experimental results and the model show that the slope of the S-N curve and the FAT class are both higher than the categories of not post-treated specimens or post-treated by the TIG remelting process. Fig. 2 summarises all the S-N curves for small samples, plates, welded plates and welded post-treated plates showing each effect on the fatigue endurance and proving that the PIT post-treatment is clearly the most efficient post-process in term of fatigue endurance increase.

From the experiments on the small cases A, it is clear that the stress ratio has also an impact on the FAT classes and on their slopes m which are both reduced when R increases (Fig. 2.22).

Compared to the small scale tests with PIT post-treatment, the beam test results show a lower fatigue strength, which can be explicitly seen on the S-N-diagram, for the nominal stress range level of 315 N/mm² (Fig. 2.23). Since only one beam test did break on the welded post-treated joint between the girder bottom flange and the stiffener, it is difficult to determine the slope of the FAT curve for the beams but the same slope m=5 as the one of the small cases is consistent.

Nonetheless, it is possible to identify a reduction factor due to size effects for the present test data by evaluating S-N curves with linear regressions and a fixed slope of m = 5 for small and beam tests. A reduction factor of 0.78 (=190/242) is defined for PIT-treated high strength steel welded joints with a stress ratio R= 0.1.

A numerical model has been generated to describe the cyclic bending moment applied on the beams and to study the damage on the critical welded joint localised at mid-length, on the welded PIT post-treated connection between the stiffener and the bottom flange. The number of cycles at the crack initiation in the experiments are used to revised the fatigue material data and, by this way, to take into account of the size effect and the actual welding conditions. From this model associated to the new sets of fatigue data, the fatigue endurance limit is predicted for several stress ranges, showing that a slope m= 5 is perfectly adapted to describe the FAT classification.

The fatigue data defined for the beams are used to finally study bridge details. The design C is studied here with, first, a global model useful to show that the T-stiffener doesn't affect the stress distribution near the weld toe and to prove that the geometry of the connection can be simplified and include the girder bottom flange, the stiffener and the welded attachment only. Then, with the use of a sub-model, the fatigue endurance is computed for several stress ranges, aiming to the definition of the FAT class of such detail in HSS bridge with PIT post-treated welded joint. Here, the FAT 190 class is once again defined with a slope m= 5.

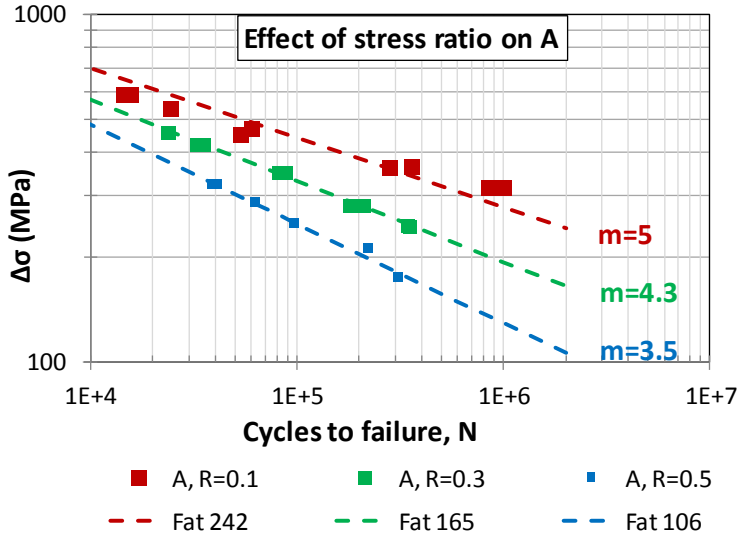

Figure 2.22: : Fatigue tests results on S690QL PIT post-treated small cases specimens A for different stress ratios R and S-N curves with an adjusted slope m

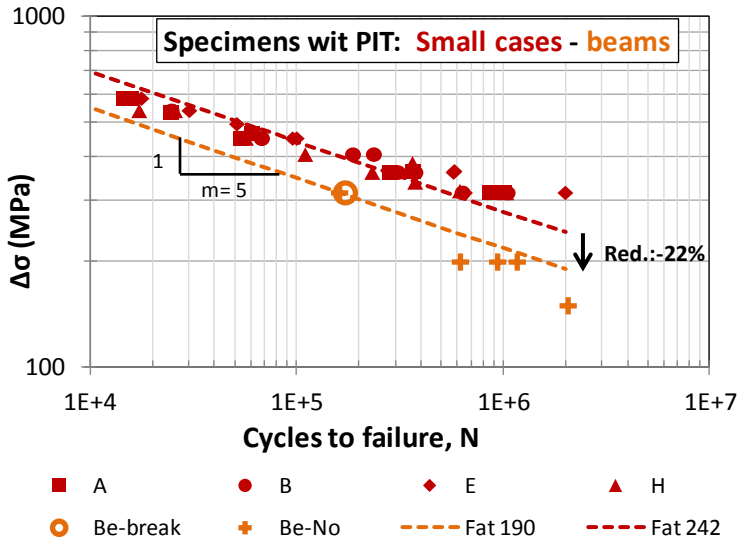

Figure 2.23: Fatigue tests results on S690QL PIT post-treated specimens: small cases ("A", "B", "E", "H") and beams ("BE-break" for the beam with rupture and "Be-No" for the beams without rupture on the PIT treated welded joint) + S-N curves with a slope m=5 : FAT242 for small cases and FAT190 for beams

WP 3. Buckling of multiaxial stressed plates

Motivation

Application of high strength steels such as S690 allows for more slender plates in bridge design than usual design with S355. As a result, plate buckling might get decisive for the ultimate load capacity of the cross-section. Since the cross-section is affected by several internal forces the plates are then stressed multiaxially.

However, the design process of plated structures provided by the current state of (EN 1993-1-5:2006) [2] does not provide reliable verification for multiaxially loaded plates. For instance the "effective width method" does not provide any possibility of checking plates subjected to biaxial loading and the "reduced stress method" does not allow taking into account tensile stresses and their positive effect on the buckling behaviour. Although, the positive effect of tensile stresses is

well known, it cannot be quantified since no investigation has been conducted in this field, neither for the case tension/compression nor tension/shear.

The main objective of WP3 is to evaluate the influence of multiaxial stress states on the buckling behaviour of slender plates and to improve the existing design rules in order to count for the positive effect of tensile stresses.

WP 3.1 Experimental study on multiaxially stressed plate panels

Target

Experimental investigations on unstiffened plates subjected to multiaxial stress states had been conducted, in order to study the effect of tensile stresses on the buckling behaviour. Existing experimental investigations are known only with uni-axial loading and biaxial compression. In order to investigate the buckling behaviour of slender plates subjected to multiaxial stress states, six large size tests were realized at the laboratory of the Material Testing Institute (MPA) in University of Stuttgart.

Dimensions and test parameters

For the experimental investigations simple isolated steel panels were regarded, which were loaded with tension (σ_z) in horizontal and with compression (σ_x) in vertical direction.
In Table 3.1, the defined test parameters for the investigated plates are listed. The tests were done subdivided into two groups as "A" and "B". The "A" tests were conducted on plates with a width of 900 mm having a square test panel of 900 mm x 900 mm. The tension/compression ratio $\beta = \sigma_z/\sigma_x$ also varied between 0, -0.25 and -0.5. The "B" tests were conducted on plates with a width of 500 mm having a test panel of 1500 mm x 500 mm. The tension/compression ratio β varied between 0, -1.5 and -1.0. In each group β=0 (without tension) was investigated as a reference for the evaluation of the test results.
The "B"-tests therefore had a panel aspect ratio of $\alpha = \frac{a}{b} = 3$ which allowed for investigating the so called column-like buckling behaviour. The schematic representation of the test specimens and dimensions are demonstrated in Fig. 3.1 and the stress ratios $\beta = \sigma_z/\sigma_x$ are summarized in Table 3.1. In order to investigate different $\frac{b}{t}$ ratios the plate dimensions a and b have been varied keeping the plate thickness constant as $t = 6$ mm, so that the same hinged lateral support could be used for all tests.

Table 3.1: Test parameters as planned (S690), t= thickness, a and b: see Fig. 3.1.

Geometry details	Identification name					
	A1	A2	A3	B1	B2	B3
a [mm]	900	900	900	1500	1500	1500
b [mm]	900	900	900	500	500	500
α = a/b	1	1	1	3	3	3
t [mm]	6	6	6	6	6	6
b/t	150	150	150	83	83	83
$\beta = \sigma_z / \sigma_x$	0	-0.25	-0.5	0	-1.5	-1.0

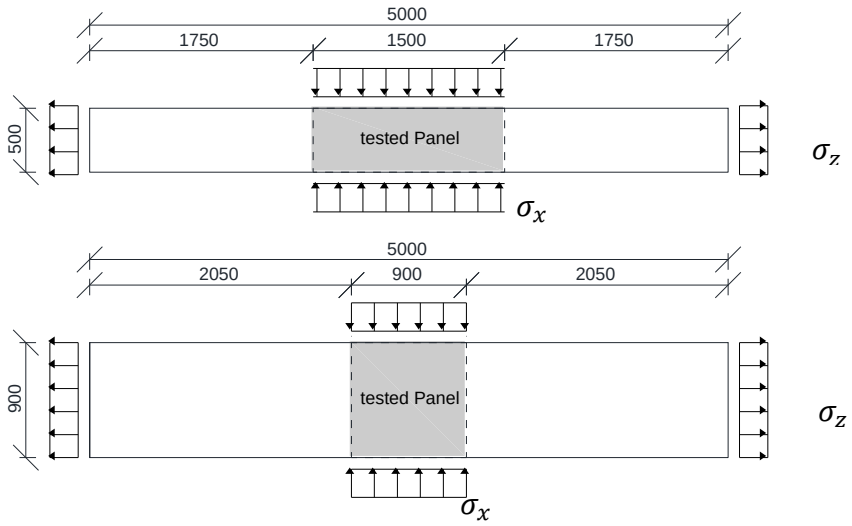

Figure 3.1: Schematic representation of the test specimens in groups A and B

Material tests

The tensile tests were conducted according to (DIN EN ISO 6892-1:2009) [37]. The dimensions of the specimens were defined according to shape ”E” of (DIN 50125:2009) [38]. In the notation the letters ”L” and ”Q” describe if the test specimen was extracted in longitudinal (”L”) or transverse (”Q”) direction of the plate.

The results of tensile coupon tests are summarized in Table A3.2. The material curves of high strength steel do not exhibit a certain yield point in contrast to normal steel. Therefore, the yield point is set at 0.2% plastic strain of material curve and is indicated as $R_{p,0.2}$ (DIN EN ISO 6892-1:2009) [37]. To clarify the parameters, which are defined below and used in Table A3.2.

A Failure strain (with a strain measuring device or directly on the specimen)
A_g Plastic extensometer-strain at ultimate load
A_{gt} Total extensometer-strain at ultimate load
A_t Total extensometer-strain at failure
ε Extensometer-strain
m_E Slope of the elastic section of the stress/Extensometer-strain curve
R Stress
R_m Tensile strength

Test Setup

The test setup included a portal frame equipped with a hydraulic jack for introducing compression to the plate in transverse direction. Additional hydraulic jacks were arranged laterally for introducing tension stresses to the plate in the longitudinal direction and generating the desired multiaxial stress state. The latter mentioned hydraulic jacks were supported by special trestles as shown in Fig. 3.2. Furthermore lateral supports were arranged for the investigated plates. In order to have the desired hinged boundary conditions for the investigated plate, special supports were developed.

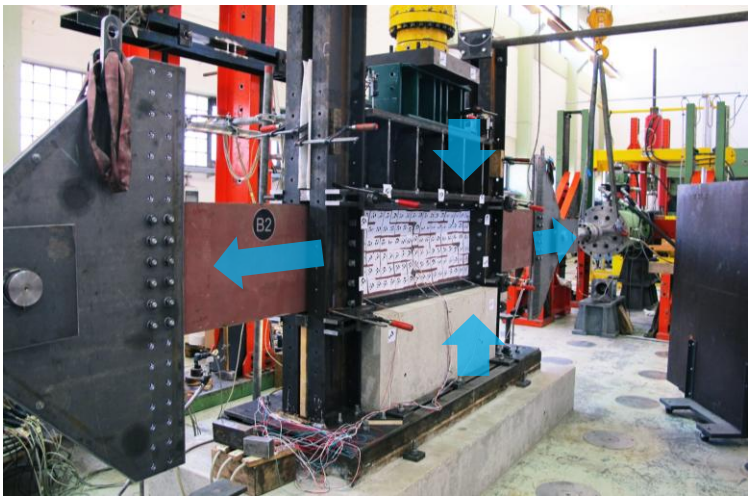

Figure 3.2: Test setup

Test Procedure

The test specimens were preloaded with approximately 15% of the estimated ultimate load before the beginning of the "real" loading phase. The loading was applied displacement-controlled. The used displacement-rate was chosen as 0.005 mm/sec in order to have quasi static loading conditions. Every 50 kN the loading was stopped and the out-of-plane deformations were measured. After reaching the ultimate load the displacement rate was raised to 0.01 mm/sec and the out-of-plane measurements took place every 0.5 - 1.0 mm.
As it was technically not possible to couple the hydraulic jacks to each other in order to apply the tensile force while introducing the compression force, the procedure was chosen as follows: first the tension increment was applied and then the respective compression increment. This allowed for an almost proportional load application with a constant $\frac{\sigma_z}{\sigma_x}$- ratio.

Experimental results

Imperfections

The measured initial imperfections are shown in Fig. A3.1 with reference to a x/y-plane, which is defined by the lower left and right point and the plane in the vertical direction. The absolute imperfection amplitudes vary from 2.4 mm to 4 mm being all in accordance to the allowable tolerances acc. to (EN 1090-2:2008) [39] (b/100).

Test Results

It is observed that the test series "A" a two half-wave failure mode develops. However, in the preliminary modelling, the failure modes for the Specimen "A1" under pure compression was observed as one half sinus wave, whereas for the multiaxially loaded plates subjected to tension and compression two half sinus waves came out. In the test, however, the results were different from what was expected. This difference has been then investigated in numerical recalculations of tests. At least for a ratio of β=-0.5 an increase of resistance can be recognised due to tension.
Obviously for the test series "B" a one half-wave failure mode develops, as expected from the preliminary modelling of test series "B". Acc. to (EN 1993-1-5:2006) [2] the plates are in the transition zone between the column-like and plate-like behaviour. From column-like behaviour can be understood that the longitudinal edges have little influence on the buckling behaviour of panels. From the comparison of failure modes of test series "B" it can be observed that a growth in the tension causes an increase in the effect of longitudinal edges and that the tension stress activates the membrane state of the panel. Therefore, it makes sense to consider the tension stress for the verification of panels.
The curves are summarized in Fig. 3.3, which represent the compression force independent of the displacement in direction of compression.

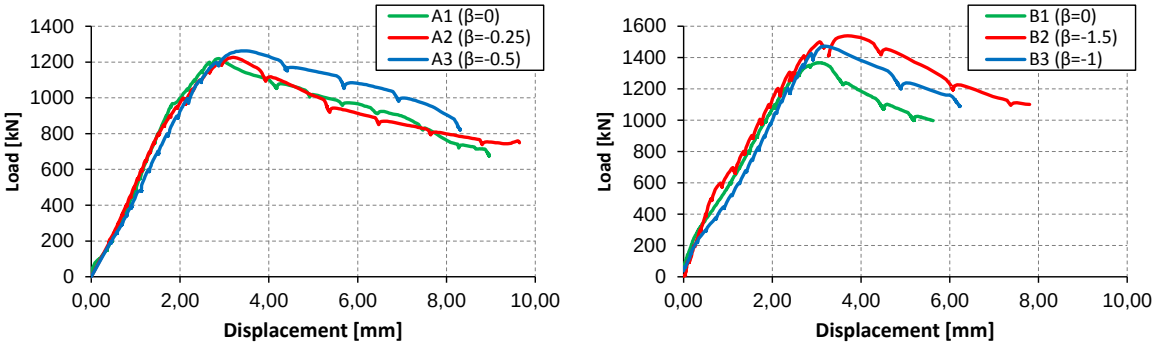

Figure 3.3: Compression load-displacement diagram for test series A(left) and B(right)

WP 3.2: Numerical parametric study on multiaxial stressed plate panels

General

The effect of tension stresses on the buckling behaviour was investigated by means of numerical simulations of the tests. The numerical models of the tests were verified by a comparison with experiments, in order to verify the procedure and the assumptions in the modelling. Furthermore, the test group A was simulated acc. to Annex C of (EN 1993-1-5:2006) [2] to investigate suitable imperfection shapes for the panels under tension and compression load. To investigate other boundary condition and parameter ranges, which are not covered by tests, a model has been developed. In this section the model is verified using the recalculation of buckling curves.

Simulations of tests

The numerical model of the whole plate was developed in ABAQUS (Dassault Systèmes Simulia Corp:2011) [40]. For the definition of the material the mean values determined from the tension coupon tests were modified into true stress-stain acc. to Annex C, (EN 1993-1-5:2006) [2]. The same boundary conditions as introduced in the experimental tests were simulated. The plates were meshed with 4 node shell elements "S4R". The initial imperfections may significantly influence the behaviour of the structural elements. The measured initial imperfections were applied in the numerical model. Concerning the results of the modelling, it has been detected that along with initial geometrical imperfections, there is another aspect affecting the buckling shapes and ultimate loads: the imperfection in load introduction. This imperfection was also considered in the model. The results of the numerical simulations are compared with the test results by using a Load Proportionality Factor (LPF = σ_{eq}/fy), which is related to the yield strength, see Fig. 3.4. In Fig. A3.2 to Fig. A3.7 failure modes and the load-displacement curves of the tests and results of the numerical models are given. In the figures compression are shorted with "comp." and tension with "ten.". Even though the deformations of the test frame had been measured during the tests, it was practically not possible to measure the deformation at the supports of specimens and the load introduction devices. So, the numerical load displacement curve of the numerical model is shifted to compare load-displacement curves just before buckling, these curves are denoted as "FEM*". The numerical results show a good agreement between the experiments and the results of the numerical calculation. Furthermore, the similarity of the buckling behaviour of the numerical model in comparison to the test results allows to consider the numerical model as validated.

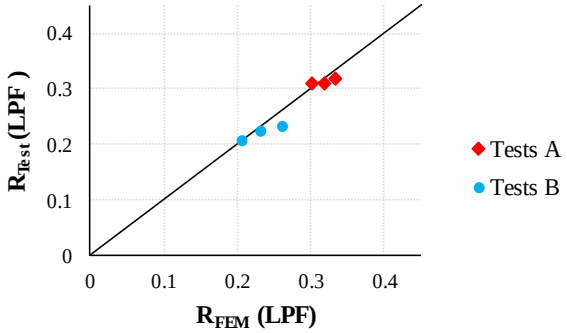

Figure 3.4: Comparison between the LPF (Load Proportionality Factor) of tests and simulations

In case of square panels subject to compression and tension stresses (Zizza:2016) [41] took the minimum ultimate load resulting from one, two and three half wave imperfection shapes as resistance of panels. Especially for panel with slenderness b/t = 150 and 250 transitions of the failure modes were observed by (Zizza:2016) [41] so that the failure shapes changed e.g. from a one-half wave to a three-half wave shape.

To check this procedure, the square panels were recalculated acc. to (EN 1993-1-5:2006) [2] applying one, two and three half-wave imperfection shapes. Fig. 3.5 (left) shows the ultimate LPF (Load Proportionality Factor) for a panel with one half-wave imperfection against the test results. It can be observed that applying one half-wave imperfection for the panel under compression and tension stress may lead to unsafe results, while as shown in Fig. 3.5 (right) the minimum LPF gained from the models with one, two and three half-wave imperfection shapes (decisive) show a good agreement with the test results.

The tension stress has not only positive influence on the ultimate load, but it can change the failure mode from one half-wave to more half-waves for a square panel. This was observed from the models acc. to Annex C, (EN 1993-1-5:2006) [2]. However, in the specimen A1 which was expected to fail with one half-wave mode, the failure mode results were different. This difference was investigated and it was due to an extra imperfection in the load introduction as mentioned before. The out-of-plane deformations of both experimental tests and numerical simulations considering the imperfection in the load introduction for different phases of the load-displacement curve are illustrated in Fig. A3.2. The out-of-plane deformations measured during the test are shown above the load-displacement curve and the shapes below the curve are the corresponding out-of-plane deformation from the numerical model. It can be seen for specimen A1 in the test and model that the out-of-plane shape changed from one half-wave to two half-waves in both. Therefore, the test and the result of the numerical model are in a good agreement. The circled point in the curve is the point below the ultimate load, where the out-of-plane deformation of the panel changes similarly, in both the numerical model and the test results, from half wave shape to two half-wave. Furthermore, it can be concluded that square panels subjected to compression and tension stress may buckle with more half-waves as shown in Fig. A3.3 and Fig. A3.4 for test A2 and A3.

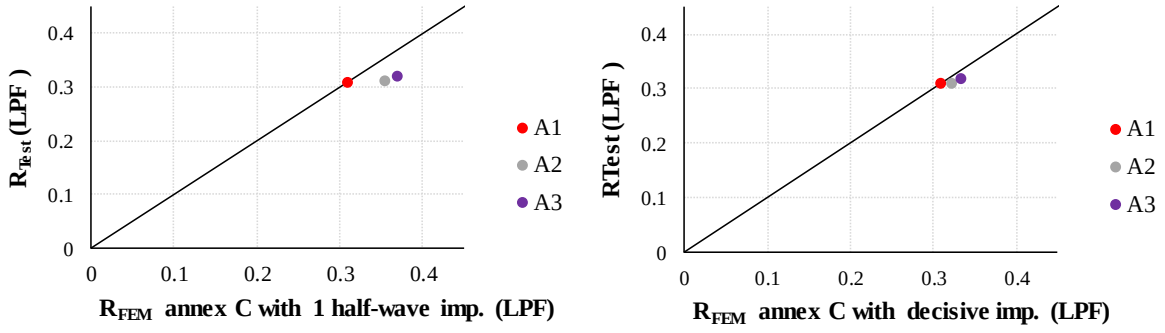

Figure 3.5: Comparison between results of the tests and simulation acc. to Annex C with one half-wave (left) and with the decisive half-wave (right) imperfection shape

Simulation of buckling curves

The buckling curves have been established empirically, mainly based on tests with mild steel specimens. Recalculating the buckling curves for high strength steel provides the possibility to verify the numerical model and to investigate further influences on the buckling behaviour such as the effect of boundary conditions, and the amplitude of imperfections, which are not covered in the experiments. In order to study the buckling behaviour of panels made of high strength steel and to validate the numerical model for other cases, the buckling curves from (EN 1993-1-5:2006) [2] for high strength steel were recalculated, which for normal steel has already been done in several studies e.g. (Lindner und Rusch:2000) [42], (Braun:2010) [43] and (Zizza:2016) [41]. (Lindner und Rusch:2000) [42] investigated the imperfection amplitude and concluded that the Winter curve can be recalculated with a reduced amplitude b/420 without considering residual stresses. Additionally, the imperfection amplitude was set to b/200 according to (EN 1993-1-5:2006) [2] to study the effect of the amplitude on the ultimate load depending on the plate slenderness. Since eigenmode-affine imperfection shapes with reduced amplitudes (w0=b/420) and without residual stresses showed to give reliable results in (Braun:2010) [43] and for a square panel the difference between eigenmode and imperfection using sine function is negligible, the recalculation of the buckling curves was conducted for square panel using sine functions for the imperfection shape. Moreover, in the numerical model for recalculation of the buckling curves, different boundary conditions were investigated as well as the effects of imperfection amplitudes. Three different types of boundary conditions and different imperfection amplitudes were taken into account. The boundary conditions BC-A refer to a panel with hinged edges in which the unloaded edges are free to move in plane, i.e. unconstrained and the loaded edges should remain straight, i.e. constrained. BC-B is constrained in all edges and BC-C is unconstrained in all. Two amplitude values w0=b/200 and w0=b/420 for boundary conditions BC-A, BC-B and BC-C were considered for the recalculation of buckling curves. For boundary condition BC-A it is visible that the Winter curve can be recalculated well with both imperfection amplitudes. For BC-B boundary conditions for stocky panel the numerical results show a good agreement with Winter curve, but with increasing slenderness the numerical results give higher results in comparison with the Winter curve. For the boundary condition BC-C, representing a plate with all four edges unconstrained, a good agreement with the buckling curve from Annex B of (EN 1993-1-5:2006) [2] can be observed.

Since in the parametric study the panel subjected to direct stresses (bending and normal forces) and shear stresses are investigated, the recalculation of buckling curves for stress ratio $\psi = 0.5;\ 0;\ -0.5$ are performed, see Fig. 3.6. For these cases the boundary conditions BC-A is applied, since with this model the Winter curve can be recalculated and Winter curve is the main buckling curve for direct stress. The same model is used for the recalculation of shear buckling curve. As in (Zizza:2016) [41][41] shown to reduce the influence of the lateral edges on resistance the panel aspect ratio increases to $\alpha = 2$. The comparison of numerical results with the shear buckling curve acc. section 5 of EN 1993-1-5 is shown in Fig. 3.7.

It can be seen that for higher slenderness the absolute values of the imperfection amplitude become less important. Moreover, it can be concluded that the amplitude has a large influence in the stocky to medium slenderness range.

It is concluded that the numerical results match very well to the buckling curves with this model for different action stresses. Thus the model is verified and can be used for the parametric study.

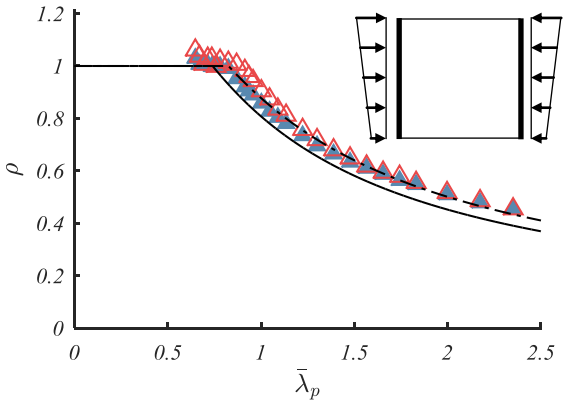

a) $\psi = 0.5$

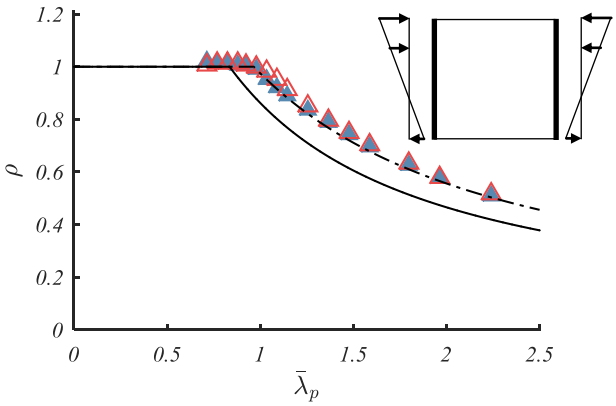

b) $\psi = -0.5$

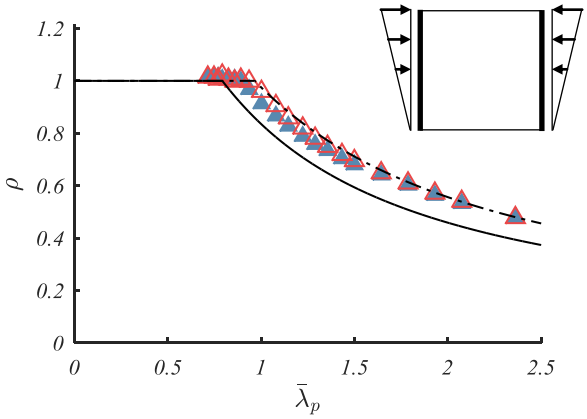

c) $\psi = 0$

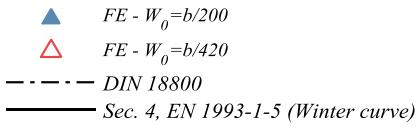

Figure 3.6: Comparison of numerical recalculation of the buckling curves with EN 1993-1-5 and DIN18800-3 (BC-A, $\alpha = 1$, $\psi = 0.5\,;0\,;-0.5$)

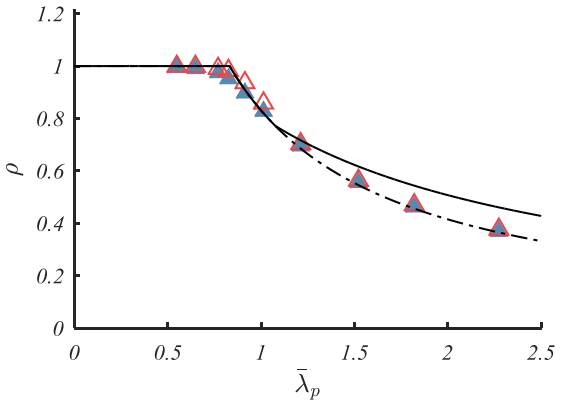

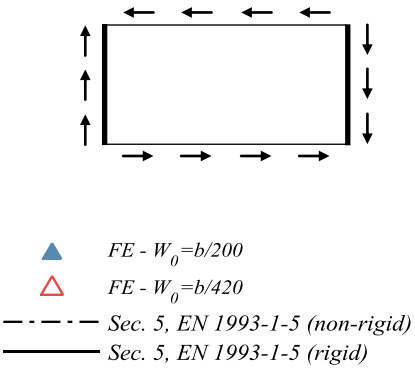

Figure 3.7: Comparison of Numerical recalculation of the buckling curves with EN 1993-1-5 (BC-A, $\alpha = 2$)

General

A modification "V-factor" was proposed by (Zizza:2016) [41] for panels under tension and compression stress states. This proposal has been checked for high strength steel, since it was developed originally for the mild steel. For panels loaded with normal and shear (Sinur:2011) [44] showed that the effective width method does not consider the benefit of tension stresses and the effective width method leads to conservative results. For interaction of bending and shear stresses in this section a design method is proposed to consider the positive effect of tension stresses in the effective width method.

Plate subjected to direct stresses

According to (Zizza:2016) [41] the positive effect of tension stresses can be considered for calculation of the reduction factors, and the tension stresses should be applied in the verification equation. Additionally, a modification factor V for panel under tensile stress was proposed by Zizza. (Zizza:2016) [41] has shown that the basis for the calculation of reduction factors is the determination of the elastic critical buckling stress, which strongly depends on the plate geometry as well as the load situation. The elastic critical buckling stress can either be determined by analytical solutions from the differential equations of buckling of a plate loaded in its plane or by software tools such as EBPLate (CTICM:2013) [45]. (Zizza:2016) [41] investigated the effect of tension stresses on the determination of the elastic critical buckling stress and showed that the buckling coefficient k_σ for several stress ratios depend on the panel aspect ratio α, see Fig. 3.8. The peaks for the linear bifurcation analysis in the determination of the buckling coefficient result from the non-continuously differential functions obtained for the solution of the differential equations. These peaks between the buckling modes affect directly the slenderness and therefore the resistance of the considered plate. With increasing tension ratio the peaks become more and more pronounced. (Zizza:2016) [41] recommend not to take the peaks into account while calculating the plate slenderness, as the effect is flattened out for high-grade non-linear calculations. Here it has been concluded, that the peaks should also be neglected for calculation of the reduction factors.

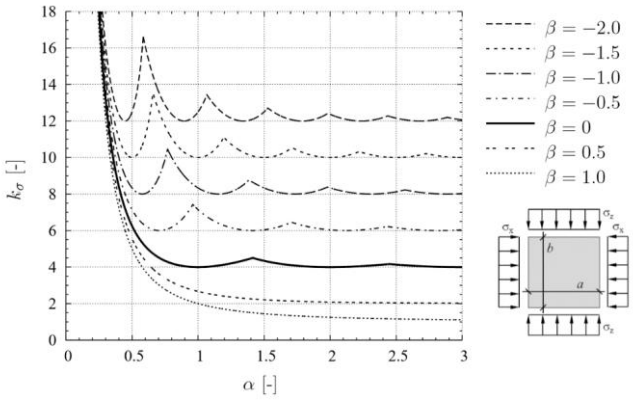

Figure 3.8: Buckling coefficient kσ depending on the stress ratio β = σz/σx and panel aspect ratio α = a/b (Zizza:2016)

The proposals of (Braun:2010) [43] and (Zizza:2016) [41][41] are summarised in Eq. 3.1.

$$\left(\frac{\sigma_{x,Ed}}{\rho_{c,x}\cdot f_y/\gamma_{M1}}\right)^2+\left(\frac{\sigma_{z,Ed}}{\rho_{c,z}\cdot f_y/\gamma_{M1}}\right)^2+V\cdot\left(\frac{\sigma_{x,Ed}}{\rho_{c,x}\cdot f_y/\gamma_{M1}}\right)\cdot\left(\frac{\sigma_{x,Ed}}{\rho_{c,x}\cdot f_y/\gamma_{M1}}\right)+3\cdot\left(\frac{\tau_{Ed}}{\chi_w\cdot f_y/\gamma_{M1}}\right)^2\leq 1.0 \qquad (3.1)$$

where:

$V=\rho_{c,x}\cdot\rho_{c,z}$ If $\sigma_{x,Ed}$ and $\sigma_{z,Ed}$ are both compression (Braun:2010) [43]

$V = 1/(\rho_{c,x} \cdot \rho_{c,z}^{2-\xi_z})$ If $\sigma_{x,Ed}$ and/ or $\sigma_{z,Ed}$ are/is tension (Zizza:2016) [41]

Current verification equation in sec.10 of (EN 1993-1-5:2006) [2] is the same equation as Eq. 3.1 but without V factor and the positive effect of tension stresses should be neglected for calculation of panels subjected to compression and tension. The current design rule has been compared with the improved design rule by (Zizza:2016) [41] in case of panels subjected to tension and compression stresses, see Fig. A3.9 and Fig. A3.10. In the Figures the green curves show the results, considering the tension in the calculation of the reduction factors and in the verification equation without considering V factor. Furthermore, in these curves the peaks from the buckling coefficient have been taken into account.

By comparing the results it can be seen that the improved design rule by (Zizza:2016) [41][41] matches well to numerical results and lead to more favourable and economic results in case of acting tension and compression stresses on the panel. The proposal is suitable to improve the design rule and for high strength steel.

Plate subjected to shear and direct stresses

Current design rules

(EN 1993-1-5:2006) [2] provides two methods for analytical calculation of panels subjected to the interaction of direct and shear stresses: "Effective Width Method" (EWM) and "Reduced Stress Method" (RSM).For verification of panels acc. to effective width method, each single internal force and moment should be met separately. In the next step the combination of acting forces should be taken into account by interaction expressions, which in sec. 7 of (EN 1993-1-5:2006) [2] are regulated. In this investigation following interaction expression is used based on section 7.1(5) of (EN 1993-1-5:2006) [2] which replaced $\bar{\eta}_1 = M_{ED}/M_{Pl,RD}$ by η_1 according Eq. 3.3:

$$\eta_1 + (2\bar{\eta}_3 - 1)^2 \leq 1.0 \qquad (3.2)$$

With:

$$\eta_1 = \frac{N_{Ed}}{\frac{f_y A_{eff}}{\gamma_{M0}}} + \frac{M_{Ed} + N_{Ed} e_N}{\frac{f_y W_{eff}}{\gamma_{M0}}}, \bar{\eta}_3 = \frac{V_{Ed}}{V_{bw,Rd}} \qquad (3.3)$$

In contrast to EWM, the reduction factors acc. to RSM are determined only with single panel slenderness and the stresses are checked with only one interaction verification expression.
In the Fig. 3.9 to Fig. 3.12 the application of EWM and RSM are plotted. The investigation on plates subjected to tension and shear stresses using RSM method is in a good agreement with numerical results and the curves follow the numerical simulations, so that an enhancement of RSM for this case is not necessary. Application of the EWM leads to conservative results therefore, a new design procedure proposed to reach the more economic design. Though (EN 1993-1-5:2006) [2] is one of the most advanced standards regarding plate buckling, the beneficial effect of tension stresses is not explicitly taken into account in the effective width method, even if those have a significant positive impact on the stability of panels. In Fig. 3.9 to Fig. 3.12 it can be seen that the results of EWM is conservative in comparison to RSM, in which the positive effects of tension are considered. In order to consider beneficial effects of tension stresses, an enhancement is proposed, see next section. The proposal deals with the resistance of panels subjected to shear combined with direct stresses.
It should be mentioned that α_{cr} for calculation of $\bar{\lambda}_p$ acc. to RSM is determined with EBPlate program (CTICM:2013) [45] and the partial factors in this study were set to 1.0.

Enhancement on effective width method

This proposal relies on extensive parametric studies based on FE simulations of the verified model of unstiffened panel. It should be noted that just a sub-panel without flanges was simulated. As mentioned, in contrast to the reduced stress method the effective width method does not consider

the positive effect of tension stresses and the reduces the shear resistance in the same way as for compression stresses (Sinur:2011) [44]. In order to consider the beneficial effects of tension stresses following proposal in case of panels subjected to normal, bending and shear forces is made:

If $|\sigma_t| > |\sigma_c|$ and the stress ratio $\psi \geq -0.5$ the slenderness $\bar{\lambda}_w$ may be taken the same $\bar{\lambda}_p$ acc. to eq. (10.2) from section 10 of (EN 1993-1-5:2006).

⇨ $\bar{\lambda}_w = \bar{\lambda}_p = \sqrt{\frac{\alpha_{ult,k}}{\alpha_{cr}}}$ if $|\sigma_t| > |\sigma_c|$ and the stress ratio $\psi \geq -0.5$

where:

σ_t: Tension stress

σ_c: Compression stress

$\bar{\lambda}_w$: Slenderness for calculation of shear buckling resistance

$\bar{\lambda}_p$: Slenderness acc. to eq. (10.2) from section 10 of (EN 1993-1-5:2006)

The resistance of panels should be determined according to the following interaction acc. to 7.1(5) :

$$\eta_1 + (2\bar{\eta}_3 - 1)^2 \leq 1.0$$

with:

$$\eta_1 = \frac{N_{Ed}}{\frac{f_y A_{eff}}{\gamma_{M1}}} + \frac{M_{Ed} + N_{Ed} e_N}{\frac{f_y W_{eff}}{\gamma_{M1}}}, \bar{\eta}_3 = \frac{V_{Ed}}{V_{bw,Rd}}$$

The results obtained from this proposal and the current methods acc. to (EN 1993-1-5:2006) [2]for plates respectively with $\psi = -0.5, 0, 0.5, 1$ are presented in Fig. 3.9 to Fig. 3.12. It can be observed that the ultimate load provided by the FEM simulations have good agreement with the values predicted by the proposal.

It should be noted that in this study the maximum acting stresses of the numerical models were limited to the equivalent stresses (von Mises stresses).

Statistical evaluation of the improved design rules

The partial factors were determined for the proposed procedure in Sec. "Enhancement on effective width method" according to the method given in (EN 1990: 2002) [46], Annex D, which gives a procedure for the assessment of the characteristic and the design values. The same procedure suggested by (Zizza:2016) [41] is used and reported in detail in (Kuhlmann et al.:2018) [47]. The final partial factor are summarized in Table 3.2. It can be seen that the required partial factors justify using of $\gamma_{M1} = 1.1$.

Table 3.2: The partial factor γ_{M^*}

$\psi = -0.5$	$\psi = 0$	$\psi = 0.5$	$\psi = 1$
1.1106	1.0527	1.0345	1.0926

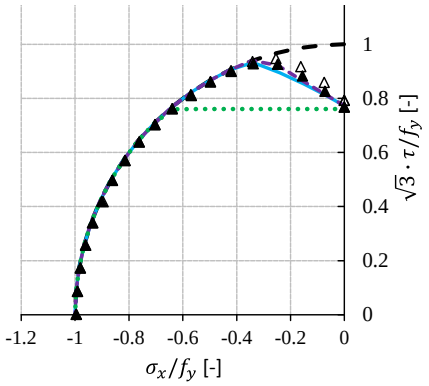

a) $b/t = 60$

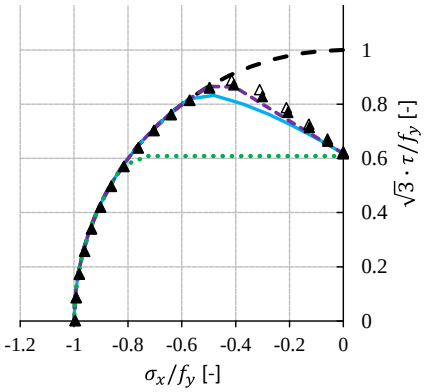

b) $b/t = 75$

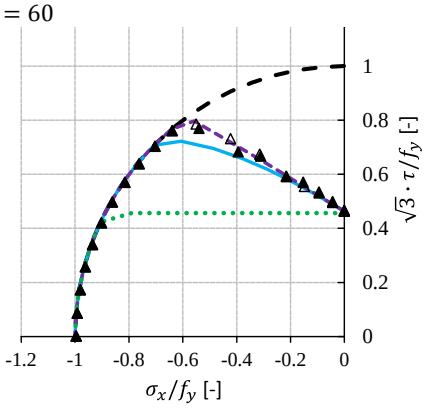

c) $b/t = 100$

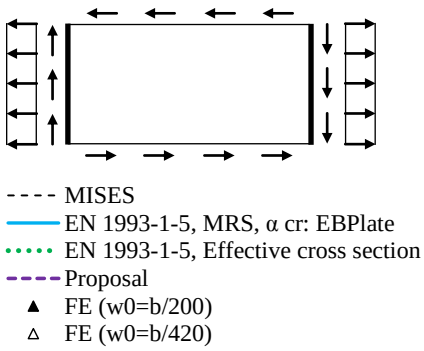

Figure 3.9: Comparison between the results of the numerical calculation with the results of the current design rule EN 1993-1-5 and the improved design rule in case of panels subjected to bending-shear (Boundary condition BC-A; $\psi = 1.0; \alpha = 2$)

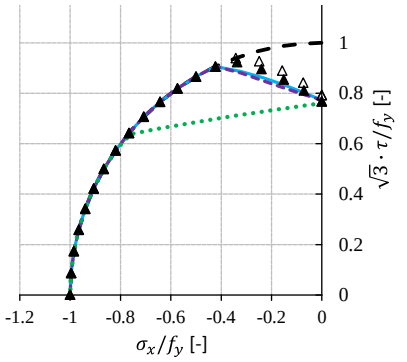

a) $b/t = 60$

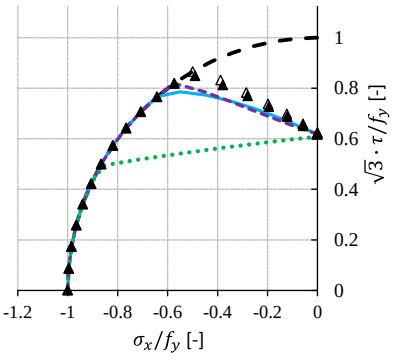

b) $b/t = 75$

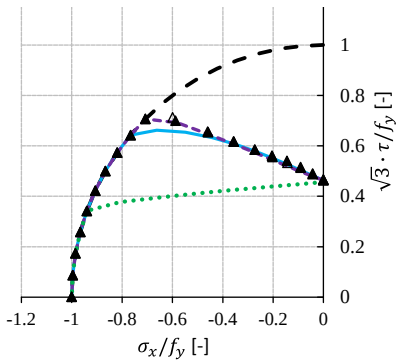

c) $b/t = 100$

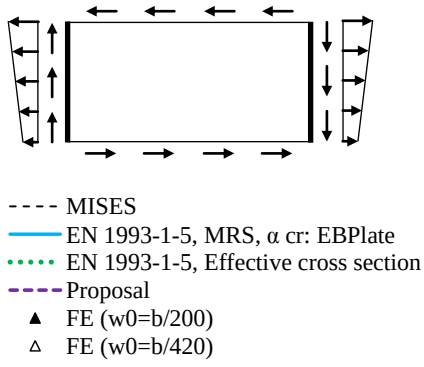

Figure 3.10: Comparison between the results of the numerical calculation with the results of the current design rule EN 1993-1-5 and the improved design rule in case of panels subjected to bending-shear (Boundary condition BC-A; $\psi = 0.5; \alpha = 2$)

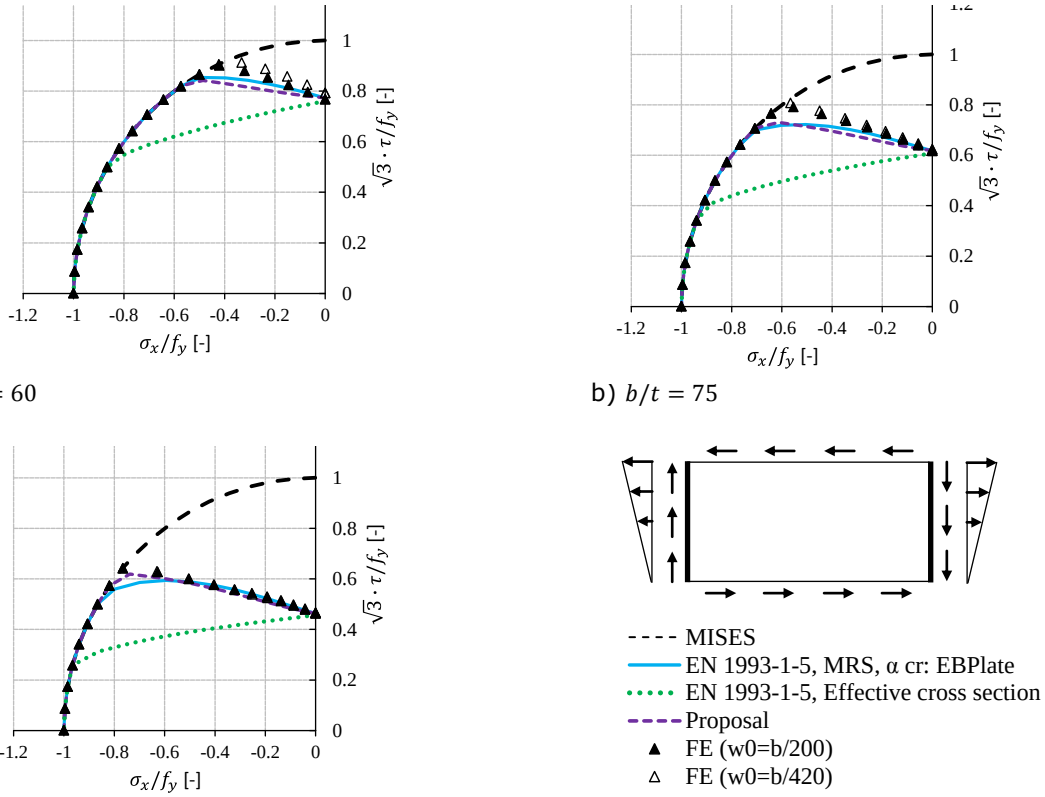

a) $b/t = 60$

b) $b/t = 75$

c) $b/t = 100$

Figure 3.11: Comparison between the results of the numerical calculation with the results of the current design rule EN 1993-1-5 and the improved design rule in case of panels subjected to bending-shear (Boundary condition BC-A; $\psi = 0; \alpha = 2$)

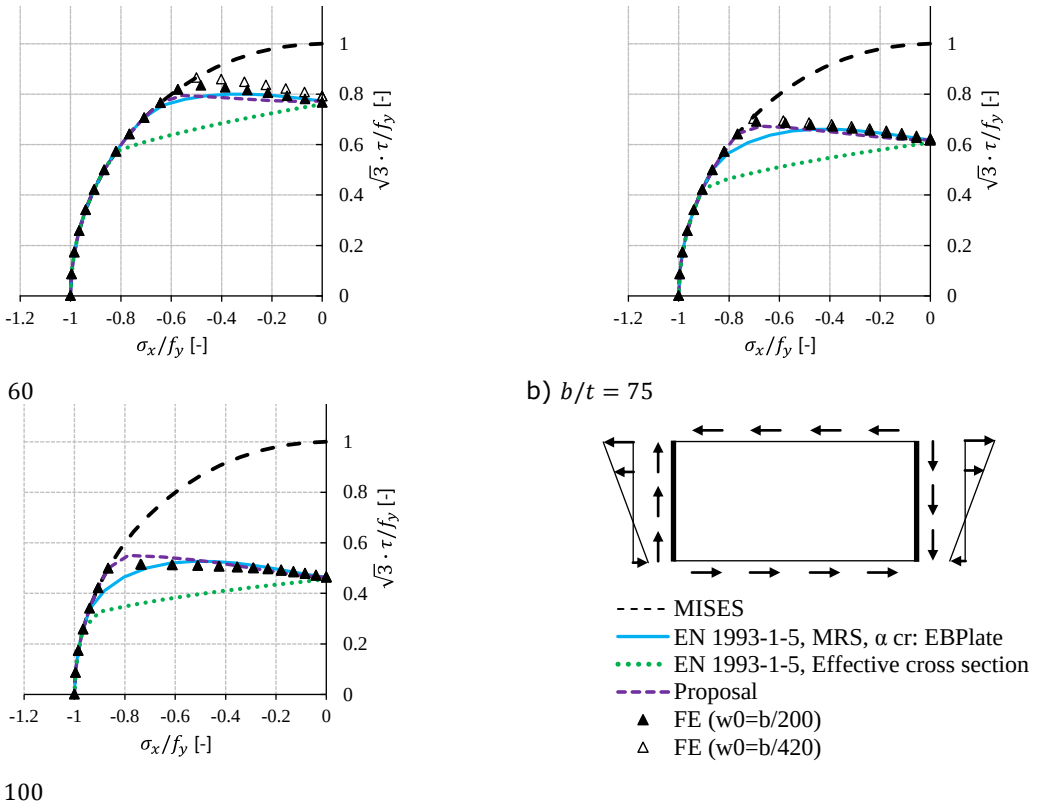

a) $b/t = 60$

b) $b/t = 75$

c) b/t = 100

Figure 3.12: Comparison between the results of the numerical calculation with the results of the current design rule EN 1993-1-5 and the improved design rule in case of panels subjected to bending-shear (Boundary condition BC-A; $\psi = -0.5; \alpha = 2$)

Conclusions of WP3

The influence of the tension stresses on the buckling behaviour can be seen on the out-of-panel deformations and on the ultimate load. The tension stresses may change the failure mode of a square panel from one half-wave into more half-waves. Furthermore, the results show that tensile stresses increase the buckling resistance of the panels. The proposal of (Zizza, 2016) [41][41] developed for mild steel is investigated for panels subjected to compression and tension in S690. It is concluded, that the proposal of (Zizza, 2016) [41] leads to good results for this case. It is concluded that considering the positive effect of tension stresses on the reduction factors, enhances the accuracy of the "reduced stress method" and leads to a more economic design of the panels, so at this point it seems reasonable to take into account tensile stresses in the design of multiaxially loaded plates. Application of reduced stress method for panels subjected to shear and direct stresses shows a good agreement with numerical results. In contrast to the reduced stress method the effective width method does not consider the positive effect of tension stresses and reduces the shear resistance in the same way as for compression stresses. In order to consider the beneficial effects of tension stresses a new proposal in case of panels subjected to normal, bending and shear forces is made and the proposal is statistically evaluated.
However, the basis of this investigation is limited on unstiffened panels neglecting the load shedding with flanges, so that in future the effect of tension stresses should be further numerically investigated for panels with stiffeners being part of a section with flanges.

WP 4: Samples generation and post-weld treatment qualification

WP 4.1: Weld simulation, characterisation, generation of samples

For 2 different cases (HAZ 1 – welding case A and HAZ 2 – welding case H) metallographic examinations of the cross sections have focussed on the exact HAZ structures. Figs. 4.1 to 4.3 show the metallographic cross sections.. Starting from the left, one can distinguish the weld metal, the **coarse grained HAZ (CG)**, the **fine grained HAZ (FG)** and the **intercritical HAZ (IC)** which runs out into the base material. The base material is fine grained. The most part of the heat affected zone is the coarse grained HAZ.

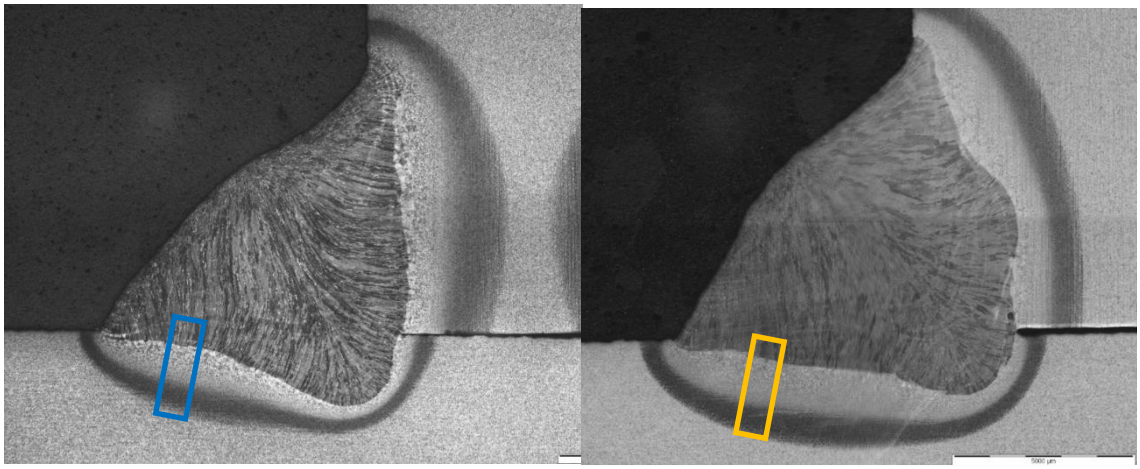

Figure 4.1: Welding Case A (HAZ 1) – detailed view of zone marked in bleu shown in Fig. 4.2 (left) and Welding Case H (HAZ 2) – detailed view of zone marked in orange shown in Fig.4.3 (right)

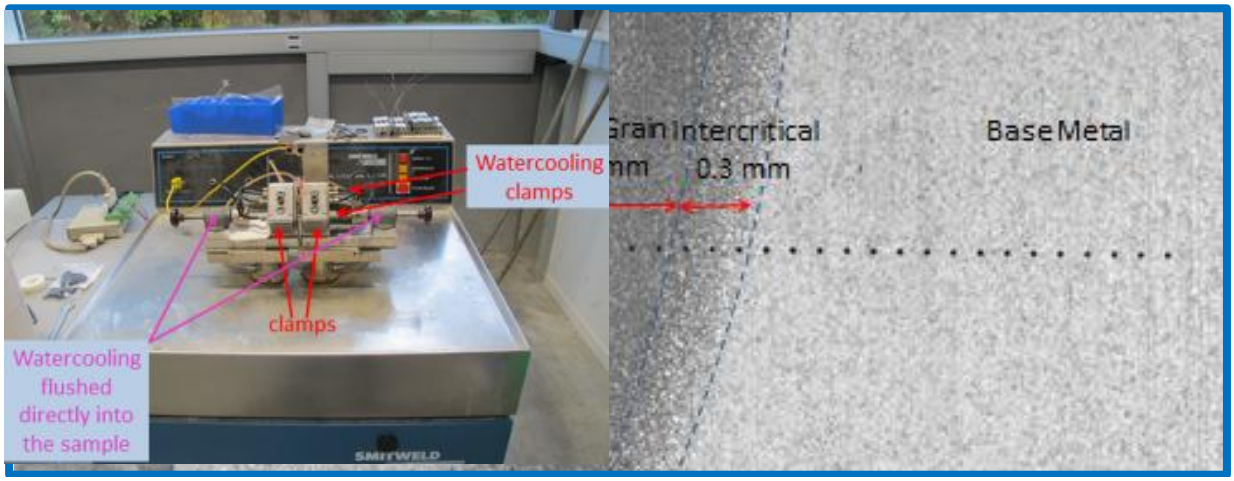

Figure 4.2: Heat affected zone 1 of fillet weld case A – location indicated in Fig. 4.1 (left)

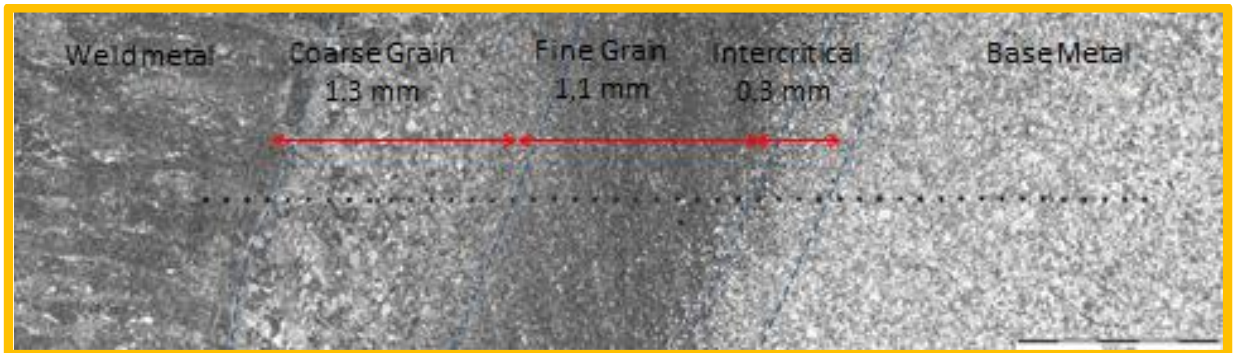

Figure 4.3: Heat affected zone 1 of fillet weld case H – location indicated in Fig.4.1, right

Based on these actual microstructures, and the obtained (micro)hardness measurements, it was decided to recreate full coarse grain heat affected zone specimens for further investigations for characterization.

The weld simulations of HAZ1 (welding case A) were executed with a cooling rate of 4.4s (as measured on the real welding sample). The ones covering HAZ 2 (welding H), were executed with a cooling rate of 7 s.

All tests for weld simulation are done on round trial samples, except for the Bauchinger test samples which are made of flat weld simulations. Weld simulations for **round test samples** are made on a Smitweld weld simulator (Fig. 4.4, left and right).

The length of the homogenous simulated zone was measured to be 11 mm long by means of hardness measurements. Fig. 4.5 shows the hardness which is significantly higher in the centre of the test samples. Fig. 4.6 shows the location of the hardness indents.

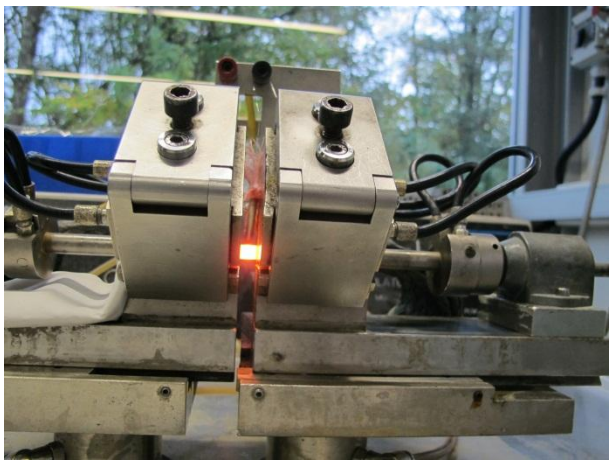

Figure 4.4: Smitweld weld simulator (left) and Thermal cycle applied on sample (right)

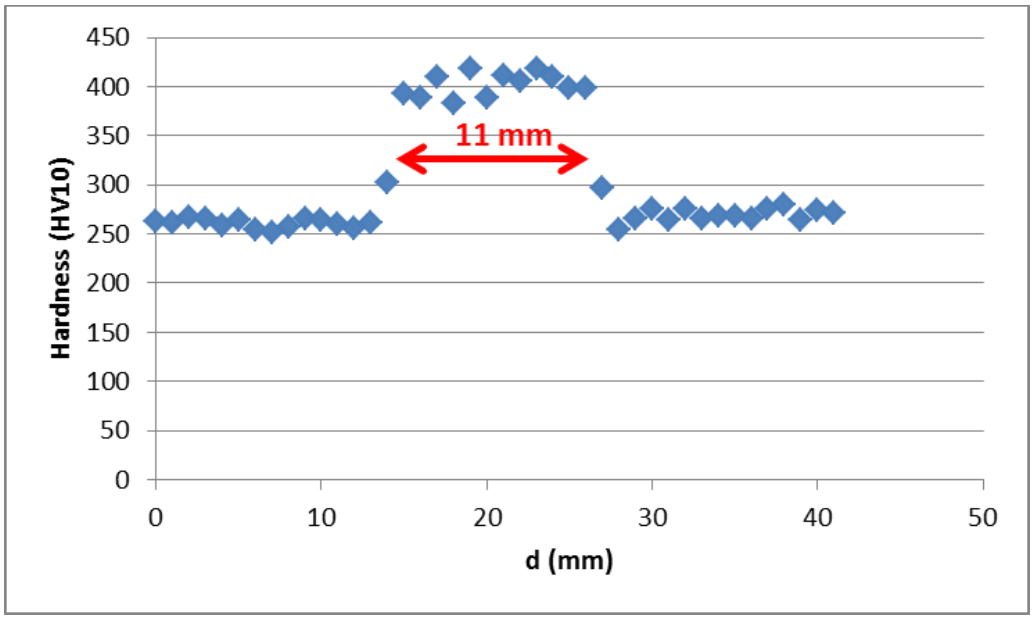

Figure 4.5: Hardness measurement on the material submitted to the physical simulation of the thermal history of HAZ 2, showing the homogeneous simulated zone of 11mm length

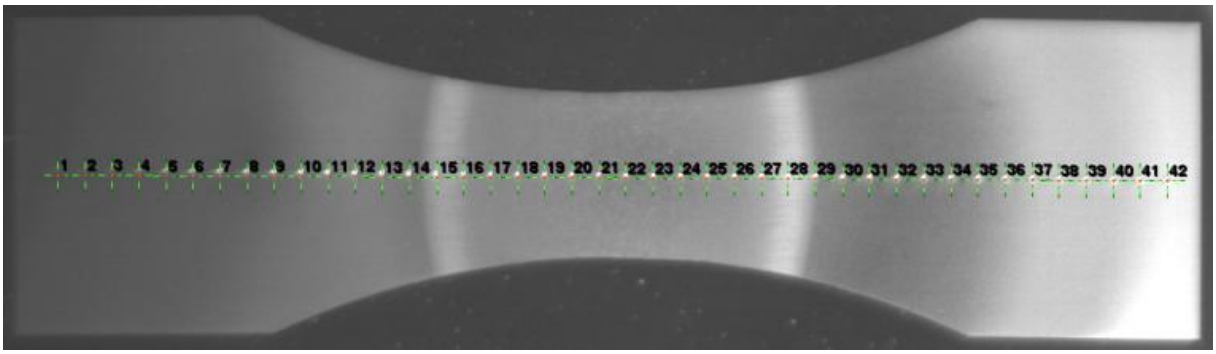

Figure 4.6: Hardness traverse over the physical simulation of the thermal history of heat affected zone 2 - location of the hardness indents

WP 4.2: Welding and post treatment of small scale fatigue tests

All welded samples prepared for the project have been following the '*EN ISO 15614-1 - Specification and qualification of welding procedures for metallic materials - Welding procedure test - Part 1 Arc and gas welding of steels for the welding procedure qualification*' standard. This standard refers to the required quality level for each possible weld imperfection. Most often quality level B is required. The WPS (Welding Procedure Specification) is given in annex 4.

All welded joints in OPTIBRI project were welded by robot, to obtain a consistent weld quality, using MAG-welding (Metal Active Gas) of S690QL steel with different thicknesses and different stiffeners. Conventional filler material matching the strength of S690QL has been used. The optimisation process included metallographic testing to verify the quality, repeatability, geometrical aspects and microstructure.

It was agreed with the material supplier that the preheat temperature can be low in case of welding in good conditions. The good conditions were achieved due to welding with low humidity and removal of scale on the material combined with cleaning of the welded plates. 20°C and 100°C are the preheating temperatures for respectively small scale tests on 25 mm plate and 40 mm plate (as defined by EN1011).

The filler material used for welding S690QL is solid MAG-wire "LNM MoNiVa" from Lincoln. The designation according the ISO standard is EN ISO 16834-A G69 4 M Mn3Ni1CrMo. The wire has mechanical properties that match with the base material S690QL. The datasheet of the filler material is added in annex 5.

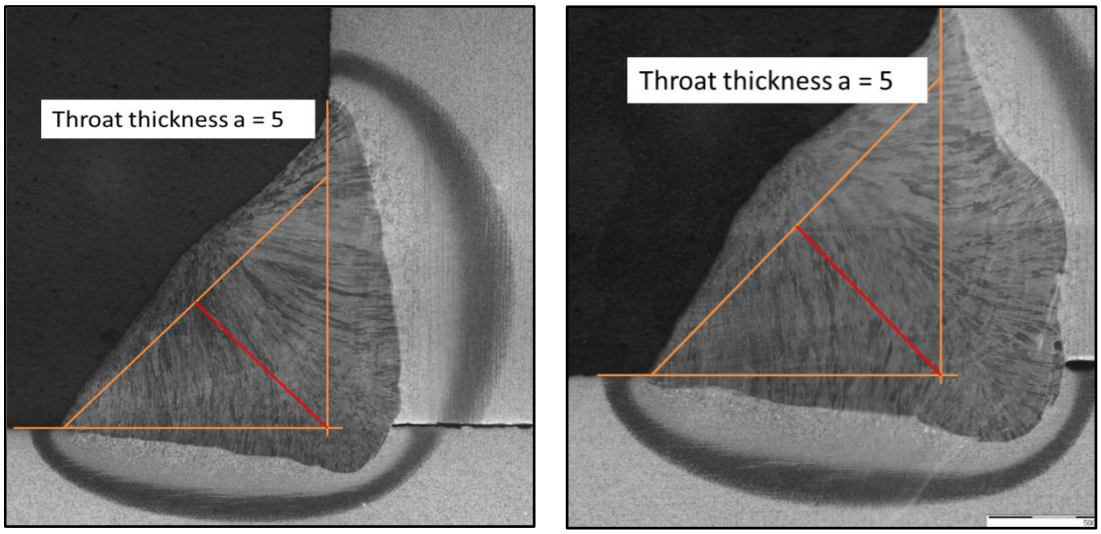

Figure 4.7: Metallographic sections on 25 and 40 mm S690QL

Fig. 4.7 shows the metallographic sections on 25 and 40 mm S690QL with a stiffener of 15 mm. The root shows good penetration and the weld toe radius is acceptable. The throat thickness is 5 mm. This is acceptable according EN ISO 15614-1.

To be able to define the exact cooling rate for the different welding set ups, measurements of T8/5 were performed at multiple locations. Figs. 4.8 to 4.10 show the measurement setup, as well as the actual recordings on the 25 and 40 mm plate (40 mm plate was preheated to 100°C).

Pneumatic impact treatment has been carried out as post-treatment process, to improve the fatigue life. For the treatment of the transverse stiffeners following parameters were used:

- Air Pressure: 6 bars
- Frequency: 90 Hz
- Pin radius: 2 mm

Gas Tungsten Arc Welding (GTAW), has been used as a second post-treatment process, by re-melting and smoothening the shape of the weld toe. The following parameters have been used:

- Voltage: 11.0V
- Current: 208A
- Travel speed: 50mm/min
- Heat input: 1.9kJ/mm
- Shielding gas: 100% Ar
- Electrode: WR2, diameter 2.4mm

GTAW dressing was carried out by a robot, in order to exclude process variations during the treatment. Fig 4.11, left and right show the result of the dressing operation.

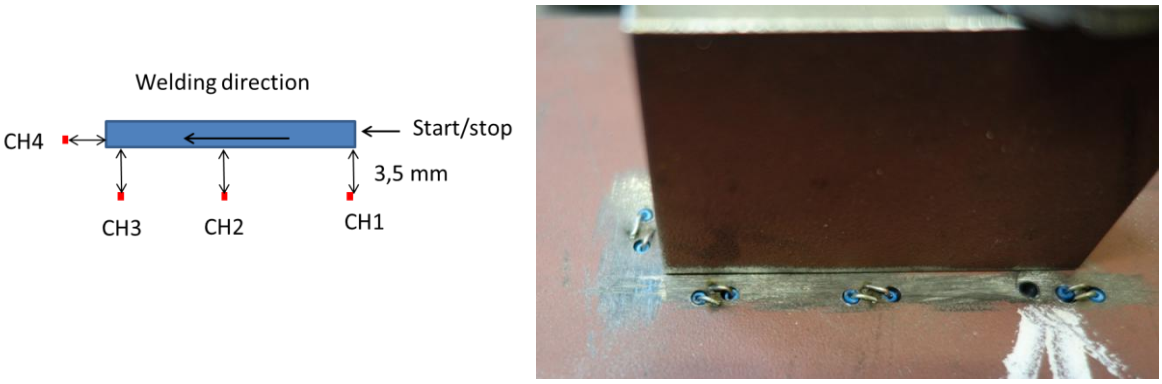

Figure 4.8: Overview where the t8/5 was measured

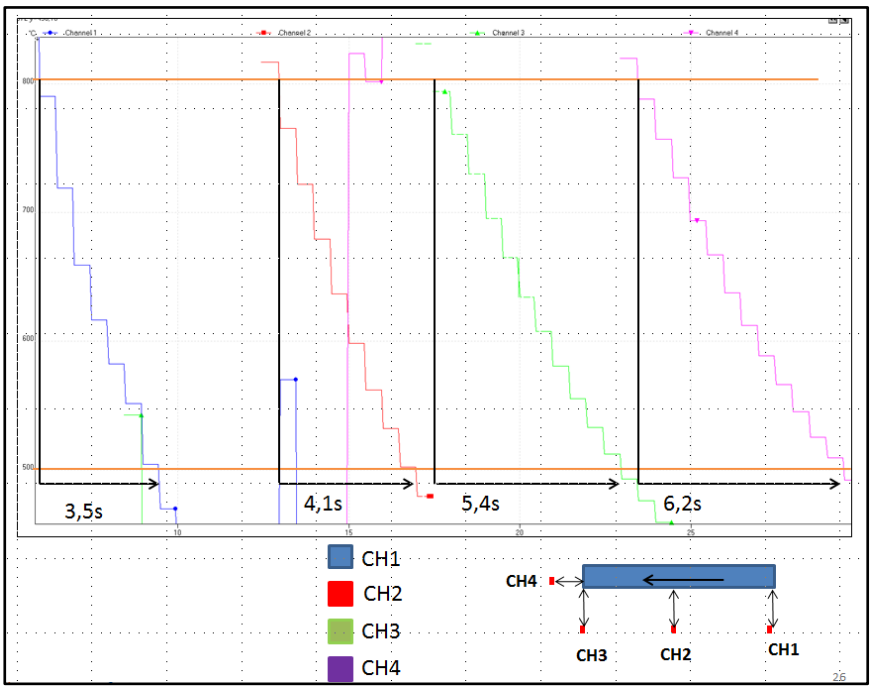

Figure 4.9: T8/5 for welding 25 mm S690QL without preheat

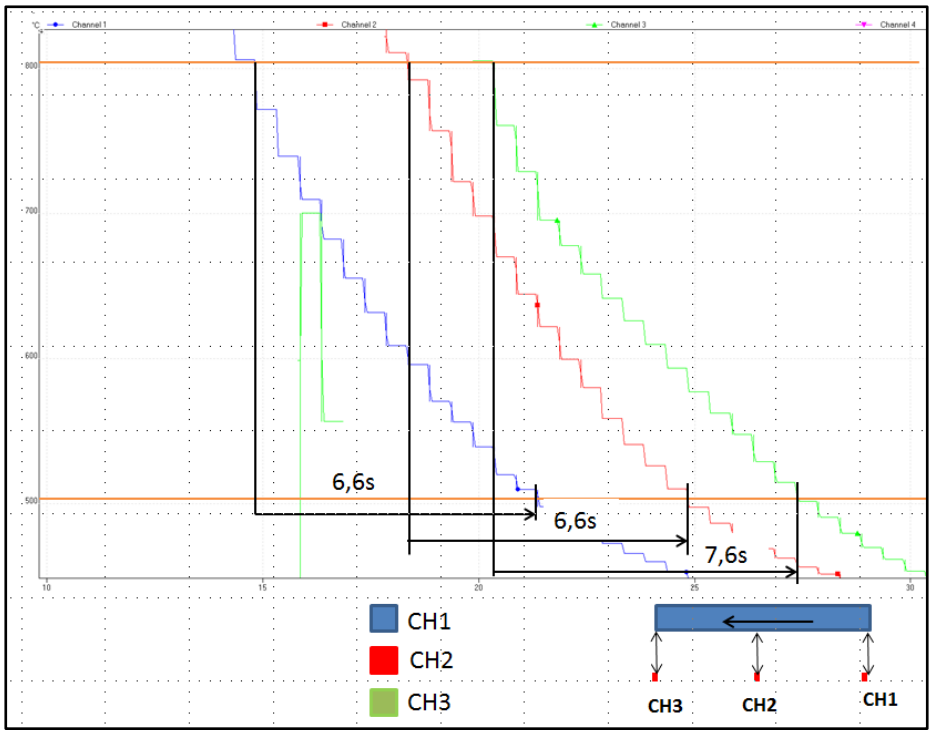

Figure 4.10: T8/5 for welding 40 mm S690QL preheated to 100°C

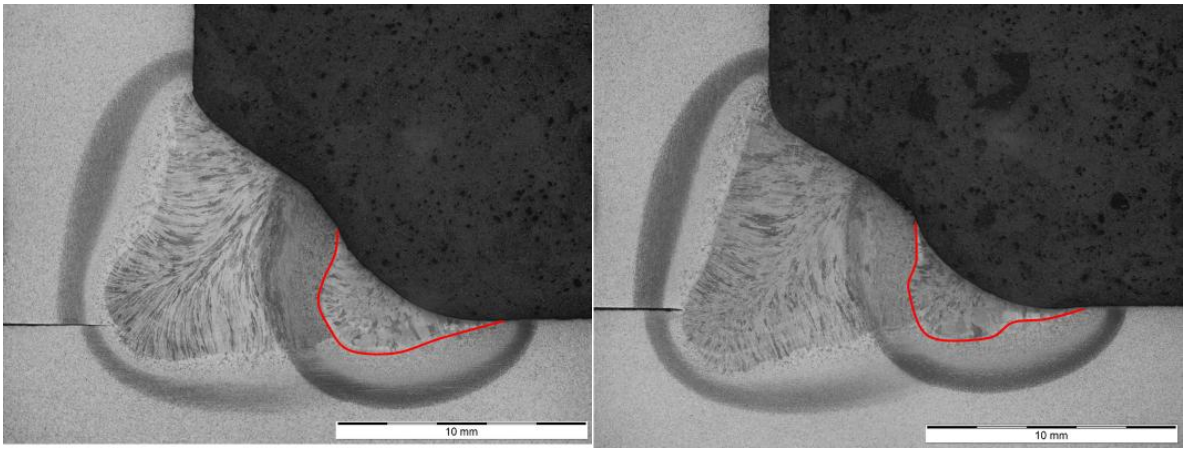

Figure 4.11: GTAW dressed weld toe, 25mm (left) and GTAW dressed weld toe, 40mm (right)

WP 4.3: Generation of beams with transverse stiffeners

The BWI interacted with Ustutt and Industeel to define the exact geometry of the beams with transverse stiffeners. The capacity of the fatigue testing machine of UStutt (in terms of maximum force) and the machine dimensions were taken into account for the determination of the dimensions of the beams. The technical drawing is shown in annex 6.

The beams are welded by subcontractor Iemants, using the SAW welding process for the longitudinal weld, and MAG welding for the transverse stiffeners. (see Fig. 4.12)

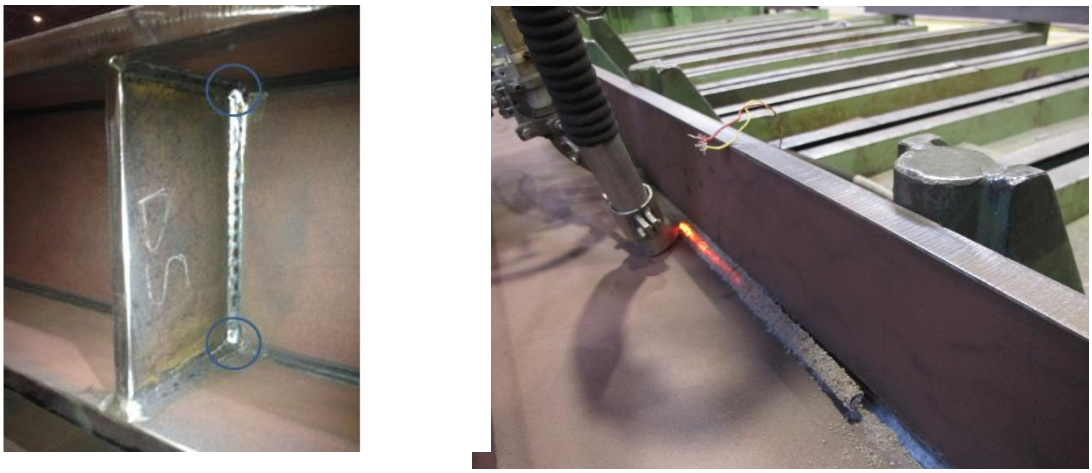

Figure 4.12:MAG welding on transverse stiffener, with weld imperfections where weds come together. (left) and SAW welding of the longitudinal weld (right)

WP 4.4: Post weld treatment qualification

For this work package post mortem analysis was carried out for a series of fatigue tested welded and post weld treated samples.

Part of the samples for this part of the work have come from a different project, but the post-weld treatment was also via Pneumatic Impact Treatment. Table 4.1 shows the different PIT parameters, these were intentionally taken well beyond the supplier's recommended parameters, to analyse the robustness of the process. The fatigue results obtained with these different parameters are shown in Fig. 4.13.

Table 4.1: Conditions and different PIT parameters (on longitudinal stiffeners)

Condition	PIT parameters
1	6 bar, 90 Hz, r=2mm
2	6 bar, 90 Hz, r=4mm
3	6 bar, 90 Hz, r=1.5mm
4	6 bar, 120 Hz, r=2mm
5	4 bar, 90 Hz, r=2mm

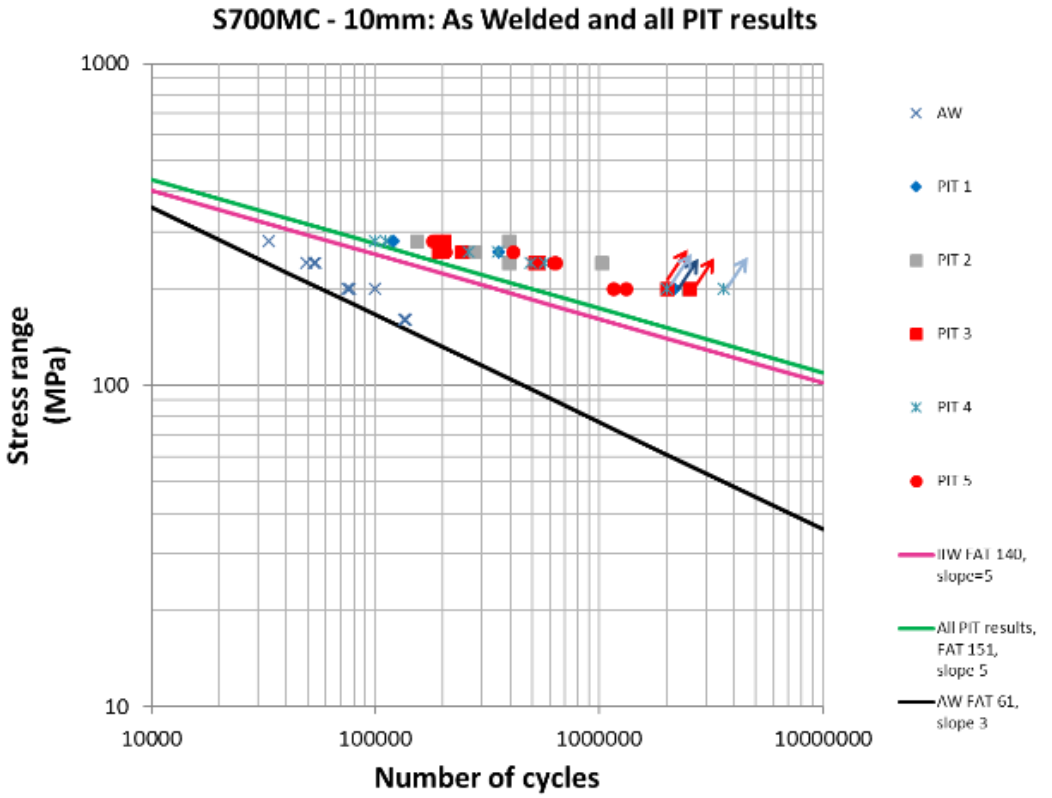

Figure 4.13: Fatigue results on S700MC. 10mm longitudinal stiffener, PIT treated.

The different PIT parameters have resulted in very similar improvements in fatigue life, indicating that the technique is very robust, and that deviations from the recommended parameters do not affect the end result much.

However, the post-mortem analysis on the OPTIBRI samples have shown that the fatigue crack often starts in the treatment zone (see example in Figs. 4.14 for PIT treatment, 4.15 for GTAW treatment).

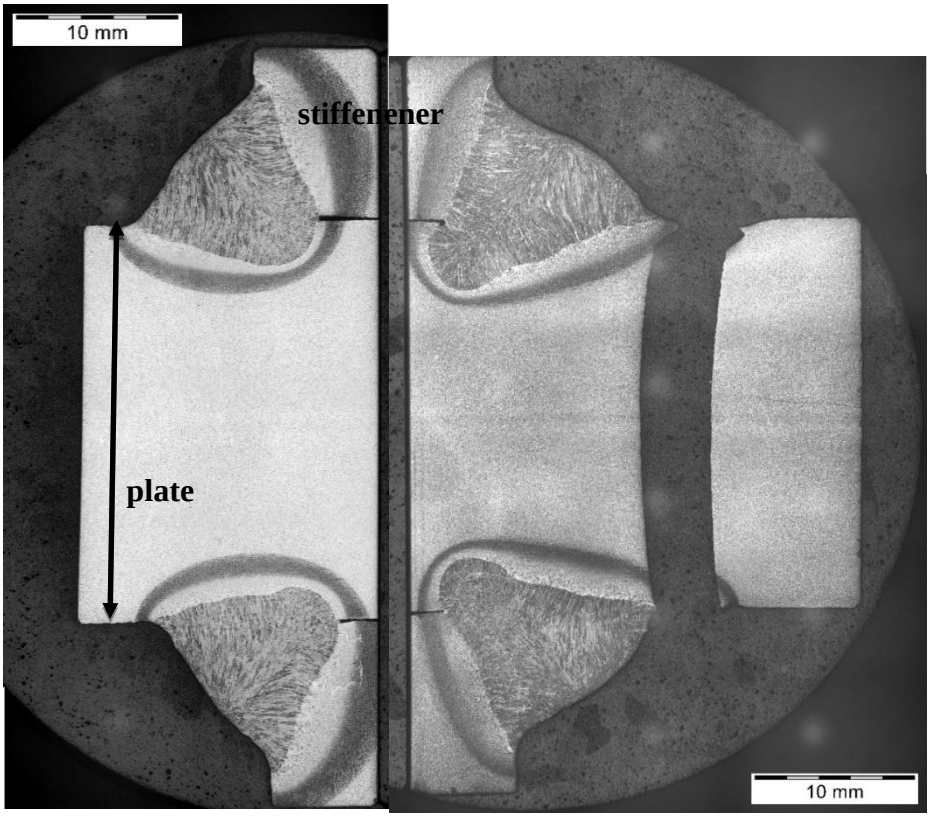

Figure 4.14: Sample SCA1 (PIT treated), crack along the peening line, fracture of the plate started in the zone of post-weld treatment

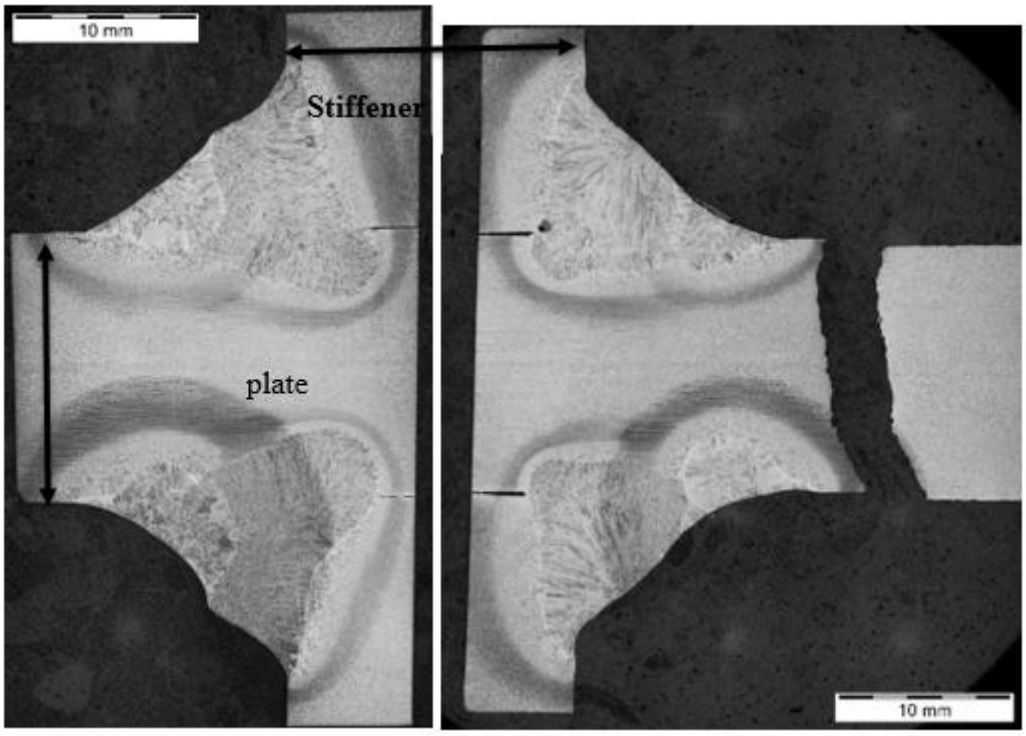

Figure 4.15: Sample SCC1 (GTAW treated), cracked at one side, going into the base material. Fracture of the plate started in the HAZ of GTAW treatment

Conclusions of WP4

It has been shown that, by replicating the thermal cycle, as measured on the actual welded joint, it has been possible to recreate samples where material characteristics of a certain area of the heat affected zone of the welded attachment can be obtained in a homogeneous zone of relative size (>10mm length). This method could be used for other applications (damage modelling, weld structure/properties modelling).

Welding of HSS Supralsim S690QL, both in a laboratory environment, and in a company workshop, has been found to be quite straightforward, with very limited preheat (only necessary for the thicker material). The time needed to carry out the post-weld heat treatment (in the industrial case) was very limited compared to the actual welding procedure, inspection and repair time.

However, it has been found, in the post-mortem analyses of the fatigued specimens, that the fatigue crack often does start in the treated area. This is something that needs to be analysed further, to see if improvements and/or adaptations of the treatments can avoid this.

WP 5: Impact of bridge design

The main aim of Work Package 5 is to provide an appropriate methodology for the lifetime assessment of High Strength Steel (HSS) bridges, from bridge construction to the end-of-life stage, taking into account structural, environmental and cost criteria. Divided in 4 steps this Work Package 5 will perform researches related to HSS bridges then will cover systematically the difference between Design A, B and C of the studied bridge cases, namely:

WP 5.1: Life cycle performance (LCP)

- To estimate the life cycle performance of HSS bridges by the definition of a deterioration curve for bridge structural performance, focussing on the fatigue behaviour;
- To established an appropriate general maintenance plan for HSS bridges, in order to keep the bridge above the required condition over its life cycle.

Since HSS bridges have a higher risk of fatigue problems in the girders, the life cycle performance analysis focuses on the fatigue behaviour.

Over the bridge life cycle, the structure deteriorates and this is a critical aspect in lifetime analysis of bridges. Without proper maintenance, the condition of a bridge may reach an unacceptable condition level (Cf) long before the required service life (SL), as illustrated in Fig. 5.1 [48].

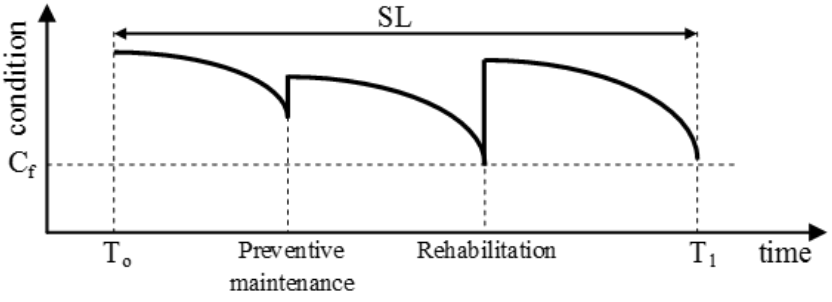

Figure 5.1: Structural behaviour over time [48]

Therefore, a key point in this WP was to estimate the time the bridge needs to be intervened (i.e. to establish the trigger point for intervention) so that relative impacts due to the use of materials, traffic congestion and costs may be estimated. In this WP5.1 the general framework for life cycle assessment is described for the life cycle performance of the bridge from the structural perspective. As already referred, the focus is on the fatigue assessment of the bridge. A software tool was also developed for the assessment of bridges.

WP 5.2: Life cycle environmental assessment (LCA)

- To establish the system boundaries for the life cycle analysis of HSS bridges;
- To collect appropriate data for the environmental analysis;
- To select the relevant environmental impact categories for life cycle assessment;
- To identify the most critical processes over the life cycle of bridges and to propose strategies for further life cycle improvement.

The evaluation of the environmental criteria over the life cycle follows the guidance from ISO standards ISO 14040 (2006) [49] and 14044 (2006) [50]. According to this set of standards, the evaluation comprehends four main steps, as represented in Fig. 5.2. However, in the proposed approach, two additional steps are added: normalization and weighting. These two steps are considered to be optional in ISO standards. Thus, the complete flowchart for the environmental life cycle analysis is represented in Fig. 5.2.

Figure 5.2: Scheme of the environmental life cycle analysis [50]

The first step defines the main goal of the analysis and the boundaries of the stage, i.e., the processes that are included in the analysis. The collection of all data needed for the environmental analysis is done in the second step. This WP5.2 focuses on the impact assessment stage. The selected indicators are described and calculation methods are introduced for its evaluation. Normalisation and weighting are here considered as two procedures of the same goal. In a decision making process, taking any decision based only in the results of the impact assessment analysis is a very complex task. Normalisation is in itself a process of weighting, as the result of an impact category is compared with a reference value of the same impact category. By means of a normalisation process, the relative importance of each impact is therefore enhanced. However, the comparison between impact categories is not taken into account in a normalisation procedure. Thus, weighting is further introduced to fulfil this aim. As already referred, these two steps are considered optional and are not further addressed in this research. Finally, in the interpretation step, the results of the environmental analysis are reviewed and complementary analyses are performed to check the consistency of the results.

WP 5.3: Life cycle cost (LCC) analysis of HSS bridges

- To collect appropriate data for the life cycle cost analysis;
- To develop a mathematical model to account for bridge deterioration and costs;
- To identify the most critical processes over the life cycle of bridges and to propose for improvements.

The lifecycle cost analysis (LCCA) has the same boundary system of the environmental analysis described in the previous chapter. Lifecycle cost calculations are based on data collected per unit process in the inventory stage.

The costs to be considered in the life cycle analysis (Eq. 5.1) may be divided into three main groups: (i) the construction costs (CC), (ii) the operation costs (OC), and (iii) the end-of-life cost (EC), as expressed by:

$$LCCA = CC + OC + EC \tag{5.1}$$

where, OC includes the costs of maintenance and rehabilitation of the bridge over the service life; and EC includes the costs of demolition and disposal minus the residual value of the structure at the time of decommission. Each of these costs are described in the deliverables D5.1 and D5.4.

WP 5.4: Application to case studies

- To apply the developed life cycle approach to the bridges analysed in WP1;
- To highlight the advantages by the use of HSS in the lifetime performance of bridges.

In this WP5.4 it is applied all previous models on the 3 bridge designs A, B and C established by GRID. Accurate application of the developed life cycle approach to the 3 bridges designed in WP1. The case studies will take into account the lifetime performance of the bridge, environmental and cost criteria. The results of the case studies will enable to identify the most critical processes in the lifetime behaviour of HSS bridges, contributing to the writing of design guidelines for optimal use of HSS bridges (see WP1.5). The results of this work package will also be used for the dissemination of the main achievements of the project.

Principal Outputs

Taken into account the activities developed in this Work Package 5, several deliverables were accomplish:

- Deliverable D 5.1: Report on "A life cycle methodology applicable for HSS bridges"

In this deliverable D5.1 the life cycle methodology to assess the performance of the bridge over its service life is described. The proposed approach enables to make the assessment of steel and/or composite bridges made from conventional steel grade and/or high strength steel grade. Furthermore, the proposed approach enables to compare different bridge solutions, i.e. bridges made from conventional steel and high strength steel, so that the advantages of the latter may be highlighted and promoted.

- Deliverable D 5.2: Report on "Identification of main advantages of HSS bridge compared to classical bridge design and effect of using Eurocode or true material behaviour"

This deliverable D5.2, summarizes the main advantages of the use of high strength steel in bridges based on the findings in WP 5.4. In WP 5.4, Lifecycle analysis was carried out on the 3 bridges designed by GRID in WP1, from the construction, over the operation and maintenance stage, until the demolition at the end-of-life. With the goal of identifying the possible advantages of using HSS, the same bridge was designed in three different ways: the first with conventional steel grade of S355 and the latter two in high strength steel of grade S690. Emphasis was placed on the steel structure as the rest of the system in all the three bridges the same in every case.

- Deliverable D 5.3: Report on "General guidelines for the lifetime assessment of HSS"

In this deliverable D5.3, general guidelines are provided for the lifetime assessment of High-Strength Steel (HSS). The lifetime assessment of the bridges includes the environmental, cost and social aspects of the bridges. LCA was carried out on three bridges of the same configuration except differences in details and material grades in WP5.4.

- Deliverable D 5.4: Report on "The comparison of Designs A, B and C through LCA, LCC, LCP analyses"

This deliverable D5.4 focuses on the entire lifecycle of the 3 bridges designed by GRID in WP1, from the construction, over the operation and maintenance stage, until the demolition at the end-of-life. The LCP of the bridges was considered in the design and is guaranteed by assuring that the fatigue life of structural details is sufficient enough to cover the full life span of the bridges. And the effect of corrosion is handled by providing sufficient inspection and maintenance of the protection layers as proposed in the standard maintenance scenario.

Conclusions of WP5

Given the lack of specific inventory data for high-strength steel, LCA was performed on the three bridges with two approaches. First, the analysis was carried out using the LCI obtained from GaBi (based on worldsteel data). This database of impacts does not differentiate between steel grades. Hence, the LCI for steel plates was used to assess the environmental impacts related to the three bridges. This assumes that the two steel grades share the same impact factors. Although this may not reflect exactly reality, the comparisons made with this assumption led to a reference case.

Given the mentioned assumption, it was found out that design options B and C cause 22.5% and 29.2% less environmental impacts, respectively, as compared to design A .

However, further sensitivity analyses were performed to gain additional confidence in the LCA. The sensitivity analysis was carried out by making the LCI for steel plates as a reference value representing the impacts of S355 steel production in a blast furnace. The impact factors of this reference steel plate were gradually increased in steps of 5% until the design options B and C reached the same LCA impacts as design option A, therefore investigating how much increase in the impact factors would be necessary to make the design options B and C, that were proven to be better in section, equally favourable as design A, the reference design, from the environmental point of view. The result was that bridge B and C would have the same environmental impact as design A only if HSS 690 steel would have 33.04% and 47.04% more impacts in every category, respectively, as compared to the reference, which was taken as S355. Since these increases are unrealistic, this clearly highlights the environmental advantages of using higher steel grades.

In terms of LCC, It was observed that the bridge design B would practically cost the same as design A, seen from a holistic lifecycle cost point of view. However, design C that uses high strength steel girders with post-weld treatment and improved design specifications proved to be 5.1% cheaper. A 7.6% reduced initial cost and 2.7% cheaper operation costs were calculated in design C as compared to design A.

The costs incurred on the users of the bridge during maintenance of the bridge throughout the lifespan are studied in the LCS analysis. As a direct consequence of the reduced steel surface area in designs B and C, lower maintenance duration, thereby lower user costs were calculated. Designs B and C were found to be 2.2% and 3.2% cheaper alternatives as compared to design A, respectively.

Clear advantages had already been seen in the early stages of the design as a significantly reduced amount of steel is required when using high-strength steel. Reduction of the steel volume is achieved by using HSS. And even more reduction is possible by using longitudinal stiffeners in place of vertical ones.

In summary, the following advantages were identified for high-strength steel:

- *LCA – Better environmental performance due to the reduction volume of steel required and subsequent reduction in welded joint volumes.*
- *LCC – Cheaper as a result of the lighter structures achieved and the use of improved knowledge on the structural behaviour of HSS*
- *LCS – reduced user costs as a result of reduced maintenance operations comes as a direct result of reduced surface are of the steel that requires corrosion protection*

Clear advantages had already been seen in the early stages of the design as a significantly reduced amount of steel is required when using high-strength steel. Reduction of the steel volume is achieved

The following paragraphs list the guidelines associated with the use of HSS as extracted from the experience gathered through the analysis done, organized according to the three dimensions of sustainability: environmental, economic and social.

From the lifecycle environmental analysis point of view, the use of high-strength steel in bridges was found to be advantageous in that significantly reduced steel volume is required when using HSS. Given the higher resistance of the material, relatively smaller dimensions (thickness and width) of steel plates were required to carry an equivalent design load. Consequent to the reductions in size mentioned above, the welding volumes, particularly related to butt welded joints, were also reduced. This caused reduced impacts in electricity use and emissions related to welding consumables. Apart from the plate girders, the type and configuration of the stiffeners played an important role in achieving better performance.

From the lifecycle costs analysis point of view, the relatively higher costs associated with the production of high-strength steel are well compensated by the reduction in steel volume. It was found out from the analyses made in WP5.4 that a bridge solution designed with high-strength steel can have practically the same LCC as those designed from conventional steel. Provided further refinement, it was proved that the HSS solution could even be cheaper.

From the lifecycle social analysis point of view, the user costs are usually associated with the maintenance operations carried out on a bridge throughout its service life. The fact that reduced sizes of plates can be achieved in using HSS has its own implication on the user costs. The lower the size of the structural steel, the lower the surface area that requires maintenance actions regarding corrosion protection layers in the operation stage of the bridge. This in turn reduces the number of days for maintenance which will pave a way to reduced user inconveniences and costs. In addition, for motor way bridges that cross highways, the smaller welded joint volumes achieved by using HSS will result in faster construction time thereby improving user convenience on the highway and lowering costs.

WP 6: Result dissemination

WP 6.1: Promotion of HSS

The results of the research programme were presented and discussed in important organizations and/or for the steel sector (e.g. European Convention for Constructional Steelwork (ECCS) and European Steel Technology Platform (ESTEP), in which the partners of the project are actively involved.

Partners contributed for the publication of scientific papers in scientific journals and conferences namely: 14th International Conference on Fracture (ICF 14), 2017, Rhodes, Greece; German seminar on steel structures "Stahlbaukalendertag 2017", Stuttgart, Germany; Eurosteel 2017, The 8th European Conference on Steel and Composite Structures, 2017, Copenhagen, Denmark; National Congress on steel and composite structures CMM 2017, Coimbra, Portugal; Conference organised by BWI, 2017.

WP 6.2: Implementation of a webpage

A webpage was implemented in the European Convention for Constructional Steelwork (ECCS) web site (https://www.steelconstruct.com/site/) for the public dissemination of the main results of the research programme.

A private part in this website was created for the organization of internal documents and project deliverables during the execution of the research programme. This private part can be accessed only by the partners of the project.

This web site publish news, international and national events organized by the partners, information and documents of the meetings, Partners, Members and documents.

WP 6.3: Organisation of a European Seminar

In order to disseminate the current state of the project and discuss the latest findings with interested designing engineers and scientific researchers a European seminar with the title "Design Guidelines for Optimal Use of HSS in Bridges" was organized. It took place at the University of Stuttgart in May 2017 and was thus mainly organized by project partner UStutt.

The content of this disseminative OptiBri-Workshop was discussed with all project partners and fixed in the frame of project meeting in January 2017 in Coimbra.

M. Habraken/University Liège:

Opening and Project-Overview

J. O. Pedro/GRID:

Challenges and Benefits of High Strength Steel (HSS) in Highway Bridges

P. Toussaint/Industeel:

Usual Application of High Strength Steel (HSS) Plates with Focus on S690

T. Baaten/Belgian Welding Institute:

Welding and Post-Weld Treatments of High Strength Steel (HSS) Joints

C. Bouffioux/University Liège:

Characterization of Fatigue Behavior, from Material Science to Civil Engineering Applications

S. Breunig/University of Stuttgart:

Categorization of Fatigue Details in View of Post-Weld Treatments

V. Pourostad/University of Stuttgart:

Buckling Behavior of Slender Plates under Multiaxial Stresses

C. Baptista /GRID:

Improved Bridge Design by Use of High Strength Steel (HSS) with OPTIBRI Developments

C. Rigueiro/University Coimbra:

Comparative Life-Time Assessment of the Use of High Strength Steel (HSS) in Bridges

M. Habraken/University Liège:

Conclusions and Closure

Therefore every project partner prepared a presentation and a corresponding handout concerning its latest results. The presentations and handouts were collected, printed and were used as seminar documents and spread to the participants in form of a ring binder.

The invitation in form of a seminar flyer (see Fig. 6.1) was sent by all project partners to possible interested engineers of industry, universities and building authorities. In sum 29 participants took part, so that a small but specialised audience came together.

Figure 6.1: Seminar flyer

Besides the distribution to the OptiBri-Workshop participants, the seminar documents were spread within a German seminar organized by the Institute of Structural Design. The "Stahlbaukalendertag" is a seminary day, where the content of the present "Stahlbaukalender" are presented by the main-authors. This seminar addresses mainly German engineers, which are interested in latest developments in guidelines and latest research results on steel structures. This year, 2017 there were 170 to 200 participants.

Exploitation and impact of the research results

The project confirms the possibility of decreasing the amount of steel volume by using HSS in bridges, even without enhanced Eurocode. In case of improved Eurocode, the advantages are increased. Note that both the environmental and the cost aspects have been demonstrated.

Due to partners involvement within Eurocode definitions, the project results will be proposed within the related expert committees.

Simões da Silva (UC) and Prof. KUHLMANN (USTUTT) are very active within Portuguese Association for Steel and Composite Construction, the Technical Management Board of ECCS, the TC8 "Stability", TC10 "Connections" of ECCS, TC14 "Sustainability & Eco-Efficiency of Steel Construction", Eurocode 3 - Steel Structures and National Portuguese Annexes of EN1993-1 and 2, CEN/TC250 SC3 Steel Structures, TC6 "fatigue" and TC11 "composite structures" of ECCS.

The dissemination of results has already begun through a dedicated seminar, conferences, journal publications, PhD dissertations are foreseen and will go on.

Dissemination

[1] Department day (poster session), 2 May, 2017, ArGEnCo department, ULiège, Liège, Belgium
A.M. Habraken, C. Bouffioux, L. Duchêne
http://hdl.handle.net/2268/212876

[2] Optibri Workshop, 3 May, 2017, UStutt, Stuttgart, Germany
Design Guidelines for Optimal Use of HSS in Bridges

[3] Distribution of the Optibri workshop documents to the 170-200 participants of the German seminar on steel structures "Stahlbaukalendertag 2017", 23 June 2017, Stuttgart, Germany, organized by USTUTT
https://www.uni-stuttgart.de/ke/konferenzen/stbkalender/beschreibung/

Publications

Conferences

[1] 14th International Conference on Fracture (ICF 14), 18-23 June, 2017, Rhodes, Greece
C. Bouffioux, C. Canales, L. Duchêne, J.P. Ponthot and A.M. Habraken
Fatigue crack propagation in HSS S690QL welded connections in bridges
http://www.icf14.org/

[2] Eurosteel 2017, The 8th European Conference on Steel and Composite Structures, 13-15 September 2017, Copenhagen, Denmark
José Oliveira Pedro; António Reis; Cláudio Baptista
High Strength Steel (HSS) S690 in highway bridges – Comparative design
http://www.eurosteel2017.dk/

[3] Eurosteel 2017, The 8th European Conference on Steel and Composite Structures, 13-15 September 2017, Copenhagen, Denmark
Antonio Zizza, Vahid Pourostad, Ulrike Kuhlmann
Investigations on the Buckling Behaviour of Slender Plates under Multiaxial Stress
http://www.eurosteel2017.dk/

[4] Portuguese XI Congress of Steel and Composite Structures, CMM2017, 23-24 November 2017, Coimbra, Portugal
J. O. Pedro; C. Vieira; C. Baptista; A. J. Reis; F. Virtuoso
Dimensionamento de Tabuleiros Rodoviários Mistos Aço-Betão utilizando o Aço de Alta Resistência S 690 QL
https://www.cmm.pt/event/event/home/index.php?target=home&event=16&defLang=1)

[5] Symposia Innovative Entwicklungen im Stahl- und Verbundbrückenbau. Neues aus Forschung und Praxis. Essen, in 06 June, 2018, organized by Fosta & Stahl
José J. Oliveira Pedro;António J. Reis
High Strength Steel (HSS) S690 in Highway Bridges – Comparative Design
https://verbundbruecken.de/files/verbundbruecken2018.pdf

[6] Breunig, S., Kuhlmann, U.: Anwendung höherfrequenter Hämmerverfahren im Stahl- und Verbundbrückenbau, 3. Brückenkolloquium – Beurteilung, Ertüchtigung und Instandsetzung von Brücken, 19th - 20th of June 2018, Stuttgart.

[7] Abstract submitted to IALCCE 2018 - The Sixth International Symposium on Life-Cycle Civil Engineering, 28-31 October 2018, Ghent, Belgium,
Helena Gervásio, Constança Rigueiro, Luis Simões da Silva, Carlos Rebelo, José Oliveira Pedro
Life cycle performance of HSS bridges
http://www.ialcce2018.org/#/home

Journal

[1] STAHLBAU Vol. 87-6, June 2018, pp 555-564,
José J. Oliveira Pedro; António J. Reis, Cláudio Baptista
High Strength Steel S690 in Highway Bridges – General Guidelines for the Design
https://doi.org/10.1002/stab.201810615

[2] Publication in journals to large technical audience (Lastechniek – Metallerie), in Dutch/French – to be submitted (BWI) http://www.bil-ibs.be/lastechniek

3. List of Figures

4. List of tables

5. Acronyms and abbreviations

- BM: Base Material
- EIO-LCA: Environmental Input-Output Life Cycle Assessment
- FEM: Finite Element Method
- GLCFM: Gradient Lemaître & Chaboche Fatigue Model
- HAZ: Heat Affected Zone
- HFMI: High Frequency Mechanical Impact
- HSS: High Strength Steel
- IIW: International Institute of Welding
- LCA: Life Cycle environmental assessment
- LCC: Life Cycle Cost
- LCP: Life Cycle Performance
- LCS: Life Cycle Society
- LTT: Low Transformation Temperature
- PFM: Probabilistic Fracture Mechanics
- PIT Pneumatic Impact Treatment
- UIT: Ultrasonic Impact Treatment
- ULS: Ultimate Limit State
- SLS: Serviceability Limit State
- WM: Weld Metal
- TIG: Tungsten Inert Gas – used for TIG dressing
- UC: University of Coimbra
- ULiège: University of Liège (Previously called ULg)
- UStutt: University of Stuttgart

6. References

[1] EN 1994-2 (2005). "Design of Composite Steel and Concrete Structures – Part 2: General rules and rules for bridges". CEN, Brussels.

[2] EN 1993-1-5 (2006). "Eurocode 3: Design of steel structures – Part 1-5: Plated structural elements". CEN, Brussels.

[3] EN10025.3 (2003). "Hot rolled products of structural steels - Part 3: Technical delivery conditions for normalized/normalized rolled weldable fine grain structural steels". CEN, Brussels.

[4] EN10025-6 (2004). "Technical delivery conditions for flat products of high yield strength structural steels in the quenched and tempered condition". CEN, Brussels.

[5] EN 1992-1 (2004). "Eurocode 2 - Design of concrete structures - Part 1: - Part 1-1: General rules and rules for buildings". CEN, Brussels.

[6] EN 10080 (2005). "Steel for the reinforcement of concrete". CEN, Brussels.

[7] EN ISO 13918 (2008). "Welding — Studs and ceramic ferrules for arc stud welding". ISO, Switzerland.

[8] EN 1991-2 (2003). "Eurocode 1: Actions on Structures – Part 2: Traffic loads on bridges". CEN, Brussels.

[9] EN1991.1.5 (2009). "Eurocode1: Actions on Structures – Part 1-5: General actions. Thermal actions". CEN, Brussels.

[10] Beg D., Kuhlmann U., Davaine L., Braun B. (2010). "Design of Plated Structures". ECCS Eurocode Design Manuals, Ernst & Sohn.

[11] Lee S.C., Yoo C.H., Yoon D.Y. (2003). "New design rule for Intermediate Transverse Stiffeners Attached on Web Panels", Journal of Structural Engineering, ASCE, vol. 129-12, pp. 1607-14.

[12] Xie, M., Chapman, J.C. (2003). "Design of web stiffeners: axial forces" – Journal of Constructional Steel Research 59.

[13] Kim Yoon Duk (2004). "Transverse stiffener requirements in straight and horizontally curved steel I-Girders", Georgia Institute of Technology.

[14] Presta F., Hendy C., Turco E. (2008). "Numerical validation of simplified theories for design rules of transversely stiffened plate girders", The Structural Engineer, nº4, pp. 37-46.

[15] Sinur F., Beg D. (2012). "Intermediate transverse stiffeners in plate girders", Steel Construction – Design and Research 5, n.º1, pp. 23-32.

[16] Johansson B., Maquoi R., Sedlacek S., Müller C., Beg D. (2007). "Commentary and worked examples to EN 1993-1-5 Plated Structural Elements". ECCS, European Convention for Constructional Steelwork.

[17] SIA260 (2003). "Bases pour l'élaboration des projets de structures porteuses, Société suisse des ingénieurs et des architectes". Zurich.

[18] EN 1993-1-9 (2009). "Eurocode 3: Design of Steel Structures – Part 1-9: Fatigue". CEN, Brussels.

[19] EN 1993-2 (2006). "Eurocode 3: Design of Steel Structures – Part 2: Steel bridges". CEN, Brussels.

[20] Nussbaumer A., Borges L., Davaine L. (2011). "Fatigue Design of Steel and Composite Structures". ECCS European Convention for Constructional Steelwork.

[21] SETRA (2007). "Eurocodes 3 and 4 – Application to steel-concrete composite road bridges". Paris.

[22] EN 1993-1-10 (2009). "Eurocode 3: Design of Steel Structures – Part 1-10: Material toughness and through-thickness properties". CEN, Brussels.

[23] Lagamine user's manual, University of Liège, 2017.

[24] PostLag_Dam user's manual, University of Liège, 2017.

[25] Flores, P., Rondia, E., Habraken, A.M., 2005. Development of an experimental equipment for the identification of constitutive laws. Int. J. Forming Processes (Special Issue), 117–137.

[26] Massonet, C.. Résistance des matériaux, Vol. II, Sciences et Lettres, Liège.

[27] Chang, K.H., Jang, G.C., Park, C.M., Gil, H.B., 2009. Strain-rate dependence of mechanical behavior and hysteretic characteristics of TMCP steel (SM570-TMC) and its modeling Computational Materials Science, vol. 45, pp. 669-673.

[28] Lamarche, C-P., 2009. Development of real-time dynamic substructuring procedures for the seismic testing of steel structures, PhD Thesis, Ecole Polytechnique de Montreal.

[29] HITUBES, RFCS project, 2012. Design and Integrity assessment of High Strength Tubular Structures for Extreme Loading Conditions. http://hdl.handle.net/2268/161260.
[30] Lemaitre, J., Chaboche, J.-L., 1996. Mécanique des matériaux solides, Dunod.
[31] Gurney, T. R.: The fatigue strength of transverse _llet welded joints. Cambridge :Abington, 1991
[32] Helms, R. ; Jaenicke, B. ; Wohler, H. ; Bork, C.-P.: Zur Schwingfestigkeit großer geschweißter Stahlträger / Bundesanstalt für Materialforschung und -prüfung (BAM),Forschungsbericht 164. 1989
[33] Duerr, A. (2006). Zur Ermüdungsfestigkeit von Schweißkonstruktionen aus höherfesten Baustählen bei Anwendung von UIT-Nachbehandlung. Dissertation Mitteilung Nr. 2006-3, Institute of Structural Design, University of Stuttgart.
[34] Breunig, S.,in preparation. Bewertung der Ermüdungsfestigkeit von Schweißnähten und ihrer Nachbehandlung im Brückenbau, Dissertation.
[35] Kuhlmann, U., Bergmann, J., Duerr, A., Thumser, R.: Effizienter Stahlbau aus höherfesten Stählen unter Ermüdungsbeanspruchung, FOSTA P620, AiF-Schlussbericht, 2006.
[36] Sedlacek, G., Hobbacher, A., et al, Commentary to Eurocode 3: EN 1993 – Part 1-9 – Fatigue. First Edition, 2007.
[37] DIN EN ISO 6892-1: Dezember 2009: Metallische Werkstoffe – Zugversuch – Teil 1: Prüfverfahren bei Raumtemperatur (ISO 6892-1:2009); ISO Norm.
[38] DIN 50125: Juli 2009: Prüfung metallischer Werkstoffe – Zugproben,DIN 50125.
[39] EN 1090-2: 2008: Execution of steel structur es and aluminium structures – Part 2: Technical requirements for the execution of steel structures, European Committee for Standardization, Brussels.
[40] Simulia., 2011. Abaqus Scripting User's Manual. Dassault Systèmes.
[41] Zizza, A., 2016. Buckling Behaviour of Unstiffened and Stiffened Steel Plates Under Multiaxial Stress States, Dissertation, Mitteilung Nr.2016-1, Institute of Structural Design, University of Stuttgart.
[42] Lindner, J., Rusch, A., 2000. Grenz (b/t)-Verhältnisse in Abhängigkeit der Belastung unter besonderer Berücksichtigung von Imperfektionen [Schlussbericht zum DIBt-Forschungsvorhaben P 32-5-16.91.32-965/00]. Stuttgart: Fraunhofer IRB Verlag.
[43] Braun, B., 2010. Stability of steel plates under combined loading. Dissertation. Mitteilung Nr. 2010-3, Institute of Structural Design, University of Stuttgart.
[44] Sinur, Franc (2011): VZDOLŽNO OJAČANI POLNOSTENSKI NOSILCI PRI INTERAKCIJI VELIKIH UPOGIBNIH IN STRIŽNIH OBREMENITEV. EN: BEHAVIOUR OF LONGITUDINALLY STIFFENED PLATE GIRDERS SUBJECTED TO BENDING-SHEAR INTERACTION. Dissertation. University of Ljubljana.
[45] EBPlate 2.01, CTICM, Piece of Software for the determination of elastic critical stresses in plates. EBPlate can be downloaded for free from www.cticm.com.
[46] EN 1990: 2002: Eurocode 0: Basis of structural design, European Committee for Standardization, Brussels.
[47] Kuhlmann, Ulrike; Pourostad, Vahid; Zizza, Antonio (2018): Optimal use of High Strength Steel grades within bridge OPTIBRI. WP.3. Buckling of multiaxially stressed plates - Deliverable D3.2. Report of the numerical investigations and proposal for the improvements of the design according to reduced stress method.
[48] M. Ryall, Bridge management. Butterworth-Heinemann, 2001.
[49] ISO 14040 Environmental management – life cycle assessment – Principles and framework, Geneva, Switzerland: International Organization for Standardization, 2006
[50] ISO 14044 Environmental management – life cycle assessment – Requirements and guidelines, Geneva, Switzerland: International Organization for Standardization, 2006.

7. Appendices

Annex 1: Geometries of the small case specimens

Table A.1.1: Plates and welded plates called "small cases"- dimensions (mm)

		Plate								Stiffeners		
Case	**Post-tr.**	**Wt**	**Wm**	**Ww**	**Wl**	**R**	**Lc**	**Lt**	**La**	**Stt**	**Stw**	**Sth**
Plate	-	25	135	235	1070	700	60	260	245	-	-	-
A	PIT	25	135	235	1070	700	60	260	245	15	60	40
B	PIT	15	105	235	1070	600	60	272	233	15	60	40
E	PIT	25	60	235	1070	400	60	250	255	15	60	40
H	PIT	40	60	235	1070	400	60	250	255	15	60	40
C	TIG R.	15	105	235	1070	600	60	272	233	15	60	40
D	TIG R.	25	135	235	1070	700	60	260	245	15	60	40
F	TIG R.	25	115	235	1070	600	60	262	243	15	40	40
G	TIG R.	15	105	235	1070	600	60	272	233	6	60	40
I	No	15	105	235	1070	600	60	272	233	15	60	40

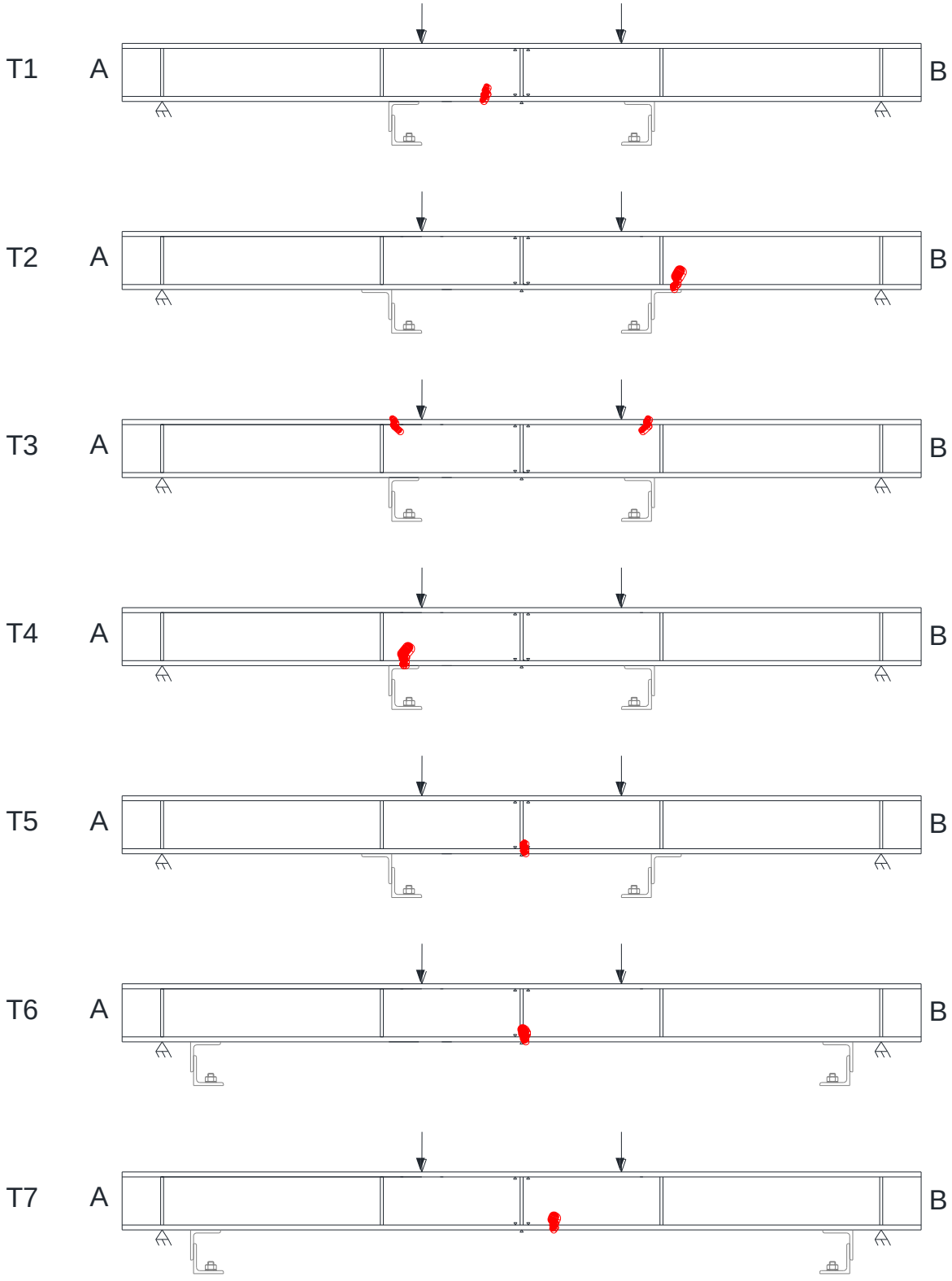

Figure A2.1: Overview of position of cracks at the beams T1 to T7

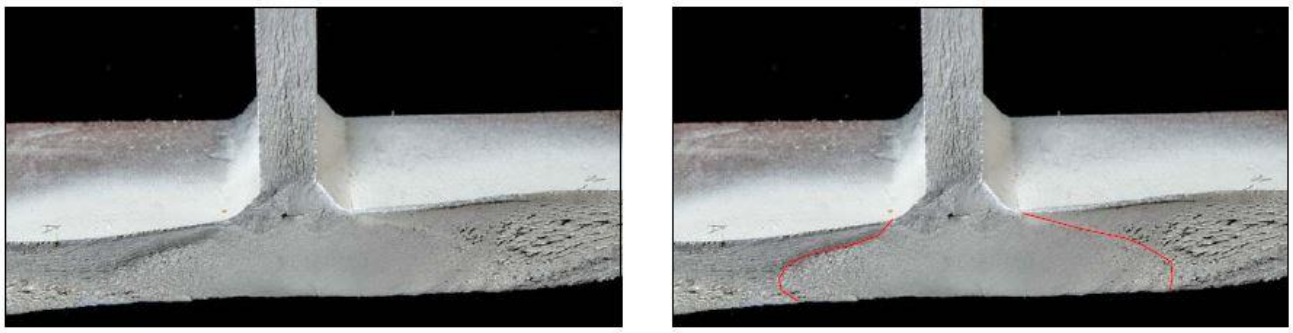

Figure A2.2: Crack surface - Specimen T1

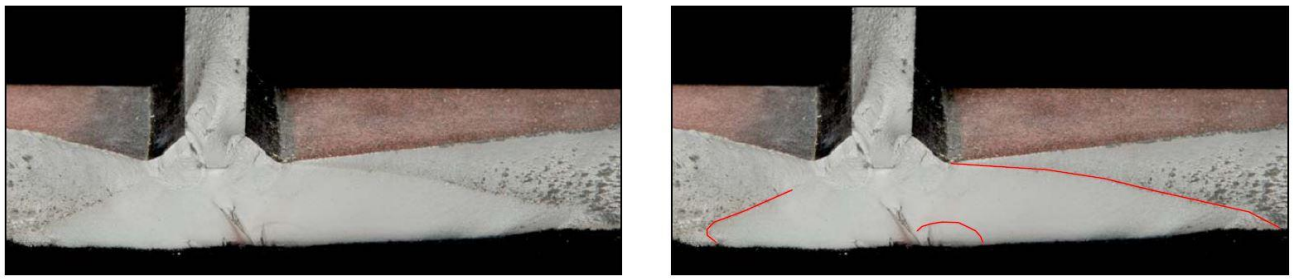

Figure A2.3: Crack surface – Specimen T2

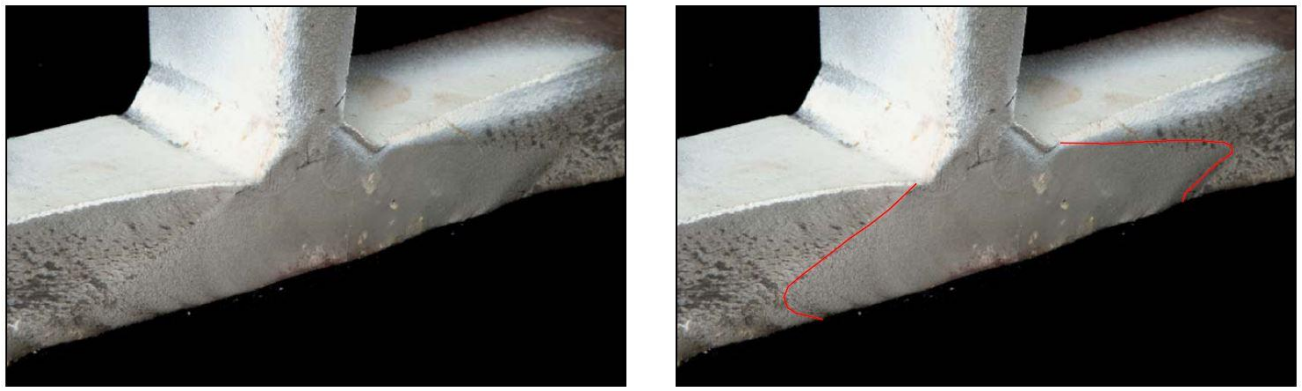

Figure A2.4: Crack surface – Specimen T4

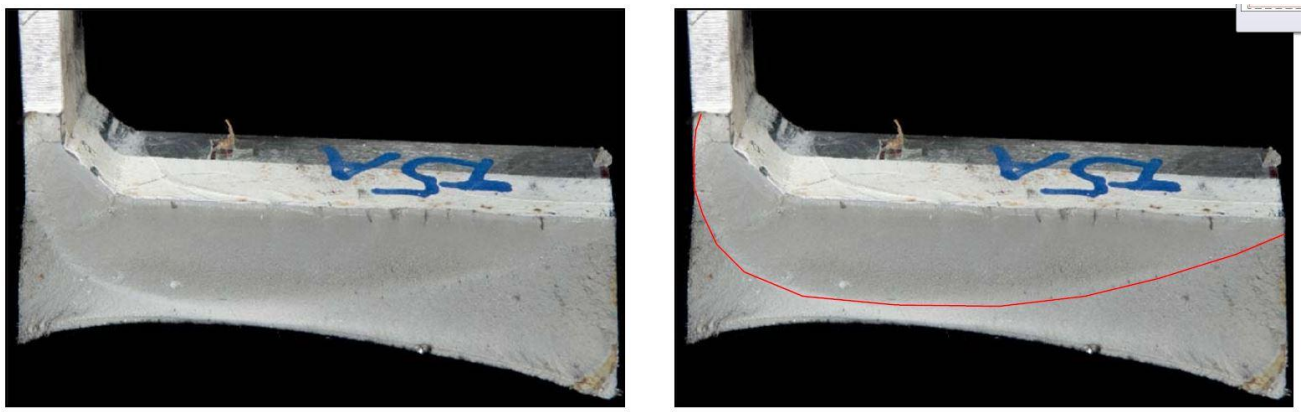

Figure A2.5: Crack surface – Specimen T5

Figure A2.6: Crack surface – Specimen T6

Figure A2.7: Crack surface – Specimen T7

Table A3.1. Results of tensile coupon tests

Tests	Name	$R_{p0.2}$	$\varepsilon_{p0.2}$	R_m	E-Modul	L_u	A_g	A_{gt}	A	A_t
		[MPa]	[%]	[MPa]	[MPa]	[mm]	[%]	[%]	[%]	[%]
1	Q1	729.8	0.56	783.2	206346	71.50	1.12	1.50	6.39	6.67
2	Q2	745.4	0.57	812.4	205392	70.40	3.13	3.53	6.37	6.63
3	L1	717.9	0.56	805.7	199740	70.50	3.15	3.55	6.39	6.65
4	L2	718.8	0.56	808.9	197265	71.30	3.41	3.82	7.24	7.48
5	G37L	723.5	0.56	815.0	200275	69.90	5.22	5.62	11.07	11.34
6	G37Q	753.8	0.56	824.6	208558	69.90	-	-	-	-

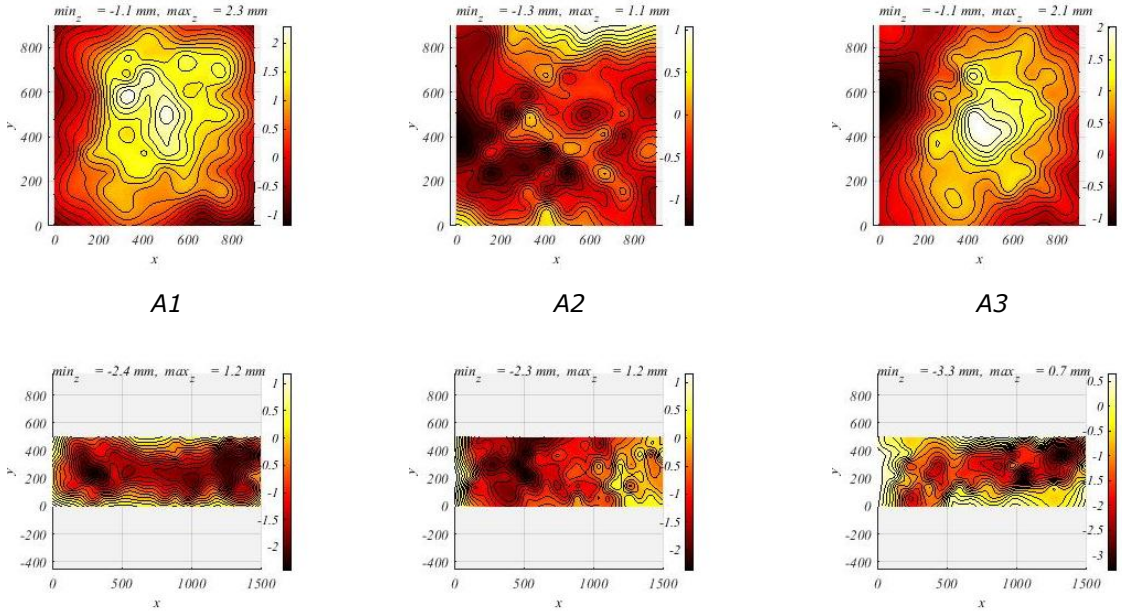

A1 *A2* *A3*

B1 *B2* *B3*

Figure A3.1. Initial imperfections of specimens

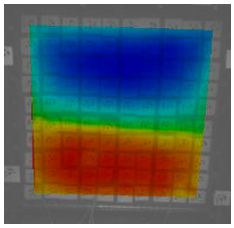

Test

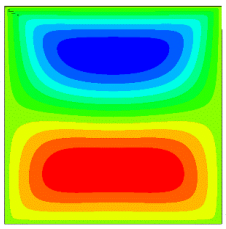

Simulation

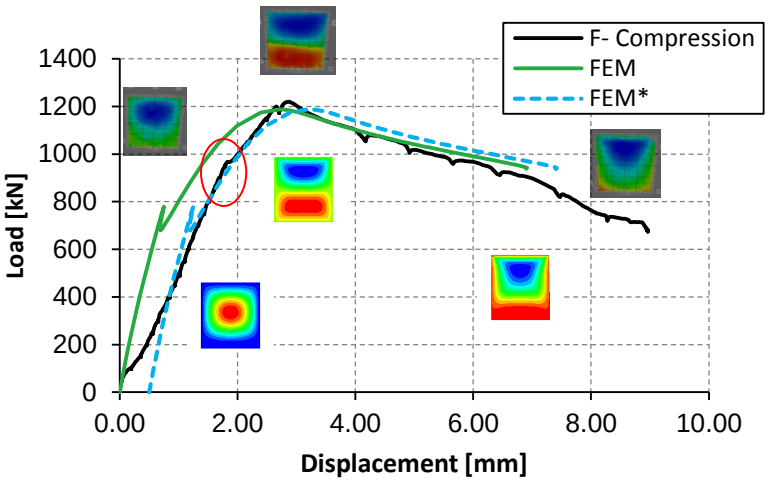

Figure A3.2. Results for test series A- Specimen A1

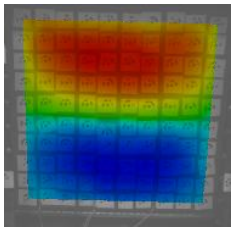

Test

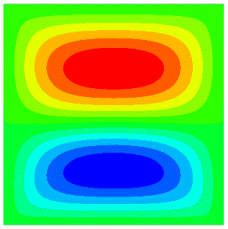

Simulation

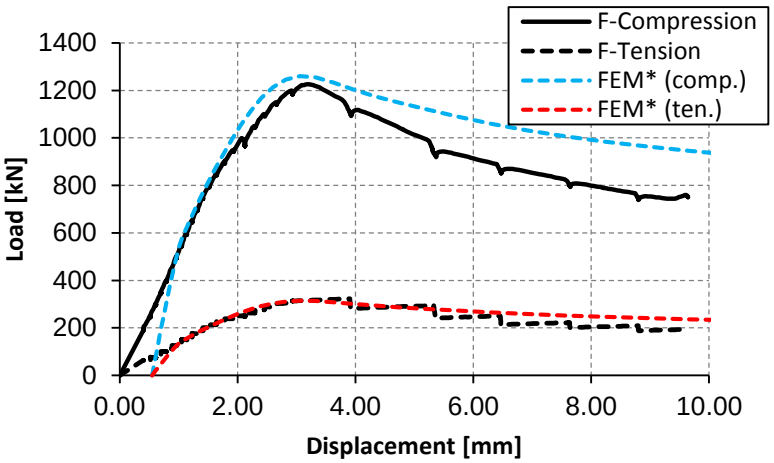

Figure A3.3. Results for test series A- Specimen A2

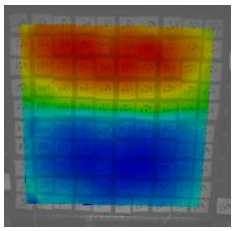

Test

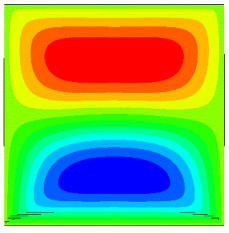

Simulation

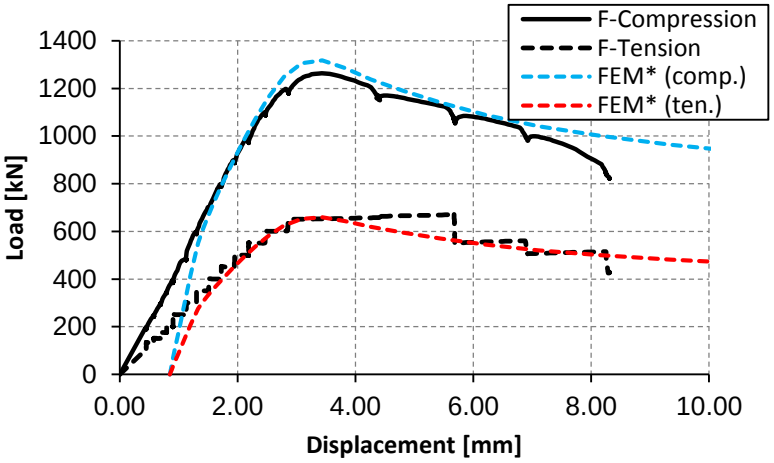

Figure A3.4. Results for test series A- Specimen A3

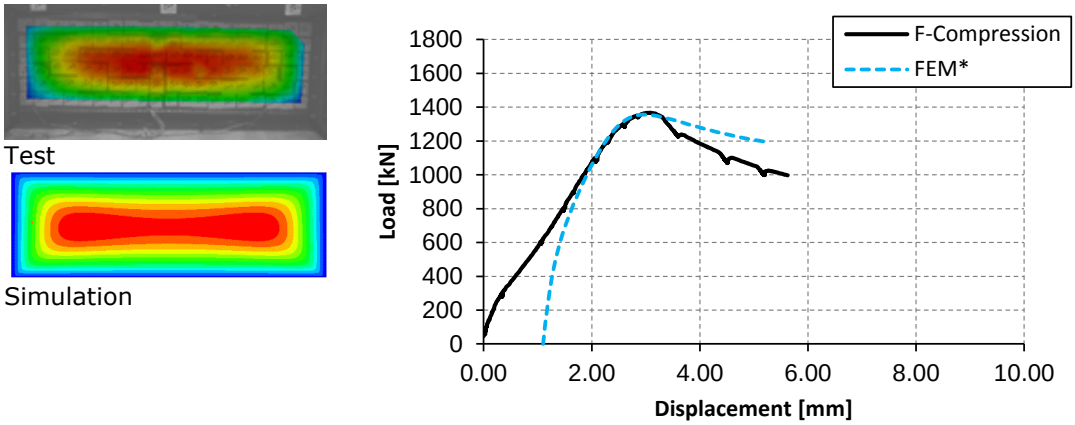

Figure A3.5. Results for test series B- Specimen B1

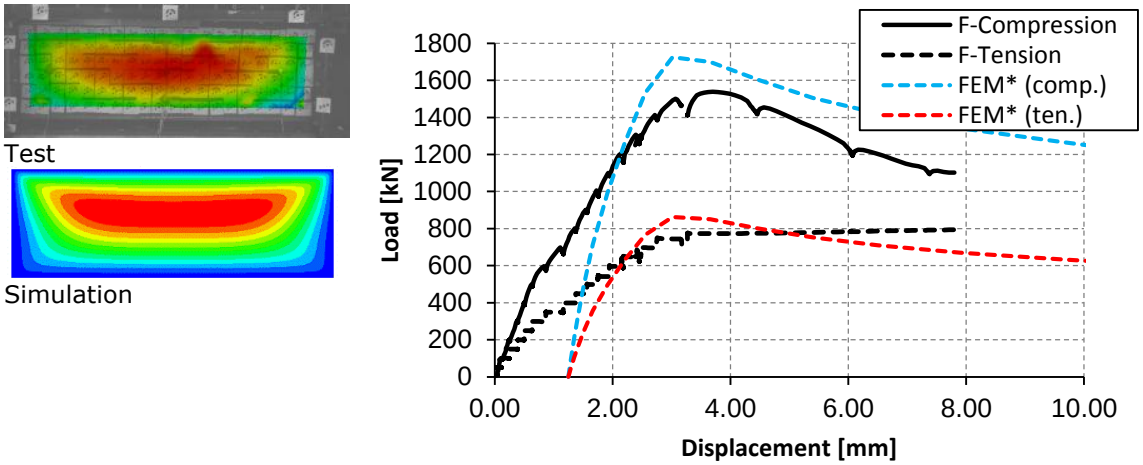

Figure A3.6. Results for test series B- Specimen B2

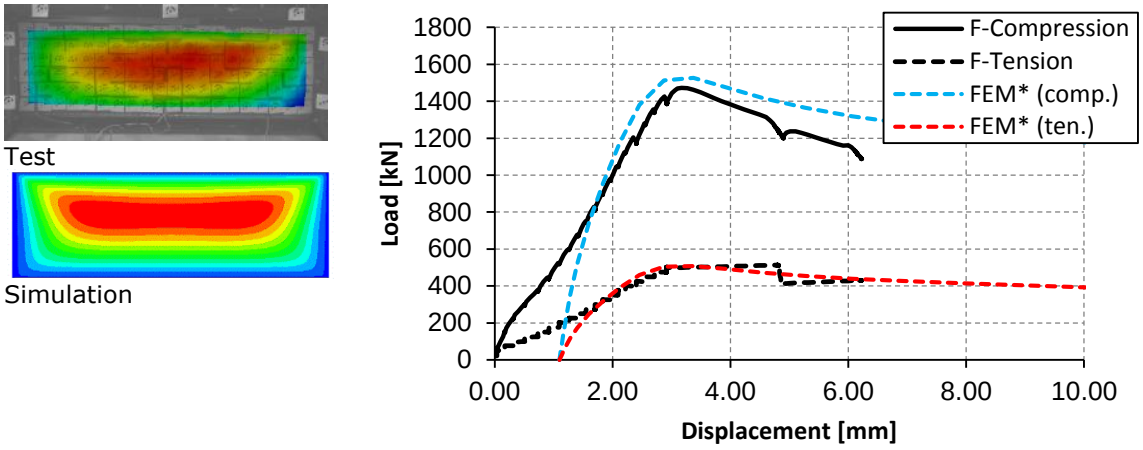

Figure A3.7. Results for test series B- Specimen B3

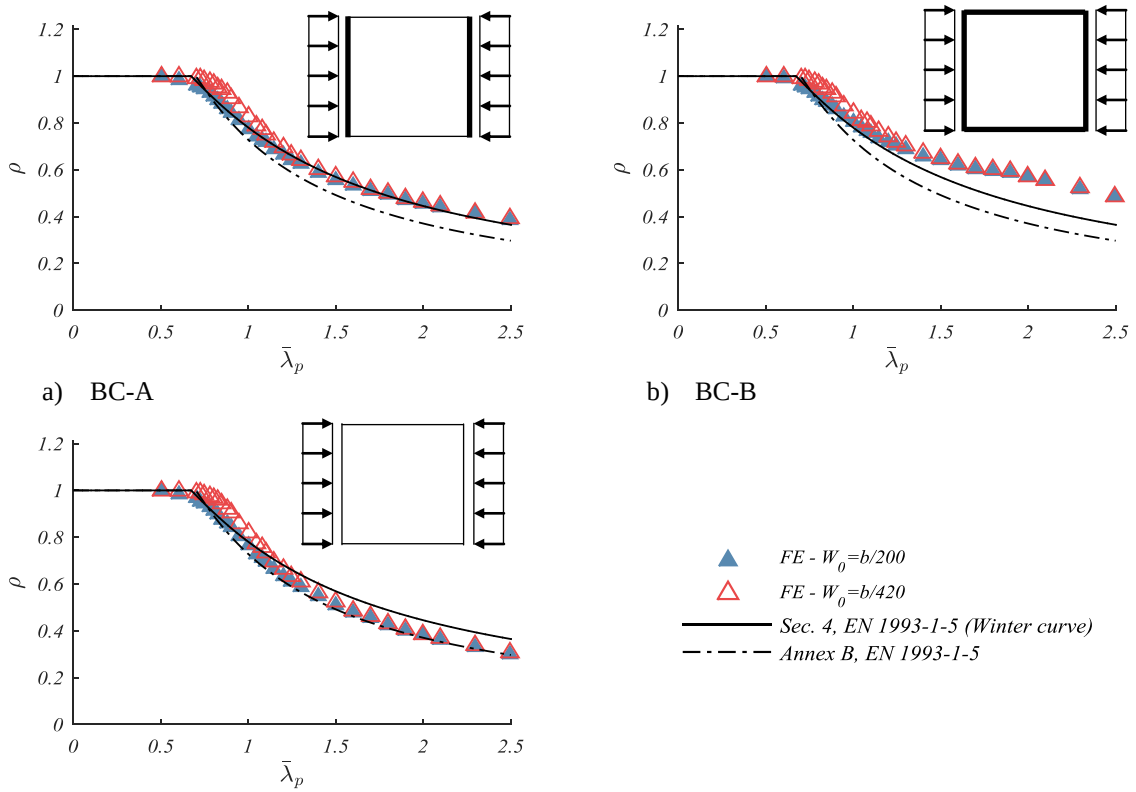

Figure A3.8. Numerical recalculation of the buckling curves acc. to EN 1993-1-5 for direct stress for different boundary conditions ($\alpha = 1$)

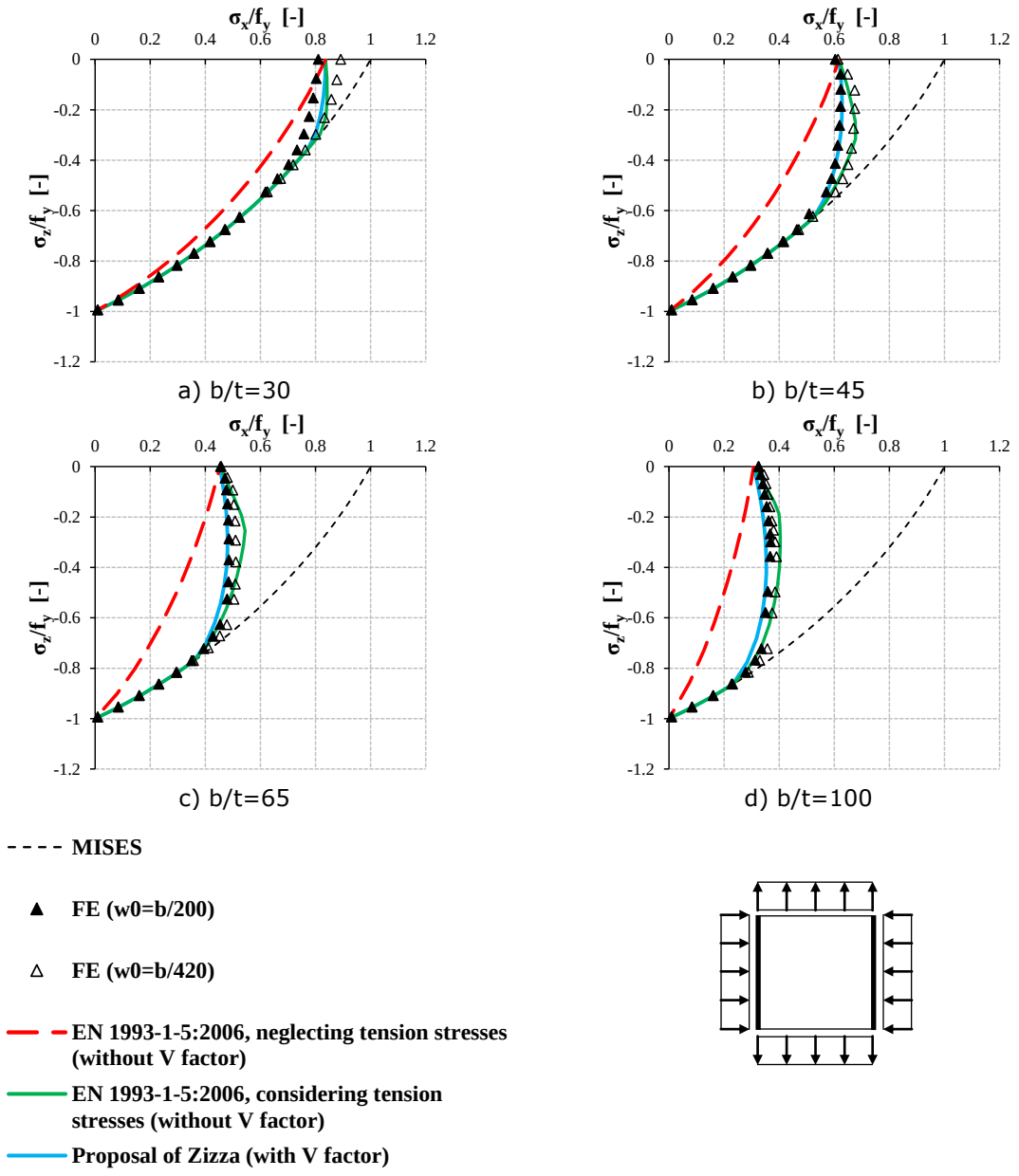

Figure A3.9. Comparison between the numerical calculation with the results of the current design rule EN 1993-1-5 and the improved design rule in case of panels subjected to compression-tension (Boundary condition BC-A: all edges hinged, loaded edges constrained and unloaded edges unconstrained; α=1; using reduction curve acc. to sec. 4 for $\rho_{c,x}$ and reduction curve acc. to Annex B for $\rho_{c,z}$)

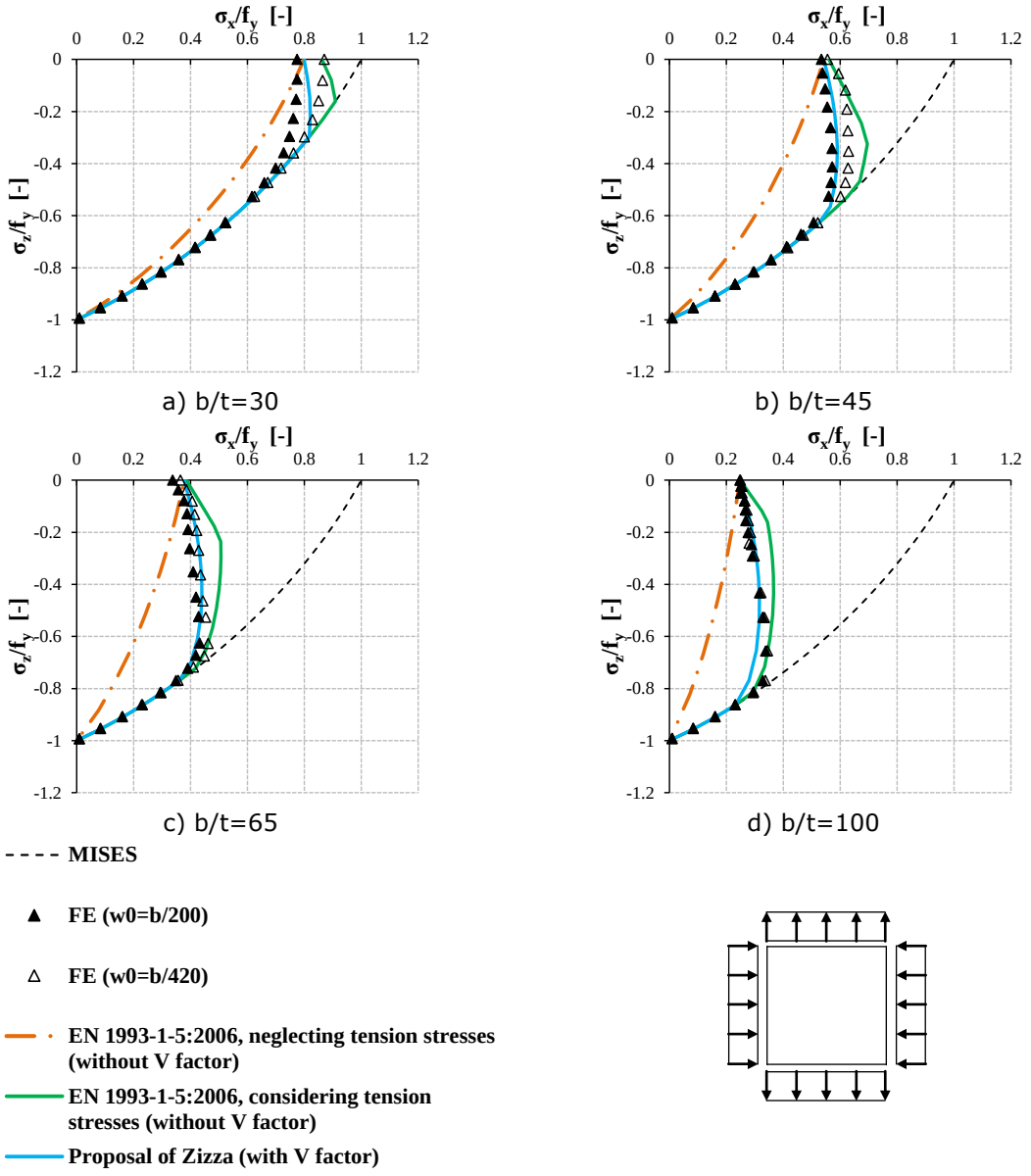

Figure A3.10. Comparison between the numerical calculation with the results of the current design rule EN 1993-1-5 and the improved design rule in case of panels subjected to compression-tension (Boundary condition BC-C: all edges hinged and free to move in plane; α=1; using reduction curve acc. to Annex B for $\rho_{c,x}$ and $\rho_{c,z}$)

Annex 4: WPS used for the samples generation, 40 and 25mm

	WELDING PROCEDURE SPECIFICATION (WPS)	WPS: S690QL_GMAW_40 REV.: 1 DATE: 2/03/2015

PROJECT: Optibri - Welding of S690QL-40mm

BASE MATERIAL:

Grade 1	S690 QL	Thickness	40 mm
Grade 2	S690 QL	Thickness	15 mm

FILLER MATERIALS:

INDEX	BRAND	NAME	EN CLASSIFICATION	DIAMETER	LOTNR.
A	LINCOLN	LNM MoNiVa	EN 12534: G69 4 M Mn3Ni1CrMo	1,2	

TEMPERATURES:

	TEMP	
Preheat , min °C	100	°C
Maintenance T. min °C	na	°C
Interpasstemp. Max. °C	na	°C

PWHT			Time	Temp.°C	Method	Heating rate		Cooling rate			
NA											

JOINT DESIGN and WELDING SEQUENCE:

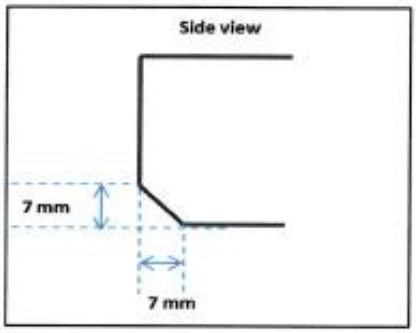

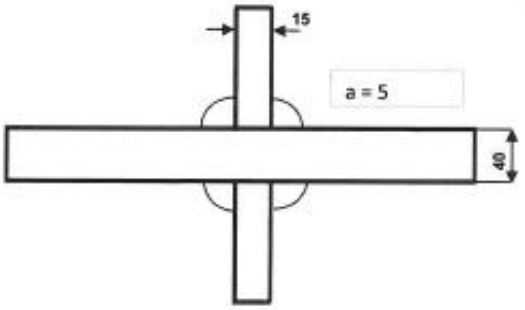

WELDING DETAILS:

Joint type	FW
Weld-edge prep.method	Cutting
Initial cleaning	NA
Interpass cleaning	NA
Welding position	PB
Backingstrip	NA
Back gouging method	NA
Shielding Gas Designation	ATAL 6 (82%Ar - 18%CO2)
Shielding Gas Flow Rate	14 l/mn.
diameter gas nozzle	15 mm
Stick out length	15 mm

WELDING PARAMETERS:

PASS NR.	INDEX Filler Mat.	WELDING PROCESS	Metal transf. Mode	CURRENT (A) ± 10%	VOLTAGE (V) ± 10%	DC/AC (+/-)	Weld.speed mm/min± 10%	Shield.gas or Flux	Interpass temp.	Ther.eff. k	HEAT INPUT kJ/mm
1	A	135-GMAW	Pulsed	250	28	DC+	220	82Ar-18CO2	na	0,8	1,527

PREPARED BY:	Benny Droesbeke		AUTHORITY	BIL
DATE:	2/03/2015		DATE:	02/03/2015

	WELDING PROCEDURE SPECIFICATION (WPS)	WPS S690QL_GMAW_25 REV. 1 DATE 2/03/2015

PROJECT: Optibri - Welding of S690QL-25mm

BASE MATERIAL:

Grade 1	S690 QL	Thickness	25 mm
Grade 2	S690 QL	Thickness	15 mm

FILLER MATERIALS:

INDEX	BRAND	NAME	EN CLASSIFICATION	DIAMETER	LOTNR.
A	LINCOLN	LNM MoNiVa	EN 12534: G69 4 M Mn3Ni1CrMo	1,2	

TEMPERATURES:

	TEMP	
Preheat , min °C	20	°C
Maintenance T. min °C	na	°C
Interpasstemp. Max. °C	na	°C

PWHT			Time	Temp.°C	Method	Heating rate		Cooling rate			
NA											

JOINT DESIGN and WELDING SEQUENCE:

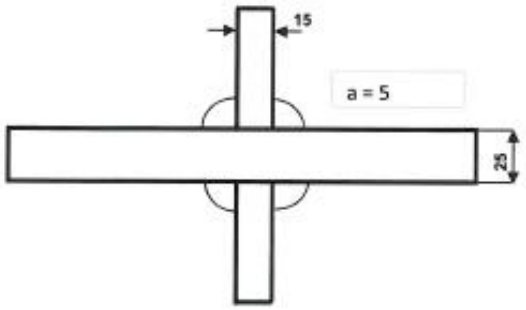

WELDING DETAILS:

Joint type	FW
Weld-edge prep.method	Cutting
Initial cleaning	NA
Interpass cleaning	NA
Welding position	PB
Backingstrip	NA
Back gouging method	NA
Shielding Gas Designation	ATAL 6 (82%Ar - 18%CO2)
Shielding Gas Flow Rate	14 l/min.
diameter gas nozzle	15 mm
Stick out length	15 mm

WELDING PARAMETERS:

PASS NR.	INDEX Filler Mat.	WELDING PROCESS	Metal transf. Mode	CURRENT (A) ± 10%	VOLTAGE (V) ± 10%	DC/AC (+/-)	Weld.speed mm/min± 10%	Shield.gas or Flux	Interpass temp.	Ther.eff. k	HEAT INPUT kJ/mm
1	A	135-GMAW	Pulsed	250	28	DC+	220	82Ar-18CO2	na	0,8	1,527

PREPARED BY:	Benny Droesbeke	AUTHORITY	BTL
DATE:	2/03/2015	DATE:	02/03/2015

Annex 5: Datasheet filler metal

LOW ALLOY SOLID WIRE

LNM MoNiVa

CLASSIFICATION

AWS A5.28 - ER110S-G
EN ISO 16834-A - G 69 4 M Mn3Ni1CrMo

GENERAL DESCRIPTION

Solid wire for welding high strength steels with yield strength up to 690 N/mm²
Good impact values at -40°C

WELDING POSITIONS (ISO/ASME)

SHIELDING GASES (ACC. ISO 14175)

M21 Mixed gas Ar+>15-25% CO_2

APPROVALS

ABS	DB	TÜV	CE
+	+	+	+

CHEMICAL COMPOSITION (W%) TYPICAL WIRE

C	Mn	Si	Ni	Cr	Mo	V	Cu
0.08	1.7	0.44	1.35	0.23	0.3	0.08	0.25

MECHANICAL PROPERTIES, TYPICAL, ALL WELD METAL

	Shielding gas	Condition	Yield strength (N/mm²)	Tensile strength (N/mm²)	Elongation (%)	Impact ISO-V(J) -40°C
Typical values	M21	AW	710	790	20	70

EXAMPLES OF MATERIALS TO BE WELDED

Steel grades	Standard	Type
Pipe material	API-5LX	X65, X70, X80
	EN 10208-2	L480, L550
Fine grained steel	EN 10025 part 6	S460, S500, S550, S620 S690
		S620Glt, S600MC, TstE620, Weldox 500, Hardox

PACKAGING AND AVAILABLE SIZES

	Diameter (mm)	0.8	1.0	1.2
Unit :	15 Kg spool B300	X	X	X

Other sizes and packaging on request

LNM MoNiVa rev. C-EN25-20/03/15

All information in this data sheet is accurate to the best of our knowledge at the time of printing. Please refer to www.lincolnelectric.eu for any updated information.
Fumes: Material Safety Data Sheets (MSDS) are available on our website.

LINCOLN ELECTRIC

www.lincolnelectric.eu

Annex 6 – Technical drawing of full beam

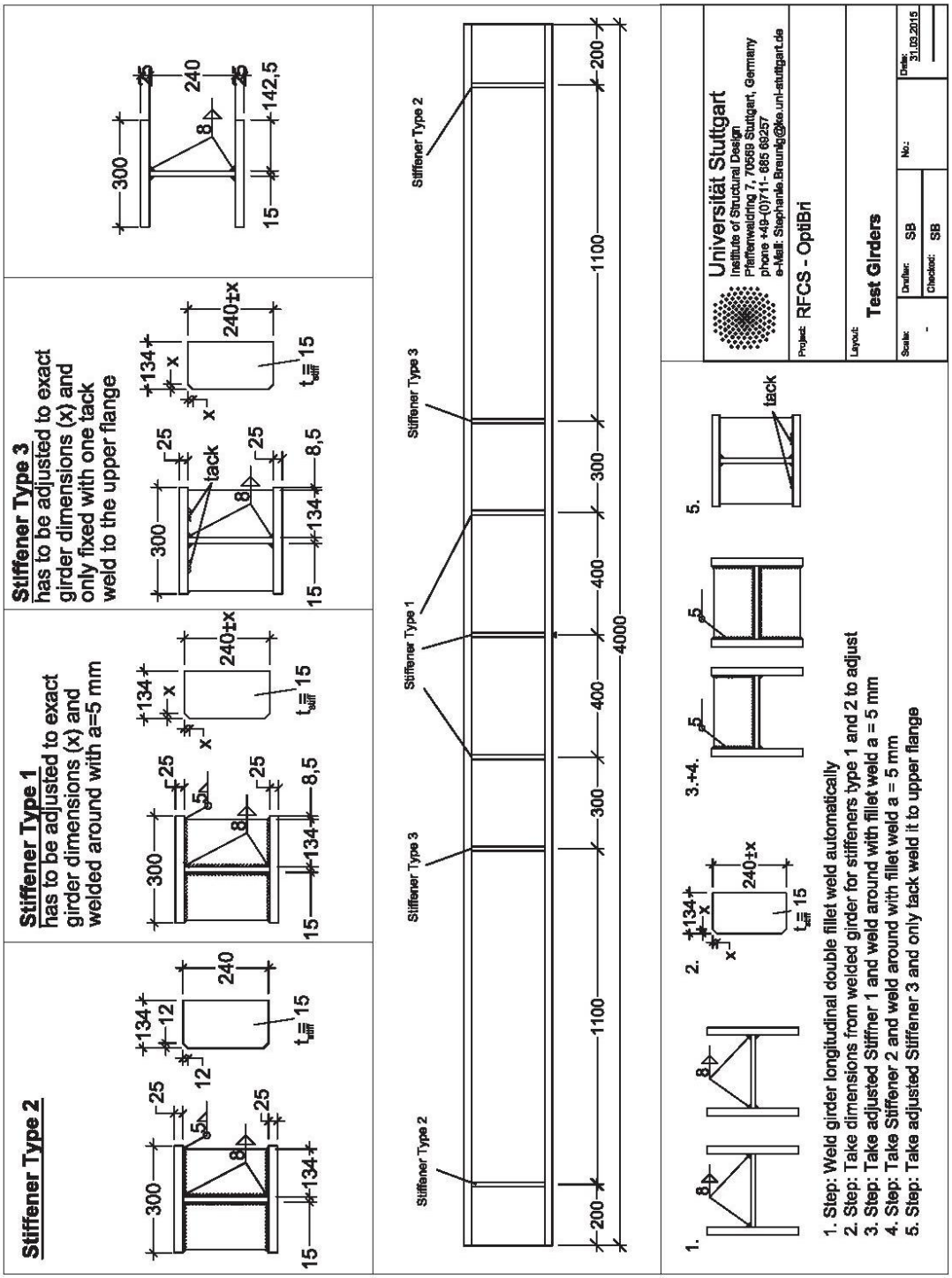

See hereafter

LONGITUDINAL VIEW - TYPICAL SPAN

ECH: 1/250

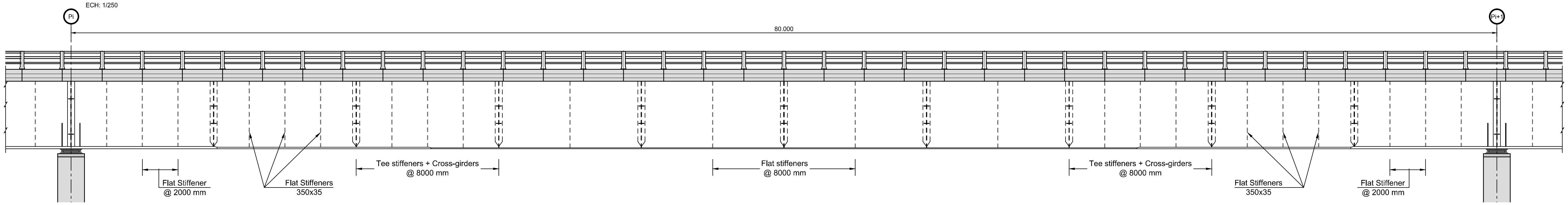

Top Flanges (mm)	1300 x 100 4000	1300 x 70 8000	1300 x 35 56000	1300 x 70 8000	1300 x 100 4000
Web thickness (mm)	26 12000	22 20000	18 16000	22 20000	26 12000
Bottom Flanges (mm)	1500 x120 8000	1500 x80 12000	1500 x50 40000	1500 x80 12000	1500 x120 8000
Head Stud Connectors	Stud Connectors 5 Ø22 // 300	Stud Connectors 5 Ø22 // 400	Stud Connectors 3 Ø22 // 400	Stud Connectors 5 Ø22 // 400	Stud Connectors 5 Ø22 // 300
Longitudinal Reinforcement	2.0% 12000	1.5% 12000	1.0% 32000	1.5% 12000	2.0% 12000

DECK TYPICAL CROSS-SECTION - SUPPORT

ESC: 1/125

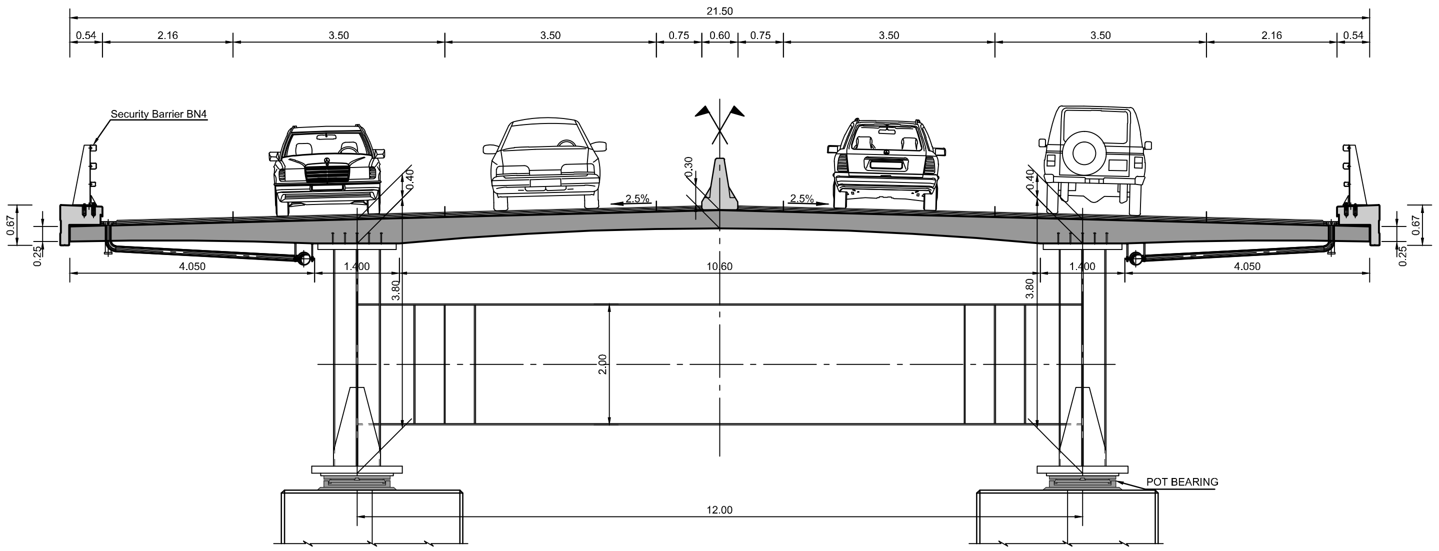

DECK TYPICAL CROSS-SECTION - SPAN

ESC: 1/125

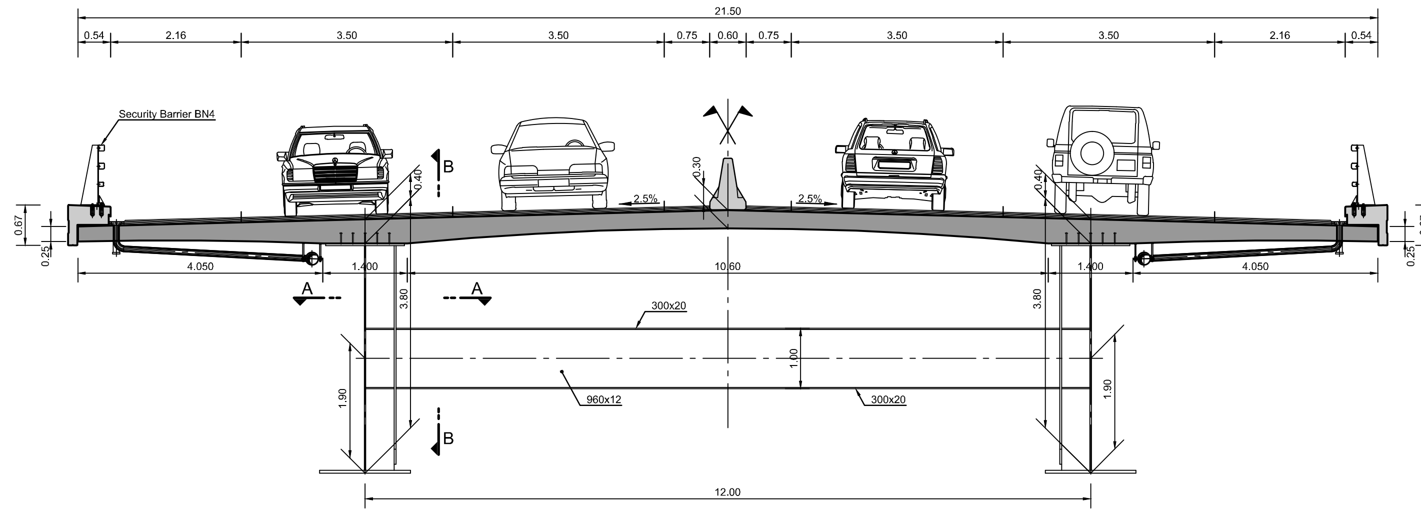

HEAD STUD CONNECTORS

ESC. 1/12.5

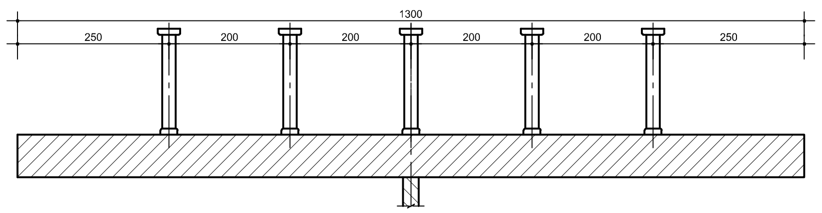

HEAD STUD CONNECTORS

ESC. 1/5

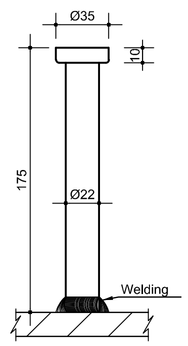

WELDING DETAILS

Scale: 1/10

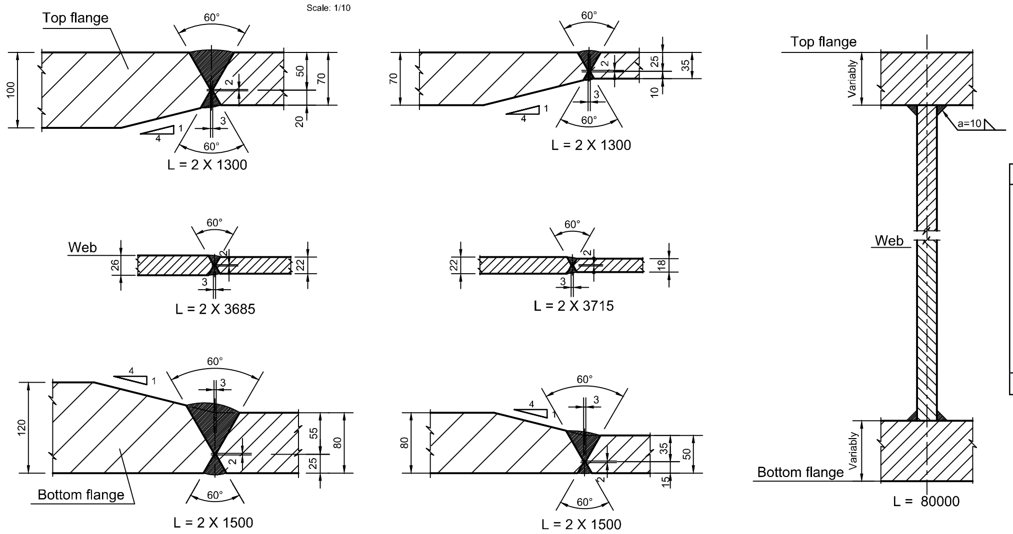

Name	Symbol	Throat	Name	Symbol	Throat
Fillet weld with no bevel			Bevel in half-V	(*)	
Fillet weld with bevel			Bevel in K	(*)	
Bevel in V			Bevel in Y		
Bevel in X			Bevel in double Y		

(*) The arrow points to the bevelled plate

SECTION A-A - TEE STIFFENERS

ESC. 1/50

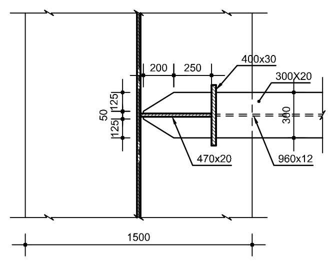

SECTION B-B - CROSS-GIRDERS

ESC. 1/50

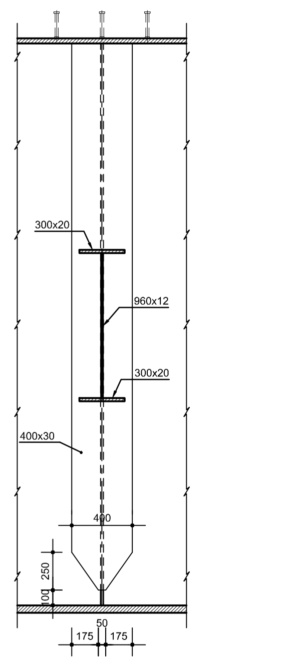

SECTION C-C - FLAT STIFFENERS

ESC. 1/50

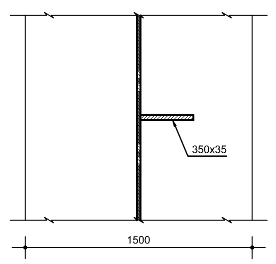

STRUCTURAL MATERIALS

CONCRETE:			
Designation	EN 206-1	Exposure Classes	Cover (mm)
Piers and Foundations	C30/37	XC3 / XF1	45
Deck - Slab	C35/45	XC4/ XF4	40
STEEL:			
Structural Steel	EN10025-2 S355 J2 (Z15 if th. ≤ 30mm) EN10025-3 S355 N (Z15 if 30 < th. ≤ 80mm) EN10025-3 S355 NL (Z25 if th. > 80mm)		
Reinforcement	B500B (EN 10080)		
Prestress Cables	$f_{p0,1k} \geq$ 1637 MPa / $f_{puk} \geq$ 1860 MPa (EN 10138)		
Stud Connectors	EN10025 S235 J2 + C450 (EN ISO 13918)		

CLIENT :

Research & Innovation
Research Fund for Coal and Steel

ULg / UStutt / UC / BWI / GRID / Industeel

AUTOR : GRID
INTERNATIONAL | CONSULTING ENGINEERS

TITLE : OPTIBRI - Optimal use of high strength steel grades within bridges

DESIGNATION :

DESIGN SOLUTION A

Rev.	Date	DESCRIPTION	Emis	Verified	Approved
0	06/01/2015	FIRST EMISSION	CC	JOP	AR
1	21/09/2015	UPDATED ACCORDING TO THE TECHNICAL REPORT	LC	JOP	AR
2	13/07/2016	WELDING DETAILS INCLUSION	VL	JOP	AR

Scale : VAR.
Format : A3

DOCUMENT CODE: GR - 1 - E128 - GE - G - A - 0100 - 2

Phase: WP 1

LONGITUDINAL VIEW - TYPICAL SPAN

ECH: 1/250

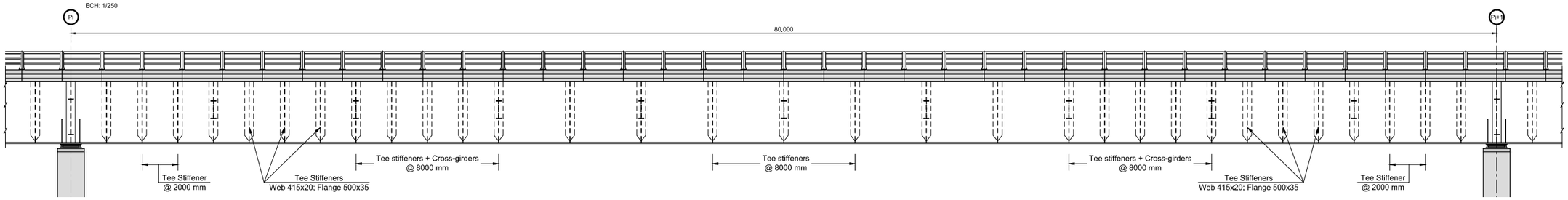

Top Flanges (mm)	1100 x 40 12000		1100 x 30 56000						1100 x 40 12000
Web thickness (mm)	20 12000		18 20000		15 16000		18 20000		20 12000
Bottom Flanges (mm)	1300 x 70 8000		1300 x 60 12000		1300 x 45 40000			1300 x 60 12000	1300 x 70 8000
Head Stud Connectors	Stud Connectors 5 Ø22 // 200		Stud Connectors 5 Ø22 // 300		Stud Connectors 3 Ø22 // 300			Stud Connectors 5 Ø22 // 300	Stud Connectors 5 Ø22 // 200
Longitudinal Reinforcement	2.0% 12000		1.5% 12000		1.0% 32000			1.5% 12000	2.0% 12000

DECK TYPICAL CROSS-SECTION - SUPPORT

ESC: 1/125

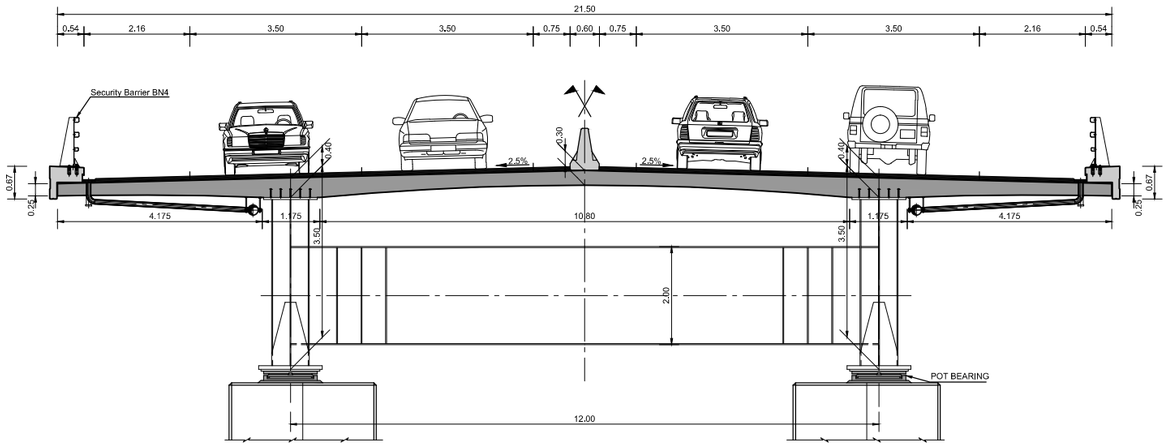

DECK TYPICAL CROSS-SECTION - SPAN

ESC: 1/125

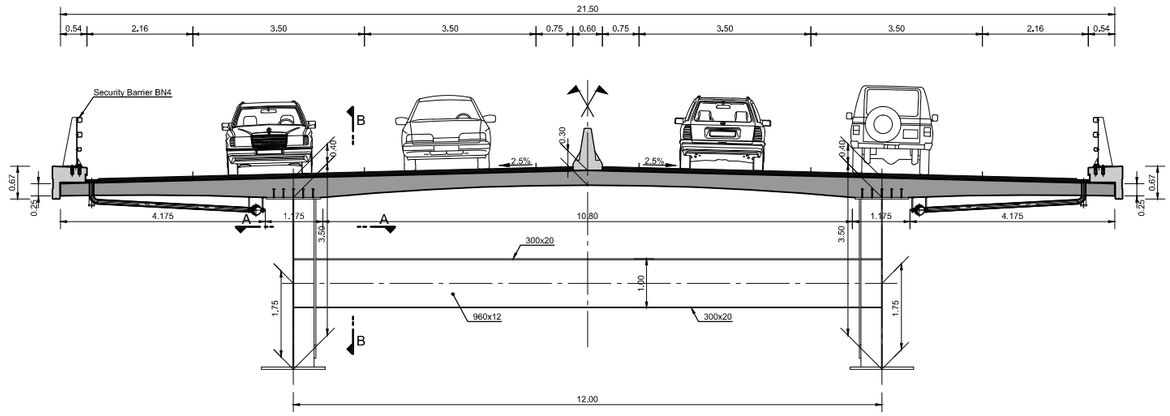

HEAD STUD CONNECTORS

ESC. 1/12.5

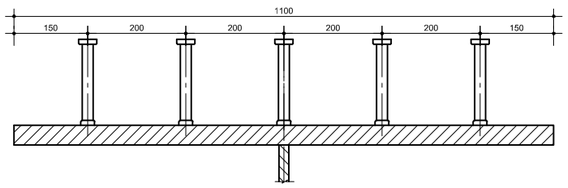

HEAD STUD CONNECTORS

ESC. 1/5

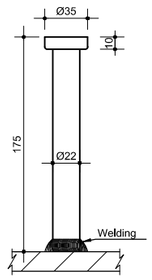

WELDING DETAILS

Scale: 1/10

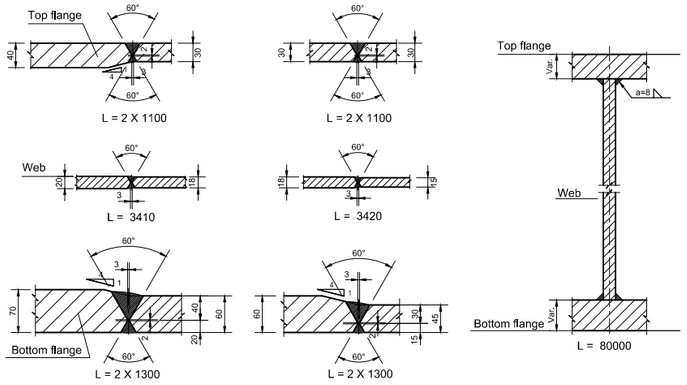

Name	Symbol	Throat	Name	Symbol	Throat
Fillet weld with no bevel			Bevel in half-V		
Fillet weld with bevel			Bevel in K		
Bevel in V			Bevel in Y		
Bevel in X			Bevel in double Y		

(*) The arrow points to the bevelled plate

SECTION A-A - TEE STIFFENERS

ESC. 1/50

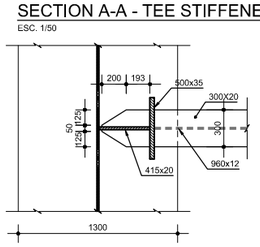

SECTION C-C - TEE STIFFENERS

ESC. 1/50

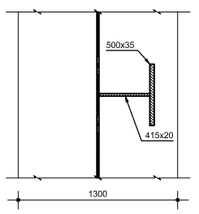

SECTION B-B - CROSS-GIRDERS

ESC. 1/50

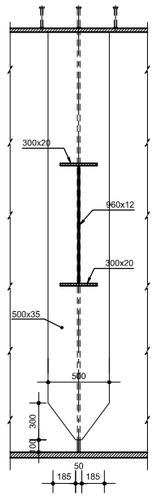

STRUCTURAL MATERIALS

CONCRETE:			
Designation	EN 206-1	Exposure Classes	Cover (mm)
Piers and Foundations	C30/37	XC3 / XF1	45
Deck - Slab	C35/45	XC4/ XF4	40
STEEL:			
Structural Steel	EN10025-6 S690 QL (40J,-40ºC) (Z15 if th. ≤ 40mm) EN10025-6 S690 QL1 (40J,-40ºC) (Z15 if th. > 40mm)		
Reinforcement	B500B (EN 10080)		
Prestress Cables	$fp_{0.1k} \geq$ 1637 MPa / $fp_{uk} \geq$ 1860 MPa (EN 10138)		
Stud Connectors	EN10025 S235 J2 + C450 (EN ISO 13918)		

CLIENT :

Research & Innovation
Research Fund for Coal and Steel

ULg / UStutt / UC / BWI / GRID / Industeel

AUTOR : GRID

TITLE : OPTIBRI - Optimal use of high strength steel grades within bridges

DESIGNATION :

DESIGN SOLUTION B

Rev.	Date	DESCRIPTION	EMISSION		
			Elab.	Verified	Approved
0	06/01/2015	FIRST EMISSION	CC.	JOP	AR
1	22/09/2015	UPDATED ACCORDING TO THE TECHNICAL REPORT	LC.	JOP	AR
2	13/01/2016	WELDING DETAILS INCLUSION	VL.	JOP	AR
3	24/01/2017	TEE STIFFENER REDESIGN	CC.	JOP	AR

Scale: VAR.
Format: A3

DOCUMENT CODE: GR - 1 - E128 - GE - G - A - 0200 - 3

Phase: WP 1

LONGITUDINAL VIEW - TYPICAL SPAN

Scale: 1/250

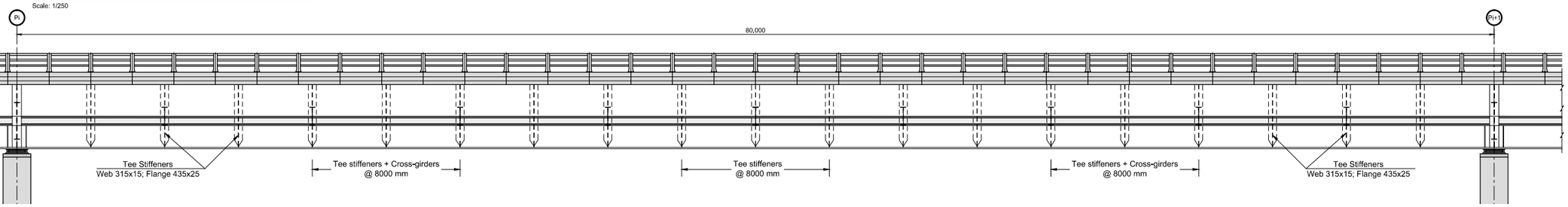

Top Flanges (mm)	1100 x 40 12000	1100 x 30 56000			1100 x 40 12000
Web thickness (mm)	20 13000	18 15000	15 24000	18 15000	20 13000
Bottom Flanges (mm)	1300 x 70 8000	1300 x 45 12000	1300 x 30 40000	1300 x 45 12000	1300 x 70 8000
Head Stud Connectors	Stud Connectors 5 Ø22 // 200	Stud Connectors 5 Ø22 // 300	Stud Connectors 3 Ø22 // 300	Stud Connectors 5 Ø22 // 300	Stud Connectors 5 Ø22 // 200
Longitudinal Reinforcement	2,0% 12000	1,5% 12000	1,0% 32000	1,5% 12000	2,0% 12000

DECK TYPICAL CROSS-SECTION - SUPPORT

Scale: 1/125

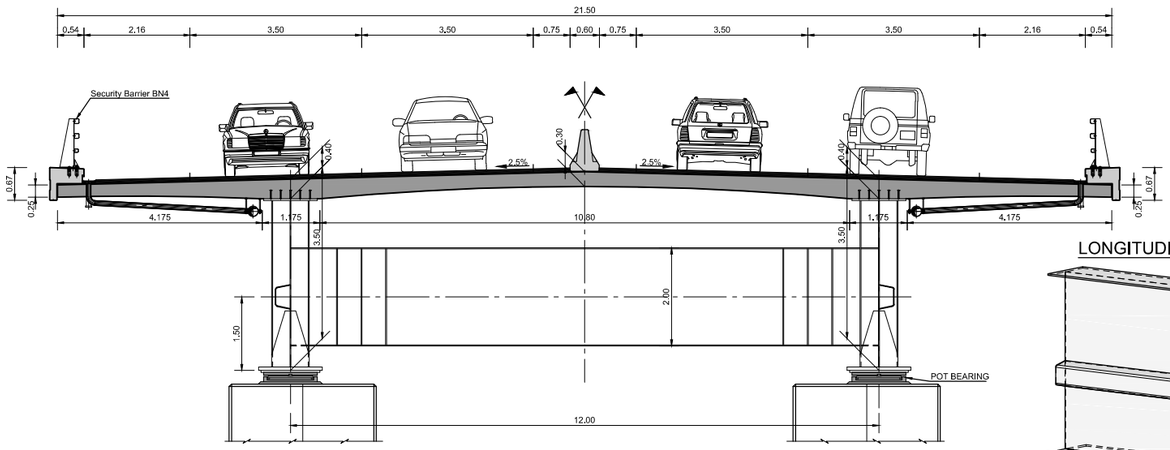

DECK TYPICAL CROSS-SECTION - SPAN

Scale: 1/125

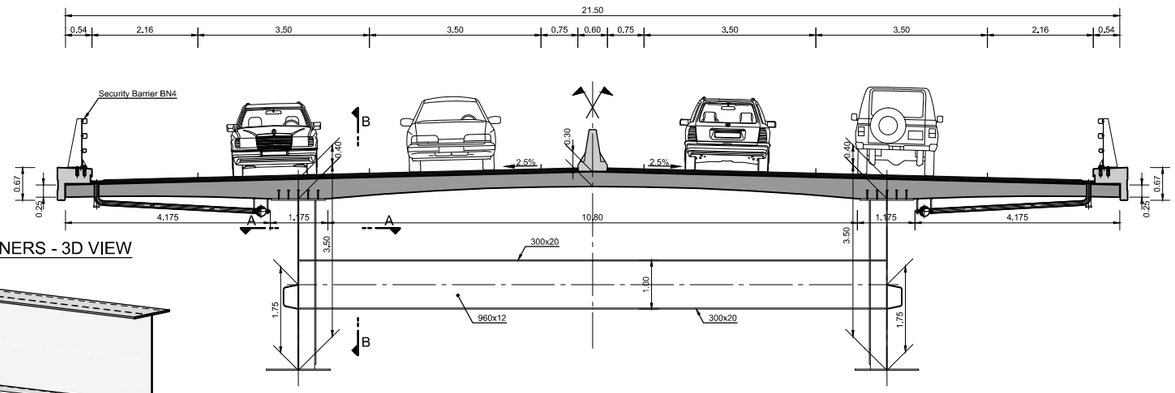

LONGITUDINAL STIFFENERS - 3D VIEW

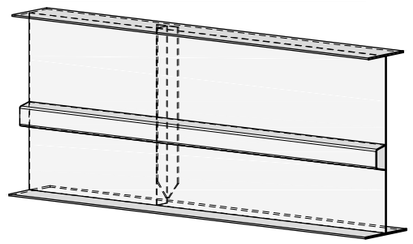

HEAD STUD CONNECTORS

Scale: 1/12.5

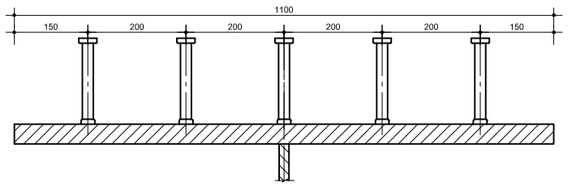

HEAD STUD CONNECTORS

Scale: 1/5

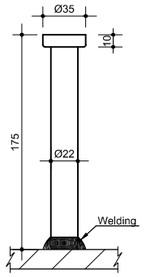

LONGITUDINAL STIFFENERS

Scale: 1/10

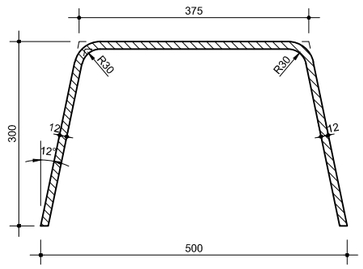

SECTION A-A - TEE STIFFENERS

Scale: 1/50

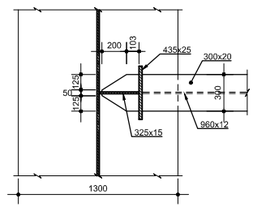

SECTION B-B - CROSS-GIRDERS

Scale: 1/50

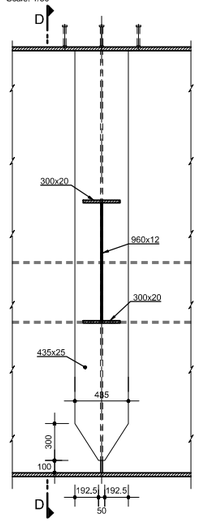

SECTION D-D - CROSS-GIRDERS

Scale: 1/50

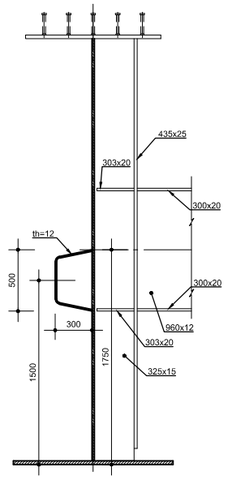

SECTION C-C - TEE STIFFENERS

Scale: 1/50

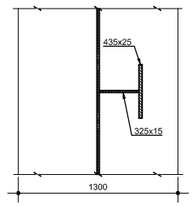

WELDING DETAILS

Scale: 1/10

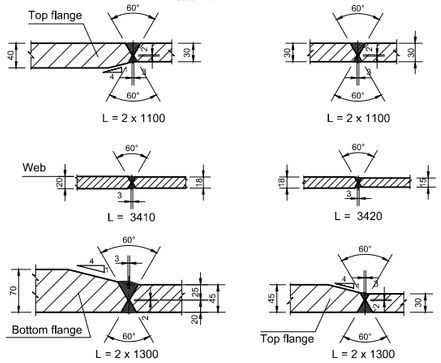

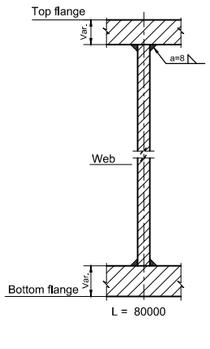

Name	Symbol	Throat	Name	Symbol	Throat
Fillet weld with no bevel			Bevel in half-V		
Fillet weld with bevel			Bevel in K		
Bevel in V			Bevel in Y		
Bevel in X			Bevel in double Y		

(*) The arrow points to the bevelled plate

STRUCTURAL MATERIALS

CONCRETE:			
Designation	EN 206-1	Exposure Classes	Cover (mm)
Piers and Foundations	C30/37	XC3 / XF1	45
Deck - Slab	C35/45	XC4/ XF4	40
STEEL:			
Structural Steel	EN10025-6 S690 QL (40J,-40ºC) (Z15 if th. ≤ 40mm) EN10025-6 S690 QL1 (40J,-40ºC) (Z15 if th. > 40mm)		
Reinforcement	B500B (EN 10080)		
Prestress Cables	$f_{p0,1k}$ ≥ 1637 MPa / f_{pk} ≥ 1860 MPa (EN 10138)		
Stud Connectors	EN10025 S235 J2 + C450 (EN ISO 13918)		

CLIENT : Research & Innovation Research Fund for Coal and Steel

ULg / UStutt / UC / BWI / GRID / Industeel

AUTOR : GRID

TITLE : OPTIBRI - Optimal use of high strength steel grades within bridges

DESIGNATION : DESIGN SOLUTION C

Rev.	Date	DESCRIPTION	EMISSION		
			Elms	Verified	Approved
0	20/09/2017	FIRST EMISSION	CC	JOP	AR
1	12/09/2017	UPDATE OF STIFFENERS	CC	JOP	AR

Scale: VAR. Format: A3

DOCUMENT CODE: GR - 1 - E128 - GE - G - A - 0200 - 3

Phase: WP 1

Getting in touch with the EU

In person

All over the European Union there are hundreds of Europe Direct information centres. You can find the address
of the centre nearest you at: https://europa.eu/european-union/contact_en

On the phone or by email

Europe Direct is a service that answers your questions about the European Union. You can contact this service:

– by freephone: 00 800 6 7 8 9 10 11 (certain operators may charge for these calls),

– at the following standard number: +32 22999696 or

– by email via: https://europa.eu/european-union/contact_en

Finding information about the EU

Online

Information about the European Union in all the official languages of the EU is available on the Europa website
at: https://europa.eu/european-union/index_en

EU publications

You can download or order free and priced EU publications at:
https://publications.europa.eu/en/publications. Multiple copies of free publications may be obtained by contacting Europe Direct or your local information centre (see https://europa.eu/european-union/contact_en).

EU law and related documents

For access to legal information from the EU, including all EU law since 1952 in all the official language versions,
go to EUR-Lex at: http://eur-lex.europa.eu

Open data from the EU

The EU Open Data Portal (http://data.europa.eu/euodp/en) provides access to datasets from the EU. Data can be downloaded and reused for free, for both commercial and non-commercial purposes.

The project aims to generate guide lines for welded bridges using High Strength Steel. The quantification of the advantage of using HSS within bridges is performed on a 21.5 m wide highway bridge, with a typical 80 m long inner span and a composite steel-concrete twin plate girder deck. It presents clear fatigue and stability issues. An extensive experimental and numerical campaign of fatigue on HSS samples, welded plates and welded beams as well as an experimental and numerical study of multiaxial stressed plates allow a better understanding of HSS material and HSS welded joint behaviour with or without weld post treatment.

The results enhance the need of an Eurocode review. Three designs of this bridge are compared: the first bridge design (A) uses only standard S355 steel grade whereas the second design (B) uses also HSS S690 QL steel but relies on current state of Eurocodes. Finally, the third design (C) is performed based on the real measured behaviour of HSS S690 QL steel and post treated welded joints. Through different variants of the design (C), the project results demonstrate the need of updating of Eurocode to take into account the enhanced material properties of HSS and the buckling of multiaxial stressed plates. The use of S690 QL in design B (C) enables reductions of steel weight of 25% (32%) on the steel deck and 34% (39%) on main girder compared to Design A and these designs save about 50% on full penetration welding volume compared to design A.

Studies and reports

Publications Office